Scuola Normale Superiore

Classe di Scienze

Corso di Perfezionamento

Multi-Terminal Thermoelectric Machines in Nanostructures

Tesi di Perfezionamento

Francesco MAZZA

Relatori Prof. Rosario FAZIO
Dott. Fabio TADDEI

Anno Accademico 2015-2016

Contents

List of Figures

Introduction

The research on sustainable energy sources for the world's population is becoming increasingly important. In the last years the number of scientists working in this field has increased accordingly, and it is likely that in the following years this trend will continue in this direction. Different scientific communities (chemistry, physics, engineering,...) are devoting more and more efforts and resources to this problem.

Standard thermal machines produce energy by converting heat into work. As first recognized by Nicoals Léonard Sadi Carnot [Carnot1824], this conversion cannot overcame a certain efficiency, the *Carnot efficiency*. For instance, the efficiency of heat engines, as the ones used in cars, is about 25%, this means that most of the heat produced by the fuel, is wasted. There are many other ways to produce energy, that may have higher efficiency rather than heat engines - electrical engines, nuclear power plants, photovoltaic panels and hydroelectric centrals - are just a few examples. Nevertheless, the very thing that these energy sources have in common, is that they all waste some heat. Being able to re-use or to control this heat would be a solid and sustainable contribution to the energy problems of the world. This is the main reason why thermoelectricity has being receiving so much attention by the scientific community. In fact, an efficient thermoelectric power generator would be albe to re-use the wasted heat, and to convert it into work.

The first observation of thermoelectric phenomena dates back to 1794, when Alessandro Volta that a thermoelectromotive force arise under the influence of a temperature gradient [Volta1794]. However, it was in 1821 that Thomas Johann Seebeck performed the first actual experiment on thermoelectricity [Seebeck1822]. He noticed that a needle can be deflected

by a closed circuit made by two different metals joined in two places, with a temperature difference across the junction: the metals respond differently to the temperature gradient, thus creating a current in the loop and a magnetic field. It is interesting to know that Seebeck called this phenomenon *thermomagnetic effect*, it was H. C. Ørsted who correctly understood it and coined the word *thermoelectricity*. Then in 1931 Lars Onsager bridged thermoelectric phenomena with the rising field of irreversible thermodynamics [Onsager1931], but the scientific community almost neglected it for 20 years. It was only in the 1950s with Ioffe's book on thermoelectricity [Ioffe1958] that this field could advance rapidly: the important role of doped semiconductors as good thermoelectric material was understood, and the thermoelectric material Bi_2Te_3 was developed for commercialization. The thermoelectric efficiency was linked to an adimensional figure of merit, called ZT, high ZT values imply high efficiency. In the thirty years from 1960 to 1990 few progresses had been made in the material science industry, and the best commercial material was operating at ZT values around 1, while it is generally accepted that the target value for efficient thermoelectric generators is around $ZT = 3$, to be competitive with conventional refrigerators and generators. The situation was about to change at the beginning of the 1990s, in fact in the last years of the 1980s the first nanostructure systems were fabricated. This opened a completely new field in the physics of matter, and gave new life to the field of thermoelectricity. This motivates the researchers to investigate different approaches, starting from the fundamental microscopic mechanisms which determine the phenomenological laws of transport of heat and particles. It was soon recognized that low dimensional materials could have very large thermoelectric response [Hicks1993]. The main ideas that were motivating the researchers were the fact that the arising quantum confinement effects could enhance the extracted power, while the internal interfaces of the nanostructure could reduce the thermal conductance more than the electrical conductance. Later it was discovered that a sufficiently narrow energy filter could lead to arbitrary large values of ZT [Mahan1997], which implies an efficiency equal to the Carnot efficiency, but zero extracted power. Nowadays the challenge for the researchers is to find efficient and scalable nano-systems that can deliver a reasonable high power at high efficiency. The search for optimization of nanoscale heat engines and refrigerators and for a way to control the heat at the nanoscale has hence stimulated a large body of activity, recently reviewed in many papers.

Up to now many progresses have been made in systems composed by two terminals. On the other hand, the more complex design, of multi-terminal devices, may offer additional advantages in thermoelectric transport, and just begun to be investigated. An interesting perspective, for instance, is the possibility to exploit a third terminal to "decouple" the energy and charge flows and improve thermoelectric efficiency. Furthermore, fundamental questions concerning thermodynamic bounds on the efficiency of these setups has being investigated, also accounting for the effects of a magnetic field breaking the time-reversal symmetry. In most of the cases studied so far, however, all but two terminals were considered as mere probes; i.e. no net flow of energy and charge through them was allowed. In other works a purely bosonic reservoir has been used, only exchanging energy (and not charge) current with the system.

The objective of this thesis is to fill the gap in the knowledge of thermoelectric properties of multi-terminal systems. Therefore we started by studying the multi-terminal problem in its full complexity, with no constraints on the leads. We soon realized that the freedom given by three-terminal systems could be used to develop a scheme to spatially separate the heat and charge flows, obtaining a significant increase in both the power and the efficiency delivered by the engine. By adding the additional complication of a magnetic field on three-terminal systems, we were able to design a thermal magnetic switch which provides a simple way to deal with heat management at the nanoscale.

The outline of the thesis is the following. In **Chapter 1** we provide the theoretical tools needed in this Thesis. Following the standard textbook derivation we set the basis for the Irreversible Thermodynamics with a special attention to the linear response regime. Then we present the Landauer-Büttiker formalism to calculate the currents for non interacting systems. We conclude with a brief overview of the state-of-the-art of the research in this field.

In **Chapter 2** we discuss the efficiency of a thermal engine working in linear response regime in a three-terminal configuration. We provide the expressions for the local and non local transport coefficients (electrical and thermal conductances, and thermoelectric powers) and derive new generalized figures of merit that will allow us to write analytical expressions for the efficiency at maximum power. We investigate numerically, through two examples, how a third terminal can enhance the performance (in terms of the efficiency and of the power extracted) of the quantum thermal machine.

In **Chapter 3** we study a class of three-terminal devices in which the (electronic) heat and charge currents can flow in different reservoirs. We introduce the main characteristics of such *heat-charge current separation* regime and show how to realize it using normal and superconducting leads. We demonstrate that this regime allows to have an independent control on heat and charge flows and to greatly enhance thermoelectric performances at low temperatures. We analyze in details a three-terminal setup involving a superconducting lead, a normal lead and a voltage probe. For a generic scattering region we show that in the regime of heat-charge current separation both the power factor Q and the figure of merit ZT are highly increased with respect to a standard two-terminal system. These results are confirmed for the specific case of a system consisting of three coupled quantum dots.

In **Chapter 4** we analyze how in a multi-terminal setup, when time-reversal symmetry is broken by a magnetic field, the heat flows can be managed by designing a device with programmable Boolean behavior. We show that such a device can be used to implement operations, such as on/off switching, reversal, selected splitting and swap of the heat currents. For each feature, the switching from one working condition to the other is obtained by inverting the magnetic field. This offers interesting opportunities for conceiving a programmable setup, whose operation is controlled by an external parameter (the magnetic field) without need to alter voltage and thermal biases applied to the system. Our results, generic within the framework of linear response, are illustrated by means of a three-terminal electronic interferometer model.

In **Chapter 5** we investigate the consequences, on thermoelectric performance, of Coulomb interaction in multi-levels quantum dots. In particular we consider the sequential tunneling regime (where the levels' broadening is negligible) for Coulomb blockaded quantum dots. We work out analytical expressions for the currents and the Onsager coefficients in the three-terminal case. In the two-terminal limit we recover all the known results for the electrical conductance and the thermopower, and moreover study the efficiency and the efficiency at maximum power. For a three-terminal case we have shown that a third terminal can be useful to improve the thermoelectric performance of a system with respect to the two-terminal systems even for the strongly interacting case. Interestingly, oscillations of the efficiency at maximum power, that reflect the oscillations of the thermopower, arise from the interplay between the charging energy and the quantization of the levels.

Chapter 1

Irreversible Thermodynamics

The thermostatic theory of thermodynamics provides a useful characterization of the equilibrium states. However, we are very often much more interested in the processes rather than in the states. Examples of this fact can be found everywhere in science, from biology to chemistry and physics: the process that the cells, the chemical reactions and the physical systems undergo to reach equilibrium states is much more fascinating and intriguing to study than the equilibrium state itself. Thermostatics does provide some approximated method to infer information about the processes, but none of this methods confronts with the central problem of the rates of real physical processes. The extension of thermodynamics to deal with the rates of physical processes is called *irreversible thermodynamics*. This theory is based on the postulates of equilibrium thermostatics [Callen1985], with the additional postulate of time reversal symmetry of physical laws.

> *The laws of physics remains unchanged if the time t is replaced by $-t$ and simultaneously the magnetic field B is replaced by $-B$.*

The irreversible thermodynamic theory started with a very brilliant and pioneering paper by Lars Onsager [Onsager1931] (almost ignored by the scientific community for over 20 years), where he formulated his Onsager reciprocity theorem.

1.1 Fluxes and generalized forces

Before starting the discussion on the Onsager theorem, we have to define the quantities the are necessary to describe irreversible processes. We need essentially two parameters: one to describe what causes the process (we will call it "generalized force" or "affinity"), and one to describe the response in the system due to this force (we will call it "flux"). Let us consider a one dimensional system in which energy and matter can flow, driven by the appropriate forces. We choose our flux to be the (only) component of the current density vector $\mathbf{J}$. Therefore associated with the energy U we will have the flux J^u (we drop the vector notation, that would be useful only in the three dimensional generalization of this example)[1].

1.1.1 Entropy production rate

Let X^k be an extensive parameter of a generic system of interest. We characterize the response to the applied force by the rate of change of the extensive parameter X^k. Then we define the flux J^k as

$$J^k \equiv \frac{dX^k}{dt}. \tag{1.1}$$

In the same way we can define the force $\mathcal{F}^k$ as the derivative of the entropy with respect to the extensive parameter X^k (the entropy is, in general, a function of all the affinities $\mathcal{S}(X^0, X^1, \dots)$)

$$\mathcal{F}^k \equiv \frac{\partial \mathcal{S}}{\partial X^k}, \tag{1.2}$$

the system is in equilibrium if $\mathcal{F}^k$ is zero, while an irreversible process is taking place whenever $\mathcal{F}^k$ is different from zero. We can notice that the flux vanishes when the affinity vanishes, while a non zero affinity leads to a non zero flux.

The rate of an irreversible process is characterized by the relations between fluxes and affinities. Now in order to identify the correct forces it is convenient to write the entropy production rate. The rate of entropy

[1] By definition the J^u is the amount of energy that flows in a unit area in the unit time and the sign gives the direction of the energy flow.

production is found by differentiating $\mathcal{S}$ with respect to the time

$$\frac{d\mathcal{S}}{dt} = \sum_k \frac{\partial \mathcal{S}}{\partial X^k} \frac{dX^k}{dt}, \tag{1.3}$$

that can equivalently be rewritten using Eqs. (1.1)-(1.2) in the more compact form

$$\dot{\mathcal{S}} = \sum_k \mathcal{F}^k J^k. \tag{1.4}$$

This can also be taken as the definition of the entropy current density J^s. Now in order to define the entropy in a non-equilibrium system we have to assume that the functional dependence of $\mathcal{S}(X_1, X_2, \dots)$ on the local extensive parameter is the same as in the equilibrium case in any infinitesimal region of the system. Then we have that the infinitesimal variation of the entropy can be written as

$$d\mathcal{S} = \sum_k \mathcal{F}^k dX^k, \tag{1.5}$$

which implies that the entropy current density is defined as

$$J^s = \sum_k \mathcal{F}^k J^k. \tag{1.6}$$

We are now ready to define the entropy production rate, that is given by the entropy leaving a certain region plus the rate of increase of entropy in that region. In formulas we have

$$\dot{\mathcal{S}} = \frac{\partial \mathcal{S}}{\partial t} + \nabla \cdot J^s, \tag{1.7}$$

if the energy and the particle's number is conserved (we will always assume that), we can write the continuity equations for those quantities

$$0 = \frac{\partial X^k}{\partial t} + \nabla \cdot J^k. \tag{1.8}$$

Now we analyze in detail the two right-hand side terms in Eq. (1.7). The first one can be obtained from Eq. (1.5)

$$\frac{\partial \mathcal{S}}{\partial t} = \sum_k \mathcal{F}^k \frac{\partial X^k}{\partial t}. \tag{1.9}$$

The second member can be calculated by taking the divergence of Eq. (1.6)

$$\nabla \cdot J^s = \nabla \cdot \sum_k \mathcal{F}^k J^k = \sum_k \nabla \mathcal{F}^k \cdot J^k + \sum_k \mathcal{F}^k \nabla \cdot J^k. \tag{1.10}$$

With this substitutions the entropy production rate equation (1.7) becomes

$$\dot{\mathcal{S}} = \sum_k \mathcal{F}^k \frac{\partial x^k}{\partial t} + \sum_k \nabla \mathcal{F}^k \cdot J^k + \sum_k \mathcal{F}^k \nabla \cdot J^k = \sum_k \nabla \mathcal{F}^k \cdot J^k, \tag{1.11}$$

where the first and the third terms cancel due to the continuity equation (1.8). Thus the affinity is defined as the gradient of the entropy representation intensive parameters. If now J^k represent the energy current density J^u, the associated affinity would be $\mathcal{F}^u = \nabla(1/T)$. Analogously is J^k denotes the particle current density J^n, the associated affinity would be $\mathcal{F}^\mu = -\nabla(\mu/T)$.

1.2 Linear systems

There is a wide class of systems in which the fluxes do not depend on the affinities at a given instant. Such systems are known (for historical reasons) as "purely resistive" systems (in the electrical case a resistor is a purely resistive system, while a circuit with a capacitor or an inductance is not purely resistive). Although it may seem a strong condition, there are many systems (other than the electrical systems) that can be ascribed to this class. If each flux depends only on the instantaneous local affinities we can write

$$J^k = J^k(\mathcal{F}^1, \mathcal{F}^2, \dots). \tag{1.12}$$

This means that the local particle current density depends on the gradient of the inverse temperature$1/T$, on the gradients of μ/T and on so forth. Notice that this does not imply that each flux depends only on its own affinity, but rather that they depend on all the affinities. This is a crucial point that will give rise to the most interesting phenomena. Now, keeping in mind that the fluxes J^k have to vanish if the affinities vanish, we can expand J^k in series of the affinities

$$J^k = \sum_j L_{jk} \mathcal{F}^j + \frac{1}{2!} \sum_i \sum_j L_{ijk} \mathcal{F}^i \mathcal{F}^j + \dots \tag{1.13}$$

The expansion coefficients are defined by

$$L_{jk} = \frac{\partial J^k}{\partial \mathcal{F}^j}. \tag{1.14}$$

The coefficients $L_{jk} = L_{jk}(\mathbf{B})$ are called *Onsager kinetic coefficients* and depend on an external magnetic field. With all these ingredients we can now state the Onsager theorem:

> *The value of the kinetic coefficients L_{jk} measured in an external magnetic field $\mathbf{B}$ is identical to the value of L_{kj} measured in the reversed magnetic field $-\mathbf{B}$.*

$$L_{jk}(\mathbf{B}) = L_{kj}(-\mathbf{B}). \tag{1.15}$$

This means that there is a symmetry between the linear effect of the $k-$th affinity on the $j-$th flux when these effects are measured in reversed magnetic field. The Onsager theorem is a very powerful tool to study linear systems, where the affinities are so small that the second order kinetic coefficients L_{ijk} could be neglected

$$J^k = \sum_j L_{jk}\mathcal{F}^j. \tag{1.16}$$

Although the class of linear processes is sufficiently common, it is by no means all inclusive and we want to stress that the Onsager theorem is not limited to it.

1.3 The Onsager matrix

We now want to specify the general framework developed in Sections 1.1 and 1.2 to the case of a two-terminal system that can exchange both particles and energy, see Fig. 1.1. The simultaneous presence of electric and thermal currents in a system gives rise to the thermoelectric effects, where the thermal gradient produces an electrical current or an electric current produces an heat current.

We start again with the differential of the local entropy density

$$d\mathcal{S} = \frac{1}{T}du - \frac{\mu}{T}dn, \tag{1.17}$$

where u is the local energy density, μ the chemical potential of the electrons and n the number of electrons per unit volume. The relation between the currents is

$$J^s = \frac{1}{T}J^u - \frac{\mu}{T}J^n, \tag{1.18}$$

J^s, J^u and J^n are the entropy, energy and particle current densities. The entropy production rate than reads

$$\dot{\mathcal{S}} = \nabla\frac{1}{T}J^u - \nabla\frac{\mu}{T}J^n. \tag{1.19}$$

If J^n and J^u are the fluxes then the associated affinities are $\nabla(1/T)$ and $\nabla(\mu/T)$. Eq. (1.16) becomes

$$J^n = L'_{11}\nabla\frac{\mu}{T} + L'_{12}\nabla\frac{1}{T} \tag{1.20}$$

$$J^u = L'_{21}\nabla\frac{\mu}{T} + L'_{22}\nabla\frac{1}{T}. \tag{1.21}$$

Even if the energy current density is easy to compute it is often much more useful to use the heat current density. It is possible to derive it from second low of thermodynamics $dQ = TdS$:

$$J^h = TJ^s = J^u - \mu J^n. \tag{1.22}$$

By substituting Eq. (1.22) into Eq. (1.19) we obtain

$$\begin{pmatrix} J^n \\ J^h \end{pmatrix} = \begin{pmatrix} L_{11} & L_{12} \\ L_{21} & L_{22} \end{pmatrix} \begin{pmatrix} X^\mu \\ X^T \end{pmatrix}, \tag{1.23}$$

where we have defined the affinities $X^\mu = \Delta\mu/T$ and $X^T = \Delta T/T^2$. The matrix of the kinetic coefficients L_{ij} is called *Onsager matrix* and will be indicated hereafter with L. The positivity of the entropy production rate (1.19) can be rewritten in terms of the Onsager coefficients as

$$\dot{\mathcal{S}} = J^n X^\mu + J^h X^T \geq 0. \tag{1.24}$$

This implies that the Onsager matrix must be positive definite, which means that the coefficients have to fulfill the following conditions:

$$L_{11} \geq 0 \tag{1.25}$$

$$L_{22} \geq 0 \tag{1.26}$$

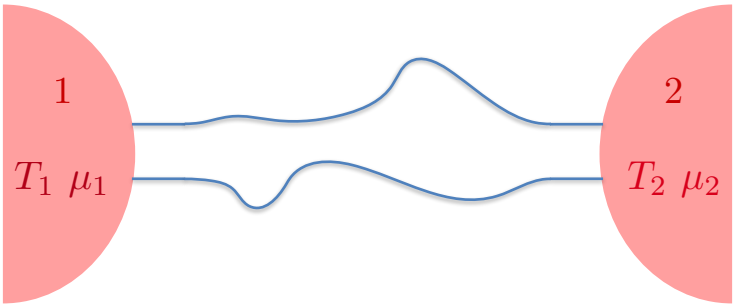

Figure 1.1 – Schematic representation of a two terminal system. A central scattering region is connected to a different reservoirs, each of them has a defined temperature T_i and chemical potential μ_i $i = (1, 2)$, and is able to exchange heat and particles with the system

$$L_{11}L_{22} \geq \frac{1}{4}(L_{12} + L_{21})^2 \tag{1.27}$$

In the next paragraphs we will describe the transport properties of a two-terminal systems as in Fig. 1.1 in terms of the Onsager coefficients, making the link between the transport coefficients (conductances and thermopowers) and the thermodynamic properties (power and efficiency) with the Onsager matrix's coefficients L_{ij}.

1.3.1 Electrical and thermal conductance

Consider a systems composed by a generic region connected to two fermionic reservoirs that can exchange both particles and heat as in Fig. 1.1. Each of the reservoirs is described by a chemical potential μ_i and a temperature T_i. If there are no magnetic fields the currents are give by Eq. (1.23) with the additional constraint $L_{21} = L_{12}$. The electrical conductance is defined as the electric current density per unit potential gradient in an isothermal system, if the gradient is small the current is proportional to it

$$G = \left(\frac{e^2 J^n}{\Delta\mu}\right)_{\Delta T=0} = \frac{e^2}{T} L_{11}. \tag{1.28}$$

Similarly the thermal conductance is defined as the heat current density per unit temperature gradient at zero electric current. Again if the gradient

is small the current is proportional to it

$$K = \left(\frac{J^h}{\Delta T}\right)_{J^n=0} = \frac{1}{T^2}\frac{L_{11}L_{22} - L_{12}L_{21}}{L_{11}}. \tag{1.29}$$

Notice that the bounds on the Onsager coefficients imposed by the positivity of the entropy production rate (1.25) is sufficient to guarantee the positivity of the electrical the thermal conductances.

1.3.2 Seebeck effect

The Seebeck effect refers to the development of a voltage difference in an open circuit (with zero electric current) in response to a temperature gradient. If the temperature gradient is small, the voltage produced is proportional to it and the proportionality constant is the Seebeck coefficient -or thermopower- S. Then using Eq. (1.23) we can define the thermopower as

$$S = -\frac{\Delta\mu}{e\Delta T} = \frac{1}{eT}\frac{L_{12}}{L_{11}}. \tag{1.30}$$

The sign of the thermopower is not fixed by the positivity of the entropy production rate (1.25), it can be showed that the sign depend on the dominant type of carriers [Ashcroft1976].

1.3.3 Peltier effect

In 1834, J. C. A. Peltier observed an effect "equal and opposite" to the Seebeck effect [Peltier1834]: in an isothermal junction, the flow of an electric current causes a modification in the heat flow. In particular if the electric current is small the heat flux at the junction is proportional to it. The coefficient of proportionality is the Peltier coefficient Π. Then again, using Eq. (1.23) we obtain

$$\Pi = \left(\frac{J^h}{eJ^n}\right)_{\Delta T=0} = \frac{1}{e}\frac{L_{21}}{L_{11}}. \tag{1.31}$$

The Peltier coefficient represent how much heat is carried per unit charge. It is related to the Seebeck coefficient by the Onsager reciprocity relations: $\Pi(\mathbf{B}) = TS(-\mathbf{B})$.

1.3.4 Power and efficiency

In this context, one can define the efficiency of a thermal machine as the ratio between the work W extracted from the engine when it absorbs heat $\mathcal{Q}$. By convention we assume positive the heat flowing into the system, hence in the steady state the definition of the efficiency is equivalent to

$$\eta = \frac{\dot{W}}{\dot{\mathcal{Q}}} = \frac{\sum_i J_i^h}{\sum_i^+ J_i^h} = \frac{-TX^\mu J_i^n}{J^h} = -TX^\mu \frac{L_{11}X^\mu + L_{12}X^T}{L_{21}X^\mu + L_{22}X^T} \tag{1.32}$$

where the dot indicates a derivative with respect to time and the apex $+$ in the denominator means that the sum is restricted to positive heat currents. The time derivative of the work $\dot{W}$ is the power and must be positive for the machine to work as a heat to work converter, otherwise we are dealing with a refrigerator and the definition of η is no longer valid. The maximum of Eq. (1.32) over X^μ, for fixed X^T, is achieved for

$$X^\mu = \frac{L_{22}}{L_{11}} \left(-1 \sqrt{\frac{\det L}{L_{11}L_{22}}} \right) X^T \tag{1.33}$$

which leads to

$$\eta_{\max} = \eta_C \frac{\sqrt{ZT+1}-1}{\sqrt{ZT+1}+1}, \tag{1.34}$$

where we introduce the following notation: $\eta_C = \Delta T/T$ is the Carnot efficiency, $ZT = TGS^2/K$ is the (a-dimensional) figure of merit. The Carnot efficiency is a bound for the efficiency in a cycle between two reservoirs and is obtained for a quasi-static transformation which requires infinite time and therefore the extracted power, in this limit, reduces to zero. The figure of merit ZT is bounded by the positivity of the entropy production to be positive. Notice that the Carnot limit is reached when $ZT \to \infty$.

Other interesting quantities are the maximum power $\dot{W}_{\max}$ and the efficiency at maximum power $\eta(\dot{W}_{\max})$. The maximum power is obtained for $X^\mu = -\frac{L12}{2L_{11}} X^T$ yielding

$$\dot{W}_{\max} = \frac{\eta_C}{4} \frac{L_{12}^2}{L_{11}} X^T \qquad \text{and} \qquad \eta(\dot{W}_{\max}) = \frac{\eta_C}{2} \frac{ZT}{2+ZT}. \tag{1.35}$$

Using the definitions of the transport coefficients (1.28)-(1.31) one can write $\dot{W}_{\max} = 1/4GS^2\Delta T^2$ and notice that the power is controlled by the

term $Q = GS^2$ which is therefore called "power factor". The bound of the efficiency at maximum power is the Curzon-Ahlborn efficiency [Curzon1975], within the linear response this limit is equal to $\eta_C/2$.

Let us specify $\eta_{\max}$ and $\eta(\dot{W}_{\max})$ to the case when time-reversal symmetry does not hold which means to introduce an asymmetry parameter x and a generalized figure of merit y

$$x = \frac{L_{12}}{L_{21}}, \qquad y = \frac{L_{12}L_{21}}{\det L}. \tag{1.36}$$

The maximum efficiency and the efficiency at maximum power now read

$$\eta_{\max} = \eta_C x \frac{\sqrt{y+1}-1}{\sqrt{y+1}+1}, \qquad \eta(\dot{W}_{\max}) = \frac{\eta_C}{2}\frac{xy}{y+2}. \tag{1.37}$$

In the next section we will see a method to calculate the Onsager kinetic coefficients for non interacting condensed matter systems.

1.4 Non-interacting systems

An exact calculation of the Onsager coefficients is possible for non interacting systems by means of the Landauer-Büttiker approach to quantum transport. Quantum transport concerns the study of how charged particles flow through a conductor whose size is comparable to or smaller than the wavelength of such particles. Under such conditions and at low temperatures the particles do not behave like classical "balls" but their wave-like behavior must be taken into account, so that quantum-mechanical effects become relevant.

In this coherent regime, if the particles do not lose energy inside the conductor (elastic processes), quantum transport can be related to scattering events in such conductor. In particular, Landauer and Büttiker [Landauer1957, Büttiker1986] demonstrated that the electrical currents can be expressed in terms of scattering probabilities, which means that knowing the scattering properties of a system implies understanding its transport properties. In this Section we will derive the currents in the Landauer-Büttiker approach for the most generic case of a multi-terminal system with a superconducting lead. The case with no superconductors or with just two-terminal are obtained as simple limits of the expressions that we will derive.

1.4.1 Landauer-Büttiker formalism

Let us consider a mesoscopic system composed of a conductor to which $n > 1$ leads are attached. Each lead is in equilibrium with a fermionic reservoir to which a Fermi distribution function is associated, so that a lead is characterized by a temperature and a chemical potential. At energy E the i-th lead has $N_i(E)$ open transverse channels. We allow the possibility to have superconductivity in the system and for simplicity we describe it using the Bogoliubov-de Gennes formalism which doubles the degrees of freedom by introducing "hole" states and by construction is particle-hole symmetric, i.e. the Hamiltonian H_{BdG} of the system is such that $\{H_{BdG}, \mathcal{C}\} = 0$, where $\mathcal{C}$ is the charge-conjugation operator and the curly parentheses stand for the anti-commutator. A hole state is the charge-conjugate of an electronic state, e.g. if the operator $c_{k,\sigma}$ destroys an electron of momentum k and spin σ, the operator $\mathcal{C}c_{k,\sigma}\mathcal{C} = c^\dagger_{k,\sigma}$ destroys a hole of momentum k and spin σ. For completeness we mention that $\mathcal{C}$ is a anti-unitary operator hence besides exchanging creation and annihilation operators one must take the complex conjugate of the numeric coefficients[2].

$$f_j^-(E) = 1 - f_j^+(-E), \tag{1.38}$$

where f_j^- is the distribution function for a hole in lead j and f_j^+ is the analogous for electrons. We can then write a generalized expression for the Fermi distribution function as follows

$$f_j^\alpha(E) = \frac{1}{1 + \exp\left[\beta_j(E - \alpha(\mu_j - \mu_s))\right]}, \tag{1.39}$$

where μ_j is the chemical potential of the $j-$th lead, μ_s is the chemical potential of the superconductors[3] which we take as a reference for the energies, $\beta_j = (k_B T_j)^{-1}$ is the inverse temperature of the j-th lead and α is equal to $+$ for electrons and - for holes. Assuming coherent transport in the conductor, one can express the charge and energy currents flowing through the normal leads in terms of scattering probabilities using the Landauer-Büttiker formalism generalized to include superconductivity

[2]The particle-hole symmetry implies that the occupation of a hole state is the complementary to the occupation of an electronic state with opposite energy.

[3]We assume every superconducting part in the system to have the same Fermi energy.

$$
\begin{aligned}
J_i^c &= \sum_j^n \Big(-\frac{e}{h}\Big) \sum_{\alpha\sigma\beta\sigma'} \alpha \int_0^{+\infty} dE\, P_{ij}^{\alpha\sigma\beta\sigma'}(E) f_j^{\beta}(E) \\
&+ \frac{e}{h} \sum_{\alpha\sigma} \alpha \int_0^{+\infty} dE\, N_i^{\alpha\sigma}(E) f_i^{\alpha}(E), \qquad (1.40) \\
J_i^u &= \sum_j^n \Big(-\frac{1}{h}\Big) \sum_{\alpha\sigma\beta\sigma'} \int_0^{+\infty} dE\, (E+\alpha\mu_s) P_{ij}^{\alpha\sigma\beta\sigma'}(E) f_j^{\beta}(E) \\
&+ \frac{1}{h} \sum_{\alpha\sigma} \int_0^{+\infty} dE\, (E+\alpha\mu_s) N_i^{\alpha\sigma}(E) f_i^{\alpha}(E), \qquad (1.41)
\end{aligned}
$$

where J_i^c is the charge current in the i-th lead, J_i^u is the energy current in the i-th lead, e is the electron charge, h is the Planck constant and $N_i^{\alpha\sigma}$ is the number of open channels at energy E for particles of type α and spin σ. In Eq. (1.40) $P_{ij}^{\alpha\sigma\beta\sigma'}(E)$ is the probability for a particle of type β, spin σ' and energy E incoming from lead j to be elastically scattered as a particle of type α and spin σ into the i-th lead. To avoid double-counting that would have been introduced by the BdG formalism, the integrals over the energies run from 0 to $+\infty$ instead of starting from $-\infty$. Here zero energy corresponds to the Fermi energy of the superconductors. Due to particle-hole symmetry the scattering matrix S of the system satisfies the following relation

$$
S_{(i,a),(j,b)}^{\alpha\sigma,\beta\sigma'}(E) = \alpha\beta \big[S_{(i,a),(j,b)}^{-\alpha\sigma,-\beta\sigma'}(-E)\big]^*, \qquad (1.42)
$$

where a and b are the transverse channels in lead i and j respectively. Since the probability of scattering from lead i to lead j is defined as $P_{ij}^{\alpha\sigma\beta\sigma'}(E) = \sum_{a,b} |S_{(i,a),(j,b)}^{\alpha\sigma,\beta\sigma'}(E)|^2$, Eq. (1.42) implies

$$
P_{ij}^{\alpha\sigma,\beta\sigma'}(E) = P_{ij}^{-\alpha\sigma,-\beta\sigma'}(-E). \qquad (1.43)
$$

The unitarity of the scattering matrix yields the following sum rules:

$$
\sum_{j,\sigma',\beta} P_{ij}^{\alpha\sigma,\beta\sigma'}(E) = N_i^{\alpha,\sigma}, \qquad \sum_{i,\sigma,\alpha} P_{ij}^{\alpha\sigma,\beta\sigma'}(E) = N_j^{\beta,\sigma'}. \qquad (1.44)
$$

The expressions of Eq. (1.40) can be simplified by substituting Eqs. (1.38), (1.43) and (1.44) resulting in

$$J_i^c = \frac{e}{h}\sum_{j\sigma\beta\sigma'}\int_{-\infty}^{+\infty} dE\left[N_i^{+\sigma}(E)\delta_{ij}\delta_{\sigma\sigma'}\delta_{\beta+} - P_{ij}^{+\sigma\beta\sigma'}(E)\right]f_j^{\beta}(E),$$
$$J_i^u = \frac{1}{h}\sum_{j\sigma\beta\sigma'}\int_{-\infty}^{+\infty} dE\,(E+\mu_s)\left[N_i^{+\sigma}(E)\delta_{ij}\delta_{\sigma\sigma'}\delta_{\beta+} - P_{ij}^{+\sigma\beta\sigma'}(E)\right]f_j^{\beta}(E). \tag{1.45}$$

Once the charge and energy currents are determined in the normal leads, the sum of the currents in the superconducting leads $J_S^c = \sum_j^{Sc} J_j^c$ and $J_S^u = \sum_j^S J_j^u$ can be calculated exploiting Kirchhoff's sum rules $\sum_i J_i^c = 0$ and $\sum_i J_i^u = 0$, which are a consequence of charge and energy conservation. From the first law of thermodynamics one can also define a heat current J_i^h in the i-th lead as

$$J_i^h = J_i^u - \frac{\mu_i}{e}J_i^c. \tag{1.46}$$

Let us remark that in a general case there is no sum rule for the heat currents. However, one can notice that in the superconducting leads the heat current is $J_i^h = J_i^u - \frac{\mu_s}{e}J_i^c$, hence the sum of the heat currents over the superconducting leads is $\sum_j^S J_j^h = J_S^h = J_S^c - \frac{\mu_s}{e}J_S^u$ which can be determined by Kirchhoff's sum rules on charge and energy currents.

1.4.2 Linear response

Each lead (say lead j) is characterized by a temperature T_j and a voltage V_j, where V_j is such that $eV_j = \mu_j$. Assuming a reference temperature T and a reference voltage V, each of the previous quantity can be written as to make explicit the difference from the reference values, e.g. $T_j = T + \Delta T_j$ and $V_j = V + \Delta V_j$, where $\Delta T_j = T_j - T$ and $\Delta\mu_j = \mu_j - \mu$. Here we assume the superconducting voltage $\mu = \mu_s$ as reference. Assuming small temperature- and voltage-biases, we can expand the Fermi distribution function of Eq. (1.39) at first order in such quantities

$$f_j^{\alpha}(E) \simeq f(E) + \left.\frac{\partial f_j^{\alpha}}{\partial\Delta T_j}\right|_{(E,T)}\Delta T_j + \left.\frac{\partial f_j^{\alpha}}{\partial\Delta\mu_j}\right|_{(E,T)}\Delta\mu_j, \tag{1.47}$$
$$\left.\frac{\partial f_j^{\alpha}}{\partial\Delta T_j}\right|_{(E,T)} = -\frac{E}{T}\frac{\partial f}{\partial E}, \qquad \left.\frac{\partial f_j^{\alpha}}{\partial\Delta\mu_j}\right|_{(E,T)} = -\alpha e\frac{\partial f}{\partial E},$$

where we defined $f(E) = \frac{1}{1+e^{\frac{E}{k_B T}}}$. Since the scattering matrix is independent of the biases, we can use Eq. (1.47) to linearize the currents of Eqs. (1.45) and (1.46) as follows

$$\begin{aligned} J_i^c &= \sum_j \mathcal{G}_{ij}\Delta\mu_j + \sum_j \mathcal{D}_{ij}\Delta T_j, \\ J_i^h &= \sum_j \mathcal{M}_{ij}\Delta\mu_j + \sum_j \mathcal{K}_{ij}\Delta T_j, \end{aligned} \tag{1.48}$$

We divided the coefficients per types: $\mathcal{G}_{ij}$ are the coefficients that relate the electrical currents with the chemical potential gradients, $\mathcal{D}_{ij}$ are the coefficients that relate the electric to the temperature gradients, $\mathcal{M}_{ij}$ are the coefficients that relate the heat currents to the chemical potential gradients and $\mathcal{K}_{ij}$ are the coefficients that relate the heat currents with the temperature gradients. Those quantities are defined as (we can always put $\mu = 0$)

$$\begin{aligned} \mathcal{G}_{ij} &= \frac{e^2}{h}\sum_{\sigma\sigma'}\int_{-\infty}^{+\infty} dE\Big[N_i^{+\sigma}(E)\delta_{ij}\delta_{\sigma\sigma'} - P_{ij}^{+\sigma+\sigma'}(E) + P_{ij}^{+\sigma-\sigma'}(E)\Big]\Big(-\frac{\partial f}{\partial E}\Big) \\ \mathcal{D}_{ij} &= \frac{e}{h}\sum_{\sigma\sigma'}\int_{-\infty}^{+\infty} dE\,\frac{E}{T}\Big[N_i^{+\sigma}(E)\delta_{ij}\delta_{\sigma\sigma'} - P_{ij}^{+\sigma+\sigma'}(E) - P_{ij}^{+\sigma-\sigma'}(E)\Big]\Big(-\frac{\partial f}{\partial E}\Big), \\ \mathcal{M}_{ij} &= \frac{e}{h}\sum_{\sigma\sigma'}\int_{-\infty}^{+\infty} dE\,E\Big[N_i^{+\sigma}(E)\delta_{ij}\delta_{\sigma\sigma'} - P_{ij}^{+\sigma+\sigma'}(E) + P_{ij}^{+\sigma-\sigma'}(E)\Big]\Big(-\frac{\partial f}{\partial E}\Big), \\ \mathcal{K}_{ij} &= \frac{1}{h}\sum_{\sigma\sigma'}\int_{-\infty}^{+\infty} dE\,\frac{E^2}{T}\Big[N_i^{+\sigma}(E)\delta_{ij}\delta_{\sigma\sigma'} - P_{ij}^{+\sigma+\sigma'}(E) - P_{ij}^{+\sigma-\sigma'}(E)\Big]\Big(-\frac{\partial f}{\partial E}\Big). \end{aligned} \tag{1.49}$$

Let us notice that from the unitarity of the scattering matrix it follows that the diagonal coefficients are always positive or zero. One could also redefine the Onsager matrix by multiplying the even columns of the matrix by the reference temperature T and dividing the temperature biases by T, i.e. by substituting $\mathcal{D}_{ij}$ with $T\mathcal{D}_{ij}$, $\mathcal{K}_{ij}$ with $T\mathcal{K}_{ij}$ and ΔT_i with $\frac{\Delta T_i}{T}$. It can be demonstrated that for a system with time-reversal symmetry such a matrix is symmetrical.

For a two terminal setup, like the one in Fig. 1.1 (with no superconducting leads and spin degeneracy) the Onsager coefficients defined in Eq.(1.49) reduce to

$$L_{11} = \mathcal{G}_{12} = \frac{2e^2}{h}\int_{-\infty}^{\infty} dE\,P_{12}(E)\left(-\frac{\partial f}{\partial E}\right), \tag{1.50}$$

$$L_{12} = T\mathcal{D}_{12} = \frac{2e}{h}\int_{-\infty}^{\infty} dE\,(E-\mu)\,P_{12}(E)\left(-\frac{\partial f}{\partial E}\right), \tag{1.51}$$

$$L_{21} = \mathcal{M}_{12} = \frac{2e}{h}\int_{-\infty}^{\infty} dE\ (E-\mu)\, P_{12}(E)\left(-\frac{\partial f}{\partial E}\right), \tag{1.52}$$

$$L_{22} = T\mathcal{K}_{12} = \frac{2}{h}\int_{-\infty}^{\infty} dE\ (E-\mu)^2\, P_{12}(E)\left(-\frac{\partial f}{\partial E}\right). \tag{1.53}$$

Notice that now the lead indices are fixed to $i = 1$ and $j = 2$, since we are interested in transport from lead 1 to lead 2 and, in fact, the only thing that matters is the transmission probability $P_{12}(E)$. If spin degeneracy holds then $P_{ij}^{+\sigma-\sigma'} = 0$ and $P_{ij}^{\sigma,\sigma'} = 2P_{ij}$.

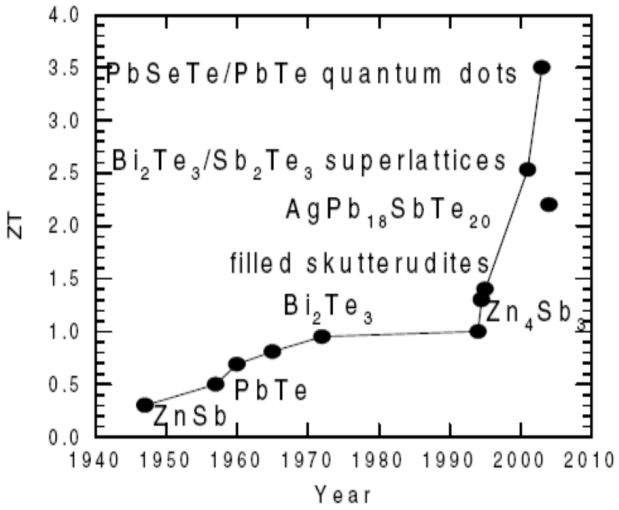

Figure 1.2 – The time evolution of the best figure of merit ZT. It is possible to see how, after the initial positive trend from 1940 to 1960 (with the discovery of theBi_2Te_3) there has been a stagnation for almost 30 years with the advent of the low dimensional systems. In the last decades a large value of ZT (greater than 1) has been observed in filled skutterudites [Fleurial1996, Morelli1995, Vineis2010], Bi_2Te_3/Sb_2Te_3 superlattice and PbSeTe/PbTe quantum dot superlattices [Harman2002]. Figure from Ref. [Zheng2008].

1.5 Quantum thermal machines: state of the art

In the last seventy years many progresses have been made in the search for the best figure of merit ZT. Figure 1.2 shows the improvement achieved for ZT in time. It is interesting to notice how, after an initial increase in the best figure of merit (from 1940 to 1960) with the discovery of the excellent thermoelectric properties of Bi_2Te_3, no further improvements have been made for almost 30 years after. Only in the last 90s, with the advent of the skutterudites materials[4] there has been an increase in the best ZT [Fleurial1996, Morelli1995, Vineis2010].

However, no substantial progresses have been made until the discovery of the large thermoelectric effects predicted in nanostructures [Hicks1993]. A very important point in this work was the observation that low-dimensional systems should result in materials with much better thermoelectric conversion than the bulk ones. Those theoretical predictions have been observed experimentally on Bi_2Te_3 superlattices [Venkatasubramanian2001] and on PbSeTe/PbTe quantum dot superlattices [Harman2002], resulting in a $ZT \geq 3$.

This is why in the last twenty years there has been a growing interest in the Condensed Matter community, which devoted a great amount of effort in the understanding of the basic mechanism of the thermoelectric effects and proposed many implementations in solid state devices of quantum thermal machines. Many review papers have been written trying to interconnect many different fields as irreversible thermodynamics, nonlinear dynamical systems, statistical mechanics, material science and condensed matter physics [Mahan1997, Majumdar2004, Dresselhaus2007, Snyder2008, Dubi2011, Shakouri2011, Benenti2013].

It is worth noticing that most of the works in this field deal with two-terminal systems, or at most two terminals and a probe lead, i.e. a lead in which neither particles nor heat can flow. For those systems, interesting bounds on the efficiency and the efficiency at maximum power have been derived, and as a consequence, the experiments in this field moved towards the design of quantum thermal machines whose efficiency and power saturate such bounds [Saito2011, Benenti2011, Horvat2012, Balachandran2013, Brandner2013a, Brandner2013b, Bosisio2014, Bosisio2015a].

Only recently the multi-terminal setup started to be investigated. The main problem in treating these systems is that as soon as the dimension of the Onsager matrix grows the expression for the power and the efficiency become really complicated. A first step has been made by considering a third bosonic lead, i.e. a lead that can exchange only heat with the system, thus providing the energy necessary for the electron transport [Entin-Wohlman2010, Entin-Wohlman2012, Jiang2012, Jiang2013, Sánchez2011b, Sánchez2011a, Sothmann2012a, Sothmann2013].

[4] Skutterudite is a cobalt arsenide mineral that has variable amounts of nickel and iron substituting for cobalt with a general formula: $(Co,Ni,Fe)As_3$.

In the same spirit also setups with a superconducting lead have been investigated, since a superconductor is a poor heat conductor and can exchange only charge current with the system (this is true providing that the temperatures and voltages are much smaller than the superconducting gap, which means, that there are no quasi-particles excitations) [Claughton1996, Eom1998, Virtanen2004a, Parsons2003, Virtanen2004b, Jiang2005, Titov2008, Marciani2014, Machon2013, Jacquod2010, Hou2013, Ozaeta2014, Engl2011, Leijnse2014, Lopez2014].

A first attempt to study the multi-terminal problem and to exploit different implementations of such devices in solid state systems has been made in the recent years [Jacquet2009, Bedkihal2013, Jordan2013, Kosloff2014, Sothmann2014, Entin-Wohlman2015, Jiang2014a, Jiang2014b], but still a full characterization of the multi-terminal setup is lacking, and no one managed to achieve a full decoupling of the heat and charge currents.

Chapter 2

Thermoelectric Efficiency of Multi-Terminal Quantum Thermal Machines

Thermoelectric transport has been mostly investigated in two-terminal systems. It just begun to be investigated in multi-terminal systems, since these more complex devices may offer many additional advantages. However in those works the third terminal was treated in a special way and could exchange only heat [Entin-Wohlman2010, Sánchez2011b, Sánchez2011a, Entin-Wohlman2012, Sothmann2012a, Sothmann2012b, Jiang2012, Jiang2013, Sothmann2013] or only particles [Benenti2011, Saito2011, Horvat2012, Brandner2013a, Brandner2013b, Balachandran2013, Bosisio2014, Bosisio2015a]. A full characterization of these systems is still lacking and motivates us to tackle this problem. A genuine multi-terminal device offers the possibility of having a separate control about the heat and particle flows, and this could enhance the thermoelectric efficiency. Here we focus on the simplest instance of three reservoirs, treated on the same footing, which can exchange both charge and energy current with the system. A sketch of the thermal machine is shown in Fig. 2.1, where a generic nanostructure, described as a scattering region, is connected to three terminals kept at different temperatures and chemical potentials. Our aim is to provide a general treatment of the linear response thermoelectric transport for this case, and for this purpose we will discuss local and non-local transport coefficients. Note that non-local transport coefficients naturally arise in a multi-terminal setup, since they connect temperature or voltage biases applied between two terminals to heat and charge transport through the remaining terminals. We will then show that the third terminal could be exploited to improve thermoelectric performance with respect to the two-terminal case. We will focus our investigations

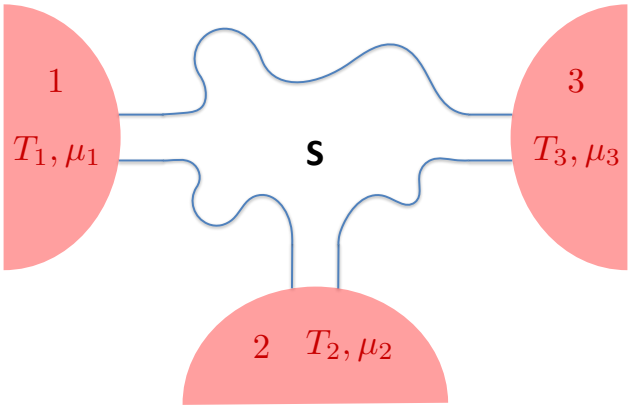

Figure 2.1 – Three-terminal thermal machine. A scattering region is connected to 3 different fermionic reservoirs, each of these is able to exchange heat and particles with the system. Reservoir 3 is taken as the reference for measuring temperature and energy: $T_3 \equiv T$; $\mu_3 = \mu$. The reservoirs 1 and 2 have small variations in temperature and chemical potential: $(T_i, \mu_i) = (T + \Delta T_i, \mu + \Delta\mu_i)$, $i \in (1, 2)$. With **S** we denote a generic coherent scattering region.

on the efficiency at maximum power [Curzon1975, Broeck2005, Schmiedl2008, Esposito2009, Esposito2010, Nakpathomkun2010, Apertet2012], i.e. a heat engine operating under conditions where the output power is maximized. Such quantity, central in the field of finite-time thermodynamics [Andresen2011], is of great fundamental and practical relevance to understand which systems offer the best trade-off between thermoelectric power and efficiency.

This chapter is organized as follows. In Section 2.1 we briefly review the linear response, Onsager formalism for a generic three-terminal setup. We will discuss the maximum output power and trace a derivation of all the local and non-local transport coefficients. In Section 2.2 we extend the concept of Carnot bound at the maximum efficiency to the three-terminal setup and we derive analytical formulas of the efficiency at maximum power in various cases, depending on the flow of the heat currents. These expressions are written in terms of generalized dimensionless figures of merit. Note that the expressions derived in Section 2.1 and 2.2 are based on the properties of the Onsager matrix and on the positivity of the entropy production. Therefore they hold for non-interacting as well as interacting systems. This framework will then be applied in Section 2.3 to specific examples of non-interacting systems in order to illustrate the salient physical picture. Namely, we will consider a single quantum dot and two dots in series coupled to the three-terminal. Finally Section 2.4 is devoted to the conclusions.

2.1 Linear response for 3-terminal systems

The system depicted in Fig. 2.1 is characterized by three energy and three charge currents ($J^u_{i=1,2,3}$ and $J^c_{i=1,2,3}$, respectively) flowing from the corresponding reservoirs, which have to fulfill the constraints:

$$\begin{aligned} &\sum_{i=1}^{3} J^u_i = 0 \quad \text{(Energy conservation)} \,, \\ &\sum_{i=1}^{3} J^c_i = 0 \quad \text{(Particle conservation)} \,, \end{aligned} \tag{2.1}$$

(positive values being associated with flows *from* the reservoir *to* the system). In what follows we will assume the reservoir 3 as a reference and the system to be operating in the linear response regime, i.e. set $(T_3, \mu_3) \equiv (T, \mu)$ and write $(T_j, \mu_j) = (T + \Delta T_j, \mu + \Delta\mu_j)$ with $|\Delta\mu_j|/k_B T \ll 1$ and $|\Delta T_j|/T \ll 1$ for $j = 1, 2$, and k_B is the Boltzmann constant. Under these assumptions the relation between currents and biases can then be expressed through the Onsager matrix L of elements L_{ij} via the identity:

$$\begin{pmatrix} J^c_1 \\ J^h_1 \\ J^c_2 \\ J^h_2 \end{pmatrix} = \begin{pmatrix} L_{11} & L_{12} & L_{13} & L_{14} \\ L_{21} & L_{22} & L_{23} & L_{24} \\ L_{31} & L_{32} & L_{33} & L_{34} \\ L_{41} & L_{42} & L_{43} & L_{44} \end{pmatrix} \begin{pmatrix} X^\mu_1 \\ X^T_1 \\ X^\mu_2 \\ X^T_2 \end{pmatrix} , \tag{2.2}$$

where $X^\mu_{1,2} = \Delta\mu_{1,2}/T$ and $X^T_{1,2} = \Delta T_{1,2}/T^2$ are the generalized forces, and where $J^h_{1,2} = J^u_{1,2} - \mu_{1,2} J^c_{1,2}$ are the heat currents of the system, the corresponding currents to reservoir 3 being determined from $J^c_{1,2}$ and $J^h_{1,2}$ via the conservation laws of Eq. (2.1). In our analysis we take L to be symmetric (i.e. $L_{ij} = L_{ji}$) by enforcing time reversal symmetry in the problem. We also remind that, due to the positivity of the entropy production rate, such matrix has to be semi-positive definite (i.e. $L \geq 0$) and that it can be used to describe a two-terminal model connecting (say) reservoir 1 to reservoir 3 by setting $L_{j3} = L_{j4} = L_{3j} = L_{4j} = 0$ for all j.

2.1.1 Transport coefficients

For a two-terminal model the elements of the Onsager matrix L can be related to four quantities which gauge the transport properties of the system under certain constraints. Specifically these are the electrical conductance G and the Peltier coefficient Π (evaluated under the assumption that both reservoirs have the same temperature), and the thermal conductance K and the thermopower (or Seebeck coefficient) S (evaluated when no net charge current is flowing through

the leads). When generalized to the multi-terminal model these quantities yield to the introduction of non-local coefficients, which describe how transport in a reservoir is influenced by a bias set between two other reservoirs.

Thermopower

For a two-terminal configuration the thermopower relates the voltage ΔV that develops between the reservoirs to their temperature difference ΔT under the assumption that no net charge current is flowing in the system, i.e. $S = -\left(\frac{\Delta V}{\Delta T}\right)_{J^c=0}$. A generalization of this quantity to the multi-terminal scenario can be obtained by introducing the matrix of elements

$$S_{ij} = -\left(\frac{\Delta\mu_i}{e\Delta T_j}\right)_{\substack{J^c_k = 0\ \forall k,\\ \Delta T_k = 0\ \forall k\neq j}}, \tag{2.3}$$

with local ($i = j$) and non-local ($i \neq j$) coefficients, e being the electron charge. In this definition, which does not require the control of the heat currents, we have imposed that the particle currents in all the leads are zero (the voltages are measured at open circuits) *and* that all but one temperature differences are zero (of course this last condition is not required in a two-terminal model). It is worth observing that Eq. (5.25) differs from other definitions proposed in the literature. For example in Ref. [Machon2013] a generalization of the two-terminal thermopower to a three-terminal system, was proposed by setting to zero one voltage instead of the corresponding particle current. While operationally well defined, this choice does not allow one to easily recover the thermopower of the two-terminal case (in our approach instead this is rather natural, see below). Finally in the probe approach presented in Refs. [Jacquet2009, Saito2011, Horvat2012, Balachandran2013, Brandner2013b, Brandner2013a] it was possible to study a multi-terminal device by using an effective two-terminal system only, because the heat and particle currents of the probe terminals are set to vanish by definition. Therefore, within this approach, there are no chances of having non-local transport coefficients.

In the three-terminal scenario we can use Eq. (2.2) to rewrite the elements of the matrix (5.25). In particular introducing the quantities

$$L^{(2)}_{ij;kl} = L_{ik}L_{lj} - L_{il}L_{kj}, \tag{2.4}$$

we get (see Appendix 2.A for details)

$$S_{11} = \frac{1}{eT}\frac{L^{(2)}_{13;32}}{L^{(2)}_{13;31}}, \qquad S_{22} = \frac{1}{eT}\frac{L^{(2)}_{14;31}}{L^{(2)}_{13;31}}, \tag{2.5}$$

$$S_{12} = \frac{1}{eT}\frac{L^{(2)}_{13;34}}{L^{(2)}_{13;31}}, \qquad S_{21} = \frac{1}{eT}\frac{L^{(2)}_{13;21}}{L^{(2)}_{13;31}}, \tag{2.6}$$

which yields, correctly, $S_{11} = \frac{1}{eT}\frac{L_{12}}{L_{11}}$ as the only non-zero element, by taking the two-terminal limits detailed at the end of the previous section.

Electrical conductance

In a two-terminal configuration the electric conductance describes how the electric current depends upon the bias voltage between the two-terminal under isothermal conditions, i.e. $G = \left(\frac{eJ^c}{\Delta V}\right)_{\Delta T=0}$. The generalization to many-terminal systems is provided by the following matrix:

$$G_{ij} = \left(\frac{eJ_i^c}{\Delta\mu_j}\right)_{\substack{\Delta T_k = 0\ \forall k,\\ \Delta\mu_k = 0\ \forall k \neq j}} . \tag{2.7}$$

Using the three-terminal Onsager matrix (2.2) we find

$$\begin{pmatrix} G_{11} & G_{12} \\ G_{21} & G_{22} \end{pmatrix} = \frac{e^2}{T}\begin{pmatrix} L_{11} & L_{13} \\ L_{13} & L_{33} \end{pmatrix}, \tag{2.8}$$

which, in the two-terminal limit where reservoir 2 is disconnected from the rest, gives $G_{11} = \frac{e}{T}L_{11}$ as the only non-zero element.

Thermal conductance

The thermal conductance for a two-terminal is the coefficient which describes how the heat current depends upon the temperature imbalance ΔT under the assumption that no net charge current is flying through the system, i.e. $K = \left(\frac{J^h}{\Delta T}\right)_{J^c=0}$. In the multi-terminal scenario this generalizes to

$$K_{ij} = \left(\frac{J_i^h}{\Delta T_j}\right)_{\substack{J_k^c = 0\ \forall k,\\ \Delta T_k = 0\ \forall k \neq j}} , \tag{2.9}$$

where one imposes the same constraints as those used for the thermopower matrix (5.25), i.e. no currents and $\Delta T_k = 0$ for all terminals but the j-th. For a three-terminal case, using Eq. (2.4) this gives

$$K_{11} = \frac{1}{T^2}\frac{L_{13}L^{(2)}_{12;32} - L_{12}L^{(2)}_{13;32} - L_{11}L^{(2)}_{23;23}}{L^{(2)}_{13;31}}, \tag{2.10}$$

$$K_{22} = \frac{1}{T^2}\frac{L_{14}L^{(2)}_{13;43} - L_{13}L^{(2)}_{14;43} - L_{11}L^{(2)}_{34;34}}{L^{(2)}_{13;31}}, \tag{2.11}$$

and

$$K_{12} = K_{21} = \frac{1}{T^2}\frac{L_{24}L^{(2)}_{13;31} + L_{14}L^{(2)}_{13;23} + L_{34}L^{(2)}_{13;12}}{L^{(2)}_{13;31}}. \tag{2.12}$$

Once more, in the two-terminal limit where the reservoir 2 is disconnected from the rest, the only non-zero element is $K_{11} = \frac{1}{T^2}\frac{L^{(2)}_{12;12}}{L_{11}}$.

Peltier coefficient

In a two-terminal configuration the Peltier coefficient relates the heat current to the charge current under isothermal condition, i.e. $\Pi = \left(\frac{J^h}{eJ^c}\right)_{\Delta T=0}$. For multi-terminal systems this generalizes to the matrix

$$\Pi_{ij} = \left(\frac{J_i^h}{eJ_j^c}\right)_{\substack{\Delta T_k = 0\ \forall k,\\ \Delta\mu_k = 0\ \forall k \neq j}} , \tag{2.13}$$

which can be shown to be related to the thermopower matrix (5.25), through the Onsager reciprocity equations, i.e. $\Pi_{ij}(\mathbf{B}) = TS_{ji}(-\mathbf{B})$ ($\mathbf{B}$ being the magnetic field on the system),[Callen1985, De Groot1962] from which, using Eqs. (2.5) and (2.6), one can easily derive for the three-terminal case the dependence upon the Onsager matrix L.

2.2 Efficiency for 3-terminal systems

In order to characterize the properties of a multi-terminal system as a heat engine we shall now analyze its efficiency. In order to generalize the definition for the efficiency of a two-terminal machine [Benenti2013, Callen1985], we have to define the steady state heat to work conversion efficiency η, for a three-terminal machine, as the power $\dot{W}$ generated by the machine (which equals to the sum of all the heat currents exchanged between the system and the reservoirs), divided by the sum of the heat currents *absorbed* by the system, i.e.

$$\eta = \frac{\dot{W}}{\sum_{i_+} J_i^h} = \frac{\sum_{i=1}^3 J_i^h}{\sum_{i_+} J_i^h} = \frac{-\sum_{i=1}^2 \Delta\mu_i J_i^c}{\sum_{i_+} J_i^h} , \tag{2.14}$$

where the symbol $\sum_{i_+}$ in the denominator indicates that the sum is restricted to positive heat currents only, and where in the last expression we used Eq. (2.1) to express J_3^h in terms of the other two independent currents[1].

The definition (2.14) applies only to the case in which $\dot{W}$ is positive. Since the signs of the heat currents J_i^h are not known *a priori* (they actually depend on the details of the system), the expression of the efficiency depends on which heat currents are positive. For the three-terminal system depicted in Fig. 2.1

[1]Note that Eq. (2.14) can be easily generalized to M terminals, after appropriate change of the numerator. By setting for instance $(T_M, \mu_M) = (T, \mu)$, $\Delta T_i = T_i - T$, and $\Delta\mu_i = \mu_i - \mu$ ($i = 1, ..., M-1$), the output power reads as follows:

$$\dot{W} = \sum_{i=1}^{M} J_i^h = -\sum_{i=1}^{M-1} \Delta\mu_i J_i^c. \tag{2.15}$$

we set for simplicity $T_3 < T_2 < T_1$ and focus on those situations where J_3^h is negative (positive values of J_3^h being associated with regimes where the machine effectively works as a refrigerator which extract heat from the coldest reservoir of the system). Under these conditions the efficiency is equal to

$$\eta_{12} = \frac{\dot{W}}{J_1^h + J_2^h} \,, \tag{2.16}$$

when both J_1^h and J_2^h are positive, or

$$\eta_i = \frac{\dot{W}}{J_i^h} \,, \tag{2.17}$$

when for $i = 1$ or 2 only J_i^h is positive.

2.2.1 Carnot efficiency

The Carnot efficiency represents an upper bound for the efficiency and is obtained for an infinite-time (Carnot) cycle. For a two-terminal thermal machine the Carnot efficiency is obtained by simply imposing the condition of zero entropy production, namely $\dot{S} = \sum_i J_i^h/T_i = 0$. If the two reservoirs are kept at temperatures T_1 and T_3 (with $T_3 < T_1$), from the definition of the efficiency, Eq. (2.14), one gets the two-terminal Carnot efficiency $\eta_C^{II} = 1 - T_3/T_1$. The Carnot efficiency for a three-terminal thermal machine is obtained analogously by imposing the condition of zero entropy production, when a reservoir at an intermediate temperature T_2 is added. If J_1^h only is positive as in Eq. (2.17), one obtains

$$\eta_{C,1} = 1 - \frac{T_3}{T_1} + \frac{J_2^h}{J_1^h}(1 - \zeta_{32}) = \eta_C^{II} + \frac{J_2^h}{J_1^h}(1 - \zeta_{32}), \tag{2.18}$$

where $\zeta_{ij} \equiv T_i/T_j$. Note that Eq. (2.18) is the sum of the two-terminal Carnot efficiency η_C^{II} and a term whose sign is determined by $(1 - \zeta_{32})$. Since $J_1^h > 0$, $J_2^h < 0$ and $\zeta_{32} < 1$, it follows that $\eta_{C,1}$ is always *reduced* with respect to its two-terminal counterpart η_C^{II}. Analogously if only J_2^h is positive, one obtains

$$\eta_{C,2} = \eta_C^{II} - \frac{T_3}{T_1}\left[\frac{J_1^h}{J_2^h}(1 - \zeta_{13}) - (1 - \zeta_{12})\right], \tag{2.19}$$

which again can be shown to be reduced with respect to η_C^{II}, since $J_1^h < 0$, $J_2^h > 0$, $\zeta_{12} > 1$, and $\zeta_{13} > 1$. We notice that this is a hybrid configuration (not a heat engine, neither a refrigerator): the hottest reservoir absorbs heat, while the intermediate-temperature reservoir releases heat. However, the heat to work conversion efficiency is legitimately defined since generation of power

($\dot{W} > 0$) can occur in this situation. Finally, if both J_1^h and J_2^h are positive as in Eq. (2.16) one obtains

$$\eta_{C,12} = 1 - \frac{T_3}{T_1}\left(1 + \frac{\zeta_{12} - 1}{1 + \frac{J_1^h}{J_2^h}}\right) = \eta_C^{II} - \frac{T_3}{T_1}\frac{\zeta_{12} - 1}{1 + \frac{J_1^h}{J_2^h}}. \tag{2.20}$$

Since $T_3 < T_2 < T_1$, the term that multiplies T_3/T_1 is positive so that $\eta_{C,12}$ is reduced with respect to the two-terminal case.

It is worth noticing that, in contrast to the two-terminal case, the Carnot efficiency cannot be written in terms of the temperatures only, but it depends on the details of the system. Moreover, note that the Carnot efficiency is unchanged with respect of the two-terminal case if $T_2 = T_3$ in (2.18) or if $T_2 = T_1$ in (2.20). Indeed, in this situation the quantities ζ_{ij} are equal to one, making the extra terms in Eqs. (2.18) or (2.20) to vanish.

The above results for the Carnot efficiency could be generalized to many-terminal systems. In particular, we conjecture that, given a system that works between T_1 and T_3 (with $T_3 < T_1$) and adding an arbitrary number of terminals at intermediate temperatures will in general lead to Carnot bounds smaller than η_C^{II}. On the other hand, adding terminals at higher (or colder) temperatures than T_1 and T_3 will make η_C increase.

Notice that within linear response and via Eq. (2.2) we can express the Carnot efficiencies (2.18)-(2.20) in terms of the generalized forces $X_{1,2}^{\mu}$.

2.2.2 Efficiency at Maximum Power

The efficiency at maximum power is the value of the efficiency evaluated at the values of chemical potentials that maximize the output power $\dot{W}$ of the engine. In the two-terminal case the efficiency at maximum power can be expressed as [Broeck2005]

$$\eta^{II}(\dot{W}_{\max}) = \frac{\eta_C^{II}}{2}\frac{ZT}{ZT+2}\,, \tag{2.21}$$

where $ZT = \frac{GS^2}{K}T$ is a dimensionless figure of merit which depends upon the transfer coefficient of the system. The positivity of the entropy production imposes that such quantity should be non-negative (i.e. $ZT \geq 0$), therefore $\eta^{II}(\dot{W}_{\max})$ is bounded to reach its maximum value $\eta_C^{II}/2$ only in the asymptotic limit of $ZT \to \infty$ (Curzon-Ahlborn limit [Curzon1975] within linear response [Broeck2005]).

For the three-terminal configuration the output power is a function of the four generalized forces $(X_1^{\mu}, X_1^T, X_2^{\mu}, X_2^T)$ introduced in Eq. (2.2), i.e.

$$\dot{W} = -T(J_1^c X_1^{\mu} + J_2^c X_2^{\mu})\,. \tag{2.22}$$

In the linear regime this is a quadratic function which can be maximized with respect to X_1^{μ} and X_2^{μ} while keeping X_1^T and X_2^T constant (the existence of a

maximum being guaranteed by the the positivity of the entropy production). The resulting expression is

$$\dot{W}_{\max} = \frac{T^4}{4}(X_1^T, X_2^T)\, M \begin{pmatrix} X_1^T \\ X_2^T \end{pmatrix} , \tag{2.23}$$

where $M = \begin{bmatrix} c & a \\ a & b \end{bmatrix}$ is a positive semi-definite matrix, see Appendix 2.B, whose elements depends on the Onsager coefficients via the identities

$$\begin{aligned} a &= G_{12}S_{12}S_{21} + G_{12}S_{11}S_{22} + G_{22}S_{21}S_{22} \\ &\quad + G_{11}S_{11}S_{12} , \\ b &= G_{11}S_{12}^2 + 2G_{12}S_{12}S_{22} + G_{22}S_{22}^2 , \\ c &= G_{11}S_{11}^2 + 2G_{12}S_{21}S_{11} + G_{22}S_{21}^2 . \end{aligned} \tag{2.24}$$

Indicating with $\alpha > \beta \geq 0$ the eigenvalues of M we can then further simplify Eq. (2.23) by writing it as

$$\dot{W}_{\max} = (\alpha \cos^2\theta + \beta \sin^2\theta) X^2 T^4/4 , \tag{2.25}$$

where $X = \sqrt{(X_1^T)^2 + (X_2^T)^2}$ is the geometric average of system temperatures, while the angle θ identify the rotation in the X_1^T, X_2^T plane which defines the eigenvectors of M. We call the parameter

$$P = \alpha \cos^2\theta + \beta \sin^2\theta \tag{2.26}$$

three-terminal power factor. It relates the maximum power to the temperature difference: by construction it fulfills the inequality $\beta \leq P \leq \alpha$, the maximum being achieved for $\theta = 0$ (i.e. by ensuring that (X_1^T, X_2^T) coincides with the eigenvector of M associated with its largest eigenvalue α). Note that in the two-terminal limit we have $\beta \to 0$, $\alpha \to G_{11}S_{11}^2$, $\cos^2\theta \to 1$, so that the usual two-terminal power factor $G_{11}S_{11}^2$ is recovered.

Exploiting Eq. (2.25) we can now write the efficiency at maximum power for the three cases detailed in Eqs. (2.16) and (2.17). Specifically we have

$$\eta_1(\dot{W}_{\max}) = \frac{1}{2T} \frac{\Delta T_1 Z_{11}^c T + \Delta T_2(\delta^{-1} Z_{11}^b T + 2Z_{11}^a T)}{\delta^{-1}(2\tilde{y} + Z_{11}^a T) + Z_{11}^c T + 2}, \tag{2.27}$$

$$\eta_2(\dot{W}_{\max}) = \frac{1}{2T} \frac{\Delta T_2 Z_{22}^b T + \Delta T_1(\delta Z_{22}^c T + 2Z_{22}^a T)}{\delta(2y + Z_{22}^a T) + Z_{22}^b T + 2}, \tag{2.28}$$

and

$$\begin{aligned} &\eta_{12}(\dot{W}_{\max}) = \\ &= \frac{1}{2T} \frac{\Delta T_1 Z_{12}^c T + \Delta T_2(2Z_{12}^a T + \delta^{-1} Z_{12}^b T)}{\delta^{-1}(2(1+y^{-1}) + Z_{12}^a T + Z_{12}^b T) + 2(1+\tilde{y}^{-1}) + Z_{12}^a T + Z_{12}^c T}, \end{aligned} \tag{2.29}$$

where we have defined the parameters $\delta = X_1^T/X_2^T = \Delta T_1/\Delta T_2$, $y = K_{12}/K_{22}$ and $\tilde{y} = K_{12}/K_{11}$ and introduced the following generalized ZT coefficients:

$$Z_{ij}^a T = \frac{aT}{K_{ij}}, \quad Z_{ij}^b T = \frac{bT}{K_{ij}}, \quad Z_{ij}^c T = \frac{cT}{K_{ij}} \,. \tag{2.30}$$

The efficiencies (2.27), (2.28) and (2.29) can also be expressed in terms of the corresponding Carnot efficiencies given in Eqs. (2.18), (2.19) and (2.20), obtaining the following equations which mimic Eq. (2.21) of the two-terminal case:

$$\begin{aligned} \eta_1(\dot{W}_{\max}) &= \frac{\eta_{C,1}}{2} \frac{Z_{11}^b T + 2\delta Z_{11}^a T + \delta^2 Z_{11}^c T}{2\tilde{y}/y + 4\delta\tilde{y} + 2\delta^2 + Z_{11}^b T + 2\delta Z_{11}^a T + \delta^2 Z_{11}^c T} \\ &= \frac{\eta_{C,1}}{2} \frac{\mathcal{Z}_{11} T}{C_1 + \mathcal{Z}_{11} T}, \end{aligned} \tag{2.31}$$

$$\begin{aligned} \eta_2(\dot{W}_{\max}) &= \frac{\eta_{C,2}}{2} \frac{Z_{22}^b T + 2\delta Z_{22}^a T + \delta^2 Z_{22}^c T}{2\delta^2 y/\tilde{y} + 4\delta y + 2 + Z_{22}^b T + 2\delta Z_{22}^a T + \delta^2 Z_{22}^c T} \\ &= \frac{\eta_{C,2}}{2} \frac{\mathcal{Z}_{22} T}{C_2 + \mathcal{Z}_{22} T}, \end{aligned} \tag{2.32}$$

$$\begin{aligned} \eta_{12}(\dot{W}_{\max}) &= \frac{\eta_{C,12}}{2} \frac{Z_{12}^b T + 2\delta Z_{12}^a T + \delta^2 Z_{12}^c T + o(\Delta T_i)}{2y^{-1} + 4\delta + 2\delta^2\tilde{y}^{-1} + Z_{12}^b T + 2\delta Z_{12}^a T + \delta^2 Z_{12}^c T + o(\Delta T_i)} \\ &\simeq \frac{\eta_{C,12}}{2} \frac{\mathcal{Z}_{12} T}{C_{12} + \mathcal{Z}_{12} T}, \end{aligned} \tag{2.33}$$

where we have introduced the constants

$$C_1 = 2\tilde{y}/y + 4\delta\tilde{y} + 2\delta^2, \tag{2.34}$$

$$C_2 = 2\delta^2 y/\tilde{y} + 4\delta y + 2, \tag{2.35}$$

$$C_{12} = \tilde{y}^{-1} + \delta^2 y^{-1} + 2\delta, \tag{2.36}$$

and the combinations of figures of merit

$$\mathcal{Z}_{ij} T = (Z_{ij}^b + 2\delta Z_{ij}^a + \delta^2 Z_{ij}^c) T \,. \tag{2.37}$$

Notice also that in writing Eq. (2.33) we retained only the leading order neglecting contributions of order ΔT_i or higher.

The above expressions can be used to provide a generalization of the Curzon-Ahlborn limit efficiency for a multi-terminal quantum thermal device. Indeed using the Cholesky decompositions on the Onsager matrix, we can prove that the constants C_1, C_2 defined in Eqs. (2.34), (2.35) are positive, see [Gentle1998] for details. This fact together with the positivity of the quantities $\mathcal{Z}_{ii}T$, that we

have checked numerically, implies that the efficiencies $\eta_i(\dot{W}_{\max})$ are always upper bounded by half of the associated Carnot efficiencies, i.e.

$$\eta_i(\dot{W}_{\max}) \leq \eta_{C,i}/2 \,, \tag{2.38}$$

the inequality being saturated when the generalized ZT coefficients (2.30) diverge. An analogous conclusion can be reached also for (2.33), yielding

$$\eta_{12}(\dot{W}_{\max}) \leq \eta_{C,12}/2 \,. \tag{2.39}$$

In this case C_{12} is no longer guaranteed to be positive due to the presence of K_{12}. Still the inequality (2.39) can be derived by observing that the quantities C_{12} and $\mathcal{Z}_{12}T$ entering in the rhs of Eq. (2.33) have always the same sign.

2.3 Examples

In this Section we shall apply the theoretical framework developed so far to two specific non-interacting systems attached to three terminals. Namely, we will discuss the case of a single dot and the case of two coupled dots, in the absence of electron-electron interaction (which cannot be dealt within the Landauer-Büttiker formalism). Our aim is to show that one can easily find situations where the efficiency and output power are enhanced with respect to the two-terminal case. Furthermore, through the example of the single dot, we find the conditions that guarantee the non-local thermopowers to vanish.

The coherent flow of particles and heat through a non-interacting conductor can be described by means of the Landauer-Büttiker formalism. Under the assumption that all dissipative and phase-breaking processes take place in the reservoirs, the electric and thermal currents are expressed in terms of the scattering properties of the system [Büttiker1988, Datta1995, Imry2008]. For instance, in a generic multi-terminal configuration the currents flowing into the system from the i-th reservoir are:

$$J_i^c = \frac{e}{h} \sum_{j \neq i} \int_{-\infty}^{\infty} dE \, \mathcal{T}_{ij}(E) \, [f_i(E) - f_j(E)], \tag{2.40}$$

$$J_i^h = \frac{1}{h} \sum_{j \neq i} \int_{-\infty}^{\infty} dE \, (E - \mu_i) \, \mathcal{T}_{ij}(E) \, [f_i(E) - f_j(E)], \tag{2.41}$$

where the sum over j is intended over all but the i-th reservoir, h is the Planck's constant, e is the electron charge, $\mathcal{T}_{ij}(E)$ is the transmission probability for a particle with energy E to transit from the reservoir j to reservoir i, and where finally $f_i(E) = \{\exp[(E - \mu_i)/k_B T_i] + 1\}^{-1}$ is the Fermi distribution of the particles injected from reservoir i (notice also that we are considering currents of spinless particles). In what follows we will use the above expressions in the linear response regime where $|\Delta\mu|/k_B T \ll 1$ and $|\Delta T|/T \ll 1$, and compute the associated Onsager coefficients (2.2), see Appendix 2.C.

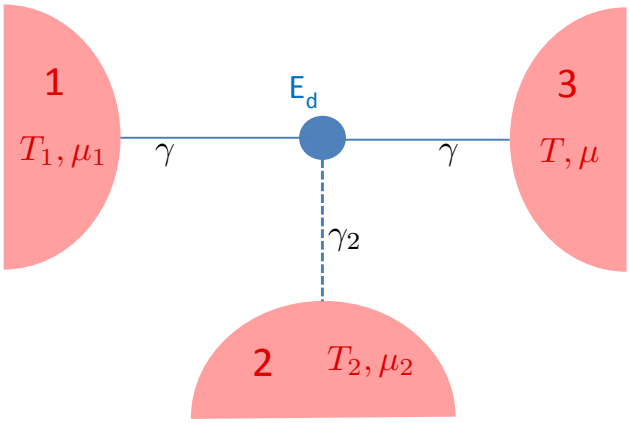

Figure 2.2 – Sketch of the single dot model used in the numerical simulations: a quantum dot with a single energy level E_d is connected to three fermionic reservoirs 1, 2, and 3. The chemical potential and temperature of the reservoir 3 are assumed as the reference values μ and T. The constants γ and γ_2 represent the coupling between the system and the various reservoirs (see Appendix 2.C.1 for details). A zero value of γ_2 corresponds to disconnecting the reservoir 2 from the system: in this regime the model describes a two-terminal device where reservoirs 1 and 3 are connected through the single dot.

2.3.1 Single dot

In this section we study numerically a simple model consisting of a quantum dot with a single energy level E_d, coupled to three fermionic reservoirs, labeled 1, 2, and 3, see Fig. 2.2. For simplicity, the coupling strength to electrodes 1 and 3 are taken equal to γ, while the coupling strength to electrode 2 is denoted by γ_2. In particular we want to investigate how the efficiencies, output powers and transport coefficients evolve when the system is driven from a two-terminal to a three-terminal configuration, that is by varying the ratio γ_2/γ. The two-terminal configuration corresponds to $\gamma_2 = 0$ and the third terminal is gradually switched on by increasing γ_2/γ. As detailed in Appendix 2.C, the transmission amplitudes between each pair of terminals can be used to evaluate the Onsager coefficients L_{ij} – the resulting expression being provided in Eqs. (2.68). Once the matrix L_{ij} is known, all the currents flowing through the system, efficiencies, output powers and transport coefficients can be calculated within the framework developed in the previous Sections.

Efficiencies and maximum power

In Fig. 2.3 we show how the Carnot efficiency η_C depends on the temperature differences ΔT_1 and ΔT_2, when the chemical potentials are chosen to guarantee maximum output power, i.e., fixing the generalized forces $X^{\mu}_{1,2}$ in order to maximize $\dot{W}$. As we can see, η_C increases linearly along any "radial" direction defined by a relation $\Delta T_2 = k\,\Delta T_1$, where k is a constant. In particular, the dashed lines corresponding to $k = 0.5$, $k = 2$, and $k = -1$ separate the different regimes discussed in Sec. 2.2.1: for $-1 < k < 0.5$ the system absorbs heat only from reservoir 1 (if $\Delta T_1 > 0$) or from 2 and 3 (if $\Delta T_1 < 0$); for $0.5 < k < 2.0$ the system absorbs heat from reservoirs from 1 and 2 (if $\Delta T_1 > 0$) or from 3 only (if $\Delta T_1 < 0$); finally, for $k > 2$ and $k < -1$ the system absorbs heat only from reservoir 2 (if $\Delta T_2 > 0$) or from 1 and 3 (if $\Delta T_2 < 0$). In the case when only one heat flux is absorbed the Carnot efficiency is given by Eq. (2.18) or Eq. (2.19), while it is given by Eq. (2.20) if two heat fluxes are absorbed.

In Figs. 2.4 and 2.5, we show how the efficiency Eq. (2.14), the output power Eq. (2.22), the efficiency at maximum output power Eqs. (2.27)-(2.29) and the maximum output power Eq. (2.23), vary when the system is driven from a two-terminal to a three-terminal configuration, *i. e.* by varying the ratio γ_2/γ. We set opposite signs for $\Delta\mu_1$ and $\Delta\mu_2$, so that the system absorbs heat only from the hottest reservoir 1, and $\Delta T_2 = 0$, in such a way that the Carnot efficiency η_C coincides with that of a two-terminal configuration, namely $\eta_C = 1 - T/T_1$. Interestingly, we proved that increasing the coupling γ_2 to the reservoir 2 may lead to an improvement of the performance of the system. In particular, as shown in Fig. 2.6, the efficiency and the output power can be enhanced *at the same time* at small couplings γ_2, exhibiting a maximum around $\gamma_2 \sim 0.3\gamma$ and $\gamma_2 \sim 0.6\gamma$, respectively. In Fig. 2.5 we show results for the same quantities but at the maximum output power [$\eta(\dot{W}_{\max})$ and $\dot{W}_{max}$]. In this case, while $\dot{W}_{max}$ still increases with γ_2, the corresponding efficiency decreases approximately linearly.

In Figs. 2.6 and 2.7 we show the same quantities as in Figs. 2.4 and 2.5, but as a function of the coupling γ for two values of γ_2 ($\gamma_2 = 0$ and $\gamma_2 = 0.5\gamma$).

From Fig. 2.6 we can see that at small γ the coupling to a third terminal can enhance both the efficiency (for $\gamma \lesssim 0.8 k_B T$) and the power (for $\gamma \lesssim k_B T$). In Fig. 2.7 we note that, both for the two- and the three-terminal system, the efficiency at maximum power tends to $\eta/\eta_C = 0.5$ in the limit $\gamma \to 0$, while the output power vanishes. For two-terminal the result is well known, since a delta-shaped transmission function leads to the divergence of the figure of merit ZT [Mahan1996, Humphrey2002, Humphrey2005]. Correspondingly, the efficiency at maximum power saturates the Curzon-Ahlborn bound $\eta/\eta_C = 0.5$. The same two-terminal energy-filtering argument explains the three-terminal result. Indeed, we found numerically that for $\gamma \to 0$ the chemical potentials optimizing the output power are such that $\mu_2 = \mu_3$. Since also the temperatures are chosen so that $T_2 = T_3$, we can conclude that terminals 2 and 3 can be seen

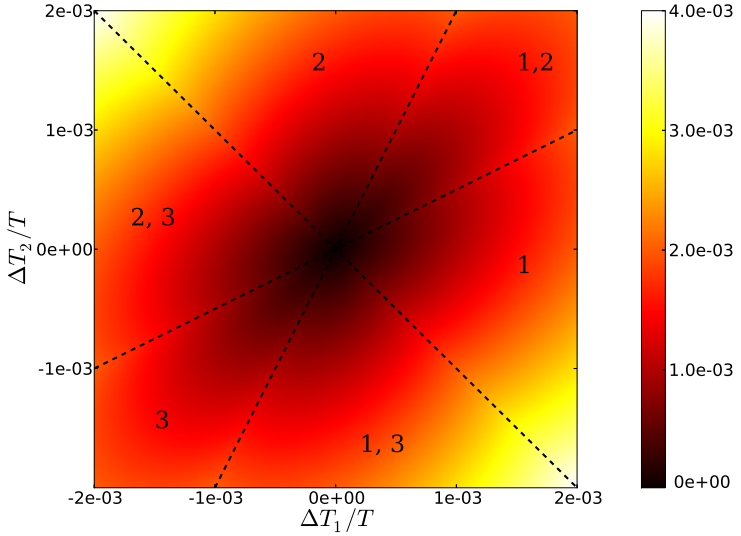

Figure 2.3 – Carnot efficiency η_C (density plot) of the three-terminal system depicted in Fig. 2.2, as a function of the gradients of temperature in reservoirs 1 and 2 (the chemical potentials μ_1 and μ_2 being chosen to guarantee maximum output power $\dot{W}$). The coupling with the reservoirs have been set to have a symmetric configuration with respect to 1 and 2 (i.e. $\gamma_2 = \gamma$). Note that η_C increases linearly along any radial direction defined by a relation $\Delta T_2 = k\Delta T_1$, where k is a constant. In particular, the dashed lines corresponding to $k = 0.5$, $k = 2$ and $k = -1$ separate different regimes discussed in Sec. 2.2.1. The numbers in each region identify the reservoirs from which the heat is absorbed. Parameter values: $\gamma = 0.2\, k_B T$, $E_d - \mu = 2.0\, k_B T$.

as a single terminal.

Thermopowers

In this section we show analytically that the non-local thermopowers are always zero in this model, while the local ones are equal. We consider a general situation, with three different coupling parameters: $\gamma_1 = \gamma$, $\gamma_2 = c\,\gamma$ and $\gamma_3 = d\,\gamma$, with $c \neq d$. Under these assumptions, the transmissions are given at the end of Appendix 2.C. Substituting these expressions in Eqs. (2.5) and (2.6), we find

$$\begin{aligned} S_{11} &= S_{22} = \frac{1}{eT}\frac{L_1}{L_0}, \\ S_{21} &= S_{12} = 0\,. \end{aligned} \tag{2.42}$$

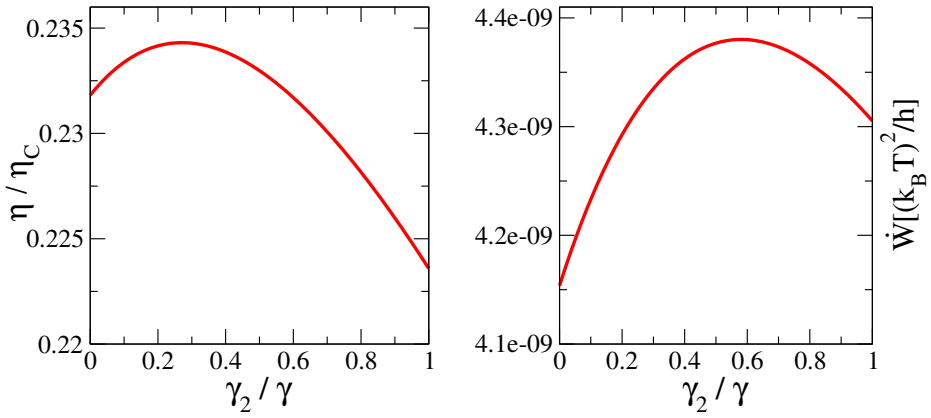

Figure 2.4 – Left panel: Efficiency η, normalized over the associated Carnot limit computed as in Sec. 2.2.1, as a function of the coupling to the reservoir 2. Note that as γ_2/γ is switched on, the efficiency increases until it reaches a maximum around $\gamma_2 \sim 0.3\gamma$, and then it decreases. Right panel: Output power $\dot{W}$ extracted from the system, as a function of the coupling to the reservoir 2. Parameters: $\gamma = 0.1\, k_B T$, $E_d - \mu = 2.0\, k_B T$, $\Delta\mu_1 = -\Delta\mu_2 = -5 \times 10^{-4}\, k_B T$, $\Delta T_1 = 10^{-3}\, T$, and $\Delta T_2 = 0$.

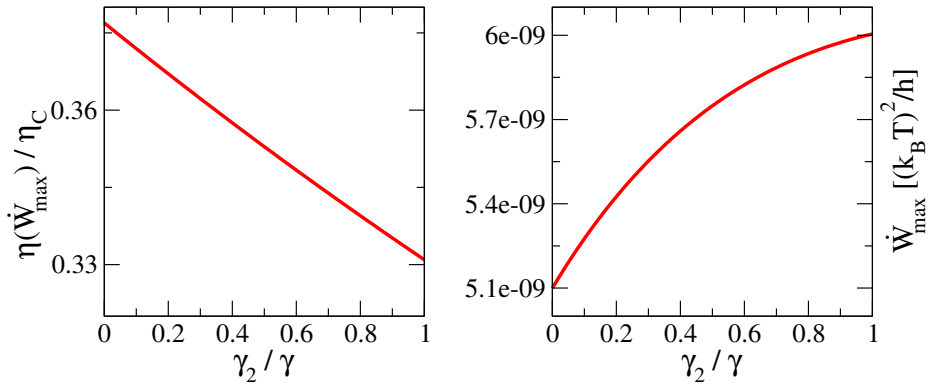

Figure 2.5 – Left panel: Efficiency at maximum power $\eta(\dot{W}_{\max})$, normalized over the Carnot limit, as a function of the coupling to the reservoir 2. Right panel: Maximum output power $\dot{W}_{max}$ extracted from the system, as a function of the coupling to the reservoir 2. Parameters: $\gamma = 0.1\, k_B T$, $E_d - \mu = 2.0\, k_B T$, $\Delta T_1 = 10^{-3}\, T$, and $\Delta T_2 = 0$.

This result is a direct consequence of the factorization of the energy dependence of the transmission probabilities, which are all proportional to the same function

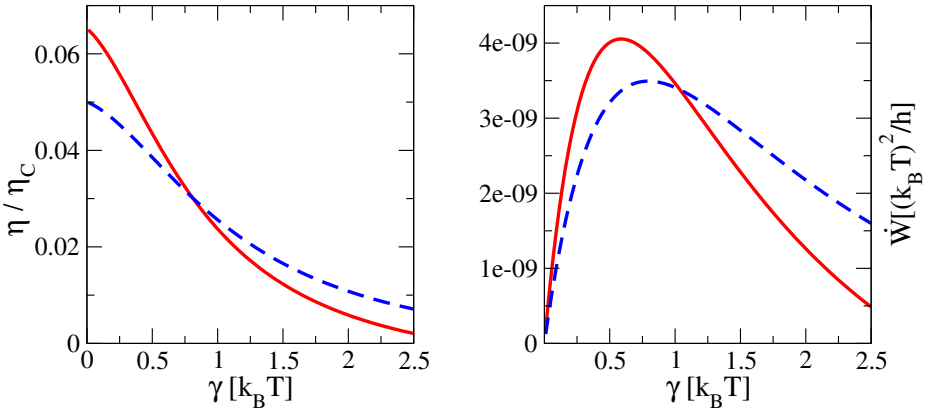

Figure 2.6 – Left panel: Efficiency η, normalized over the Carnot limit, as a function of the coupling energy γ. Right panel: Output power $\dot{W}$ extracted from the system, as a function of the coupling energy γ. In both cases, the full red curves correspond to a three-terminal configuration with $\gamma_2 = 0.5\gamma$, while the dashed blue curve refer to the two-terminal case ($\gamma_2 = 0$). Parameters: $E_d - \mu = 2.0\, k_B T$, $\Delta\mu_1 = -\Delta\mu_2 = -10^{-4}\, k_B T$, $\Delta T_1 = 10^{-3}\, T$, and $\Delta T_2 = 0$.

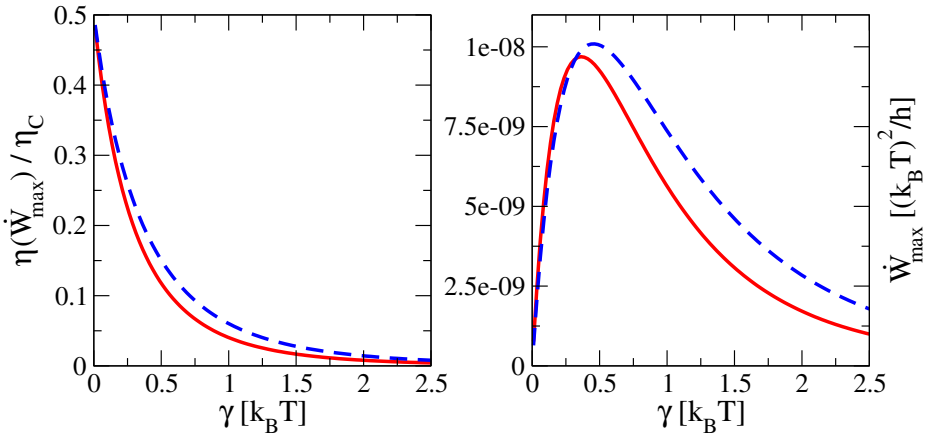

Figure 2.7 – Left panel: Efficiency at maximum power $\eta(\dot{W}_{\max})$, normalized over the Carnot limit, as a function of the coupling energy γ. Right panel: Maximum output power $\dot{W}_{max}$ extracted from the system, as a function of the coupling energy γ. In both cases, the full red curves correspond to a three-terminal configuration with $\gamma_2 = 0.5\gamma$, while the dashed blue curves refer to the two-terminal case ($\gamma_2 = 0$). Parameters: $E_d - \mu = 2.0\, k_B T$, $\Delta T_1 = 10^{-3}\, T$, and $\Delta T_2 = 0$.

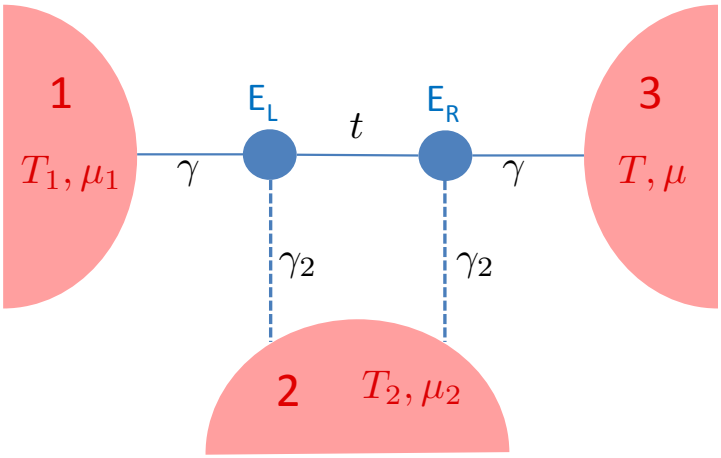

Figure 2.8 – Sketch of the double dot model used in the numerical simulations: two quantum dots with a single energy level are connected in series to three fermionic reservoirs 1, 2 and 3. The chemical potential and temperature of reservoir 3 are assumed as the reference values μ and T. A two-terminal configuration is obtained in the case in which the coupling to reservoir 2 (equal for both the dots) vanishes ($\gamma_2 = 0$).

$\mathcal{T}$, as shown in Eq. (2.67). Such factorization allows us to rewrite the Onsager's coefficients as in Eq. (2.68) and derive Eq. (2.42). The fact that the non-local thermopowers, for example S_{12}, are zero can be understood as follows. Consider first the case in which $T_1 = T_2 = T_3$ and terminal 2 behaves as a voltage probe. If so, from the condition $J_2^c = L_{31}X_1^\mu + L_{33}X_2^\mu = 0$ we derive $\Delta\mu_2 = -(L_{31}/L_{33})\,\Delta\mu_1$. Due to the factorization of the energy dependence in the transmissions we obtain $\Delta\mu_2 = (\gamma_1/(\gamma_1 + \gamma_3))\Delta\mu_1$. Hence, $\Delta\mu_1$ does not depend on the coupling γ_2. If in particular we consider $\gamma_2 = \gamma$, because of the symmetry of the system under exchange of the terminal 1 and 3 we have $\mu_1 = \mu_3$. We can therefore conclude that, independently of the coupling γ_2, the probe voltage condition for terminal 2 implies $\Delta\mu_1 = 0$. It can be shown that such result remains valid even when $\Delta T_1 = 0$ but $\Delta T_2 \neq 0$, as requested in the calculation of the thermopower S_{12}. As a result, $S_{12} = 0$. The same argument can be repeated for the current J_1^c with the terminal 1 acting as a voltage probe, leading to $S_{21} = 0$.

2.3.2 Double Dot

Let us now consider a system made of two quantum dots in series, each with a single energy level, coupled to three fermionic reservoirs. This system is described

by the Hamiltonian:

$$H = \begin{bmatrix} E_L & -t \\ -t & E_R \end{bmatrix}. \tag{2.43}$$

We call t the hopping energy between the dots, and we assume that dot L is coupled to the left lead (1), dot R is coupled to the right lead (3) and that both are coupled to a third lead (2) (see Fig. 2.8). The self energies describing these couplings are:

$$\Sigma_1 = \begin{bmatrix} \sigma_1 & 0 \\ 0 & 0 \end{bmatrix}, \quad \Sigma_2 = \begin{bmatrix} \sigma_2 & 0 \\ 0 & \sigma_2 \end{bmatrix}, \quad \Sigma_3 = \begin{bmatrix} 0 & 0 \\ 0 & \sigma_3 \end{bmatrix}. \tag{2.44}$$

In the wide-band approximation, we assume that these quantities are energy-independent and they can be written as purely imaginary numbers $\sigma_i = -i\,\gamma_i/2$. The self energies thus become:

$$\Sigma_1 = \begin{bmatrix} -i\frac{\gamma_1}{2} & 0 \\ 0 & 0 \end{bmatrix}, \quad \Sigma_2 = \begin{bmatrix} -i\frac{\gamma_2}{2} & 0 \\ 0 & -i\frac{\gamma_2}{2} \end{bmatrix}, \quad \Sigma_3 = \begin{bmatrix} 0 & 0 \\ 0 & -i\frac{\gamma_3}{2} \end{bmatrix}. \tag{2.45}$$

The retarded Green's function of the system is then:

$$\begin{aligned} \mathcal{G} = [E\mathbb{I} - H - \Sigma]^{-1} &= \begin{bmatrix} E - E_L - \sigma_1 - \sigma_2 & t \\ t & E - E_R - \sigma_3 - \sigma_2 \end{bmatrix}^{-1} = \\ &= \frac{1}{\det[\mathcal{G}]} \begin{bmatrix} E - E_R + i\frac{\gamma_3+\gamma_2}{2} & -t \\ -t & E - E_L + i\frac{\gamma_1+\gamma_2}{2} \end{bmatrix}, \end{aligned} \tag{2.46}$$

with

$$\det[\mathcal{G}] = \big(E - E_L + i\frac{\gamma_1 + \gamma_2}{2}\big)\big(E - E_R + i\frac{\gamma_3 + \gamma_2}{2}\big) - t^2. \tag{2.47}$$

Let us now define the broadening matrices as $\Gamma_i = i(\Sigma_i - \Sigma_i^\dagger)$:

$$\Gamma_1 = \begin{bmatrix} \gamma_1 & 0 \\ 0 & 0 \end{bmatrix}, \quad \Gamma_2 = \begin{bmatrix} \gamma_2 & 0 \\ 0 & \gamma_2 \end{bmatrix}, \quad \Gamma_3 = \begin{bmatrix} 0 & 0 \\ 0 & \gamma_3 \end{bmatrix}. \tag{2.48}$$

The matrix of transmission probability $\mathcal{T}_{ij}$ between each pair of reservoirs is then given by the Fisher-Lee formula [Datta1995, Fisher1981]

$$\mathcal{T}_{ij} = \mathrm{Tr}\left[\Gamma_i\,\mathcal{G}\,\Gamma_j\,\mathcal{G}^\dagger\right]. \tag{2.49}$$

For the system under consideration we obtain

$$\mathcal{T}_{13} = \frac{\gamma_1\gamma_3}{|\det[\mathcal{G}]|^2}\,t^2, \tag{2.50}$$

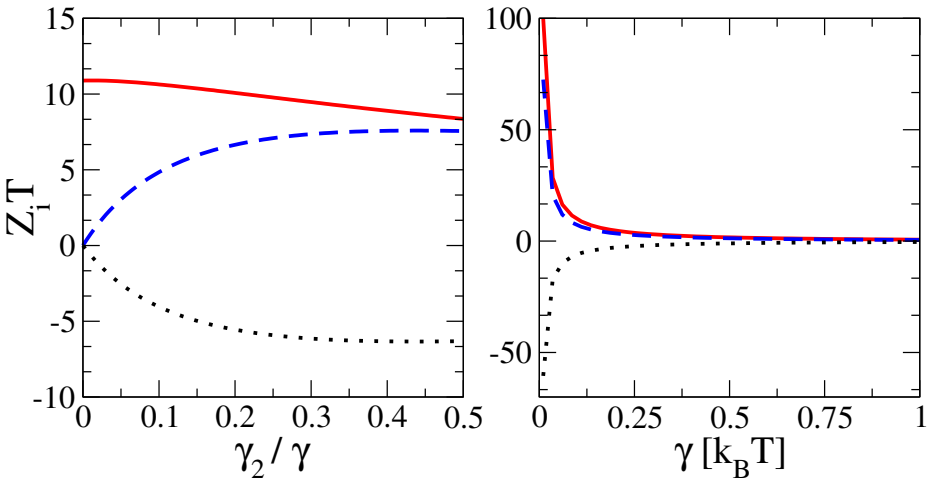

Figure 2.9 – Various figures of merit $Z^a_{11}T$ (dotted line), $Z^b_{11}T$ (dashed line) and $Z^c_{11}T$ (full line) as a function of the coupling to the bottom reservoir γ_2 (left panel), and as a function of the total coupling γ (right panel). Parameter values: $E_L - \mu = -2\ k_BT$, $E_R - \mu = -20\ k_BT$, $\gamma = 0.1\ k_BT$ (left panel) and $\gamma_2 = 0.5\ k_BT$ (right panel).

$$\mathcal{T}_{12} = \frac{\gamma_1\gamma_2}{|\det[\mathcal{G}]|^2}\left[(E-E_R)^2 + \left(\frac{\gamma_3+\gamma_2}{2}\right)^2 + t^2\right], \tag{2.51}$$

$$\mathcal{T}_{32} = \frac{\gamma_3\gamma_2}{|\det[\mathcal{G}]|^2}\left[(E-E_L)^2 + \left(\frac{\gamma_1+\gamma_2}{2}\right)^2 + t^2\right]. \tag{2.52}$$

At this point, it is clear that the energy dependence of the transmission matrix cannot be factorized as for the single dot case. This model is hence the simplest in which we can observe finite non-local thermopowers and an increase of both the power and the efficiency of the corresponding thermal machine. We find that the behavior of such quantities as functions of the various parameters is qualitatively very similar to the case of the single dot, thus confirming that a third terminal could improve the performance of a quantum machine.

Since in this system all the transport coefficients are different from zero, it is instructive to study the behavior of the generalized figures of merit defined in Eq. (2.30). In Fig. 2.9 we show, in the configuration with only one positive heat flux ($J^h_1 > 0$), $Z^a_{11}T$ (dotted line), $Z^b_{11}T$ (dashed line) and $Z^c_{11}T$ (full line). We investigate their behavior as a function of the coupling γ_2 and of the total coupling γ. Note that in the two-terminal limit ($\gamma_2 \to 0$) $Z^c_{11}T$ reduces to the standard thermoelectric figure of merit ZT, while $Z^a_{11}T$ and $Z^b_{11}T$ tend to zero. When we turn on the interaction with the reservoir 2 (left panel), we notice that the figure of merit $Z^c_{11}T$ decreases, while the figures of merit $Z^b_{11}T$ and

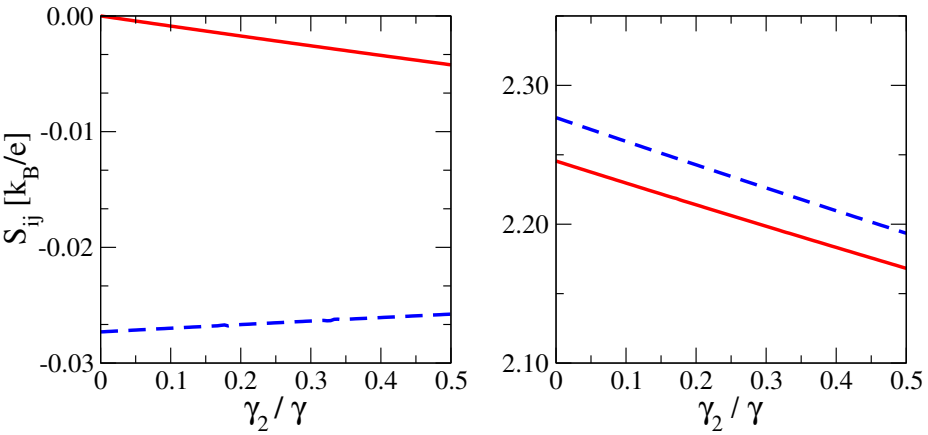

Figure 2.10 – (Left panel) Non local thermopowers as a function of the coupling γ_2 to lead 2. The full red line corresponds to $S_{12} = -\Delta\mu_1/\Delta T_2$, while the dashed (blue) line corresponds to $S_{21} = -\Delta\mu_2/\Delta T_1$. (Right panel) Local thermopowers as a function of the coupling γ_2 to lead 2. The full (red) line corresponds to $S_{11} = -\Delta\mu_1/\Delta T_1$, while the dashed (blue) line corresponds to $S_{22} = -\Delta\mu_2/\Delta T_2$. Parameter values as in Fig. 2.9.

$Z^a_{11}T$ increase their absolute values. From the behavior as a function of the total coupling γ we can see that in the limit of δ-shaped transmission function ($\gamma \to 0$), the figures of merit diverge, leading to the Carnot efficiency, while in the limit of broad transmission window ($\gamma \to \infty$), all the figures of merit go to zero and we recover the case of zero efficiency.

Thermopowers

As mentioned before, the fact that the energy-dependence of the transmission matrix for the double dot cannot be factorized is sufficient to guarantee finite non-local thermopowers, as shown in the left panel of Fig. 2.10. As a function of γ_2, S_{12} starts from zero, while S_{21} starts from a finite value. This different behavior for the two non-local thermopowers is due to the different role played by γ_2 in the two cases. As far as S_{12} is concerned, when we set a temperature difference ΔT_2 in lead 2, a chemical potential difference $\Delta\mu_1$ develops in lead 1 to annihilate the current that flows out of the lead 2. When the coupling γ_2 goes to zero, that current goes to zero and so does the chemical potential difference $\Delta\mu_1$. This argument does not hold for S_{21}, because the temperature difference ΔT_1 is set in lead 1, and γ_2 does not control the current anymore. Therefore when the coupling γ_2 approaches zero the current still have a finite value, and so the chemical potential difference $\Delta\mu_2$ needed to annihilate it. Furthermore, the local thermopowers are no more equal, as shown in the right panel of Fig. 2.10.

2.4 Summary

In this chapter we have developed a general formalism for linear-response multi-terminal thermoelectric transport. In particular, we have worked out analytical expressions for the efficiency at maximum power in the three-terminal case. By means of two simple non-interacting models (single and double quantum dot), we have shown that a third terminal can be useful to improve the thermoelectric performance of a system with respect to the two-terminal case. Moreover, we have discussed conditions under which non-local thermopowers could be observed. Our analysis could be extended also to cases in which time-reversal symmetry is broken by a magnetic field or including bosonic or superconducting terminals. It is an interesting open problem to understand in such instances both thermoelectric performance in realistic systems and fundamental bounds on efficiency for power generation and cooling.

2.A Calculation of the non-local thermopowers

To compute the multi-terminal thermopowers defined in Eqs. (2.5) and (2.6) we have to express one of the temperatures as a function of a thermal current. For example let us start from the inversion between X_1^T and J_1^h. In the Onsager's formalism this can be expressed as:

$$0 = -\begin{pmatrix} J_1^c \\ X_1^T \\ J_2^c \\ J_2^h \end{pmatrix} + \mathcal{L}\begin{pmatrix} X_1^\mu \\ J_1^h \\ X_2^\mu \\ X_2^T \end{pmatrix} = \begin{pmatrix} L & -\mathbb{I} \end{pmatrix} A\, A^{-1}\begin{pmatrix} \mathbf{X} \\ \mathbf{J} \end{pmatrix}, \tag{2.53}$$

where A is a permutation matrix that switches X_1^T and J_1^h, $\mathbf{X}$ and $\mathbf{J}$ are column vectors with components $(X_1^\mu, X_1^T, X_2^\mu, X_2^T)$ and $(J_1^c, J_1^h, J_2^c, J_2^h)$, respectively, and $\mathbb{I}$ is the 4×4 identity matrix. Then we obtain:

$$\begin{aligned} 0 &= \begin{pmatrix} L & -\mathbb{I} \end{pmatrix} A\, A^{-1}\begin{pmatrix} \mathbf{X} \\ \mathbf{J} \end{pmatrix} = \begin{pmatrix} L & -\mathbb{I} \end{pmatrix} A\begin{pmatrix} \mathbf{X}^* \\ \mathbf{J}^* \end{pmatrix} = \\ &= B\mathbf{X}^* + C\mathbf{J}^*, \end{aligned} \tag{2.54}$$

where $\mathbf{X}^*$ and $\mathbf{J}^*$ are the vectors $\mathbf{X}$ and $\mathbf{J}$ after the action of A^{-1}, that is, with $X_1^T \leftrightarrow J_1^h$; B and C are the matrices determined by the product $\begin{pmatrix} L & -\mathbb{I} \end{pmatrix} A$. We can now define the thermopower from the following equations:

$$\mathbf{X}^* = -B^{-1}\, C\mathbf{J}^* \Rightarrow \begin{pmatrix} X_1^\mu \\ J_1^h \\ X_2^\mu \\ X_2^T \end{pmatrix} = \mathcal{L}^{-1}\begin{pmatrix} J_1^c = 0 \\ X_1^T = 0 \\ J_2^c = 0 \\ J_2^h \end{pmatrix}. \tag{2.55}$$

For this choice of the parameters we have inverted, two different thermopowers can be defined, the non local S_{12}:

$$S_{12} = -\frac{\Delta\mu_1}{e\Delta T_2} = -\frac{1}{eT}\frac{X_1^\mu}{X_2^T} = \frac{1}{eT}\frac{L^{(2)}_{13;34}}{L^{(2)}_{13;31}}, \tag{2.56}$$

and the local S_{22}:

$$S_{22} = -\frac{\Delta\mu_2}{e\Delta T_2} = -\frac{1}{eT}\frac{X_2^\mu}{X_2^T} = \frac{1}{eT}\frac{L^{(2)}_{14;31}}{L^{(2)}_{13;31}}. \tag{2.57}$$

The two-terminal limit in which reservoirs 2 and 3 only are connected is obtained after setting in the Onsager matrix $L_{ij} = 0$ if $i = 1, 2$ or $j = 1, 2$. In this limit,

the previous expressions reduce to:

$$\begin{aligned} S_{12} &\to 0, \\ S_{22} &\to \frac{1}{eT}\frac{L_{34}}{L_{33}}. \end{aligned} \tag{2.58}$$

The non-local term goes to zero, while the local one goes to the correct value of the 2-terminal system. The two other terms of these generalized thermopowers are obtained with the inversion of X_2^T and J_2^h. Then we can define S_{21} as the non local quantity, and S_{11} as the local one:

$$\begin{aligned} S_{21} &= -\frac{1}{eT}\frac{X_2^\mu}{X_1^T} = \frac{1}{eT}\frac{L^{(2)}_{13;21}}{L^{(2)}_{13;31}}, \\ S_{11} &= -\frac{1}{eT}\frac{X_1^\mu}{X_1^T} = \frac{1}{eT}\frac{L^{(2)}_{13;32}}{L^{(2)}_{13;31}}. \end{aligned} \tag{2.59}$$

In a similar way all the other transport coefficients can be defined, by inverting a generalized force with a current.

2.B Cholesky decomposition for the Onsager matrix

In linear algebra, the Cholesky decomposition [Gentle1998] is a tool which allows to write a Hermitian, positive-definite (or semipositive-definite) matrix L as a product of a lower triangular matrix D and its conjugate transpose $D^\dagger$:

$$L = DD^\dagger, \tag{2.60}$$

(in particular, if L is *real*, $D^\dagger$ is simply the transpose of D). It turns out that the sign of some quantities defined throughout this work as combinations of products of Onsager coefficients L_{ij} can be easily studied by using the Cholesky decomposition on the Onsager matrix L. As an example, by writing

$$D = \begin{pmatrix} \rho_{11} & 0 & 0 & 0 \\ \rho_{12} & \rho_{22} & 0 & 0 \\ \rho_{13} & \rho_{23} & \rho_{33} & 0 \\ \rho_{14} & \rho_{24} & \rho_{34} & \rho_{44} \end{pmatrix}, \tag{2.61}$$

it can be shown that the coefficient b and c defined in Eq. (2.24) are equal to

$$b = \frac{\rho_{14}^2(\rho_{23}^2+\rho_{33}^2) + (\rho_{23}\rho_{24}+\rho_{33}\rho_{34})^2}{T^3(\rho_{23}^2+\rho_{33}^2)},$$

$$c = \frac{\rho_{22}^2\rho_{23}^2 + \rho_{12}^2(\rho_{23}^2+\rho_{33}^2)}{T^3(\rho_{23}^2+\rho_{33}^2)}\,, \tag{2.62}$$

and therefore are non-negative. The coefficient

$$a = \frac{\rho_{12}\rho_{14}(\rho_{23}^2+\rho_{33}^2) + \rho_{22}\rho_{23}(\rho_{23}\rho_{24}+\rho_{33}\rho_{34})}{T^3(\rho_{23}^2+\rho_{33}^2)}$$

instead has undefined sign. Still one can prove that it is such that the determinant of the matrix M which appears in Eq. (2.23) is non-negative. Indeed we have

$$\det(M) = \frac{(-\rho_{14}\rho_{22}\rho_{23} + \rho_{12}\rho_{23}\rho_{24} + \rho_{12}\rho_{33}\rho_{34})^2}{T^6(\rho_{23}^2+\rho_{33}^2)}\,, \tag{2.63}$$

which, together with the positivity of b and c entails that M is semi-positive definite.

The same procedure can be used to study the sign of the constants C_1, C_2 and C_{12} defined in Eqs. (2.34), (2.35), and (2.36), respectively. As it is shown here below, C_1 and C_2 are always non-negative, while C_{12} has undefined sign:

$$\begin{aligned}
C_1 &= \frac{2[(\delta\rho_{22}\rho_{33} + \rho_{24}\rho_{33} - \rho_{23}\rho_{34})^2 + (\rho_{23}^2+\rho_{33}^2)\rho_{44}^2]}{\rho_{22}^2\rho_{33}^2}\,,\\
C_2 &= \frac{2[(\delta\rho_{22}\rho_{33} + \rho_{24}\rho_{33} - \rho_{23}\rho_{34})^2 + (\rho_{23}^2+\rho_{33}^2)\rho_{44}^2]}{(\rho_{24}\rho_{33} - \rho_{23}\rho_{34})^2 + (\rho_{23}^2+\rho_{33}^2)\rho_{44}^2}\,,\\
C_{12} &= \frac{(\rho_{22}\rho_{33} + \delta\rho_{24}\rho_{33} - \delta\rho_{23}\rho_{34})^2 + \delta^2(\rho_{23}^2+\rho_{33}^2)\rho_{44}^2}{\rho_{22}\rho_{33}(\rho_{24}\rho_{33} - \rho_{23}\rho_{34})}.
\end{aligned} \tag{2.64}$$

2.C Calculation of the Onsager coefficients

For a three-terminal configuration, as in the previous sections, we choose the right reservoir 3 as the reference ($\mu_3 = \mu = 0$, $T_3 = T$), and characterize the problem in terms of the particle/heat currents flowing in linear response between the system and leads 1 (held at $\mu_1 = \mu + \Delta\mu_1$ and $T_1 = T + \Delta T_1$) and 2 (held at $\mu_2 = \mu + \Delta\mu_2$ and $T_2 = T + \Delta T_2$). The Onsager's coefficients are obtained from the linear expansion of the currents J_i^c and J_i^h ($i = 1, 2$) given by Eqs. (2.40) and (2.41). They can be written in terms of the transmission probabilities $\mathcal{T}_{ij}$, $i, j \in \{1, 2, 3\}$ as

$$
\begin{aligned}
L_{11} &= \frac{T}{h}\int dE\ (-\partial_E f)\,(\mathcal{T}_{12}+\mathcal{T}_{13}),\\
L_{12} &= \frac{T}{h}\int dE\ (-\partial_E f)\,(E-\mu)(\mathcal{T}_{12}+\mathcal{T}_{13}) = L_{21},\\
L_{13} &= \frac{T}{h}\int dE\ (-\partial_E f)\,(-\mathcal{T}_{12}) = L_{31},\\
L_{14} &= \frac{T}{h}\int dE\ (-\partial_E f)\,(-(E-\mu)\mathcal{T}_{12}) = L_{41},\\
L_{22} &= \frac{T}{h}\int dE\ (-\partial_E f)\,(E-\mu)^2(\mathcal{T}_{12}+\mathcal{T}_{13}),\\
L_{23} &= \frac{T}{h}\int dE\ (-\partial_E f)\,(-(E-\mu)\mathcal{T}_{12}) = L_{32},\\
L_{24} &= \frac{T}{h}\int dE\ (-\partial_E f)\,(-(E-\mu)^2\mathcal{T}_{12}) = L_{42},\\
L_{33} &= \frac{T}{h}\int dE\ (-\partial_E f)\,(\mathcal{T}_{12}+\mathcal{T}_{23}),\\
L_{34} &= \frac{T}{h}\int dE\ (-\partial_E f)\,(E-\mu)(\mathcal{T}_{12}+\mathcal{T}_{23}) = L_{43},\\
L_{44} &= \frac{T}{h}\int dE\ (-\partial_E f)\,(E-\mu)^2(\mathcal{T}_{12}+\mathcal{T}_{23}),
\end{aligned}
\tag{2.65}
$$

where T is the temperature, f denotes the Fermi-Dirac distribution at μ, and ∂_E is the partial derivative with respect to the energy.

2.C.1 Transmission function of a single-level dot

For a scattering region consisting of a quantum dot with a single energy level, connected to three-terminal, we can express the transmission as a function of the energy [Büttiker1988]

$$
\mathcal{T}_{ij} = \frac{\Gamma_i\Gamma_j}{(E-E_d)^2+\left(\frac{\Gamma}{2}\right)^2}, \qquad (i\neq j), \tag{2.66}
$$

where Γ_i is the contribution to the broadening due to the coupling to lead i, defined by $\Gamma_i = i(\Sigma_i - \Sigma_i^\dagger)$, Σ_i being the self-energy of lead i. In the wide-band limit approximation, we set $\Sigma_i = -i\,\gamma_i/2$, where γ_i does not depend on the energy. Note that this choice leads to the identification $\Gamma_i = \gamma_i$. Furthermore, at the denominator, $\Gamma = \Gamma_1+\Gamma_2+\Gamma_3$ is the total broadening due to the coupling to *all* leads. If we denote $\gamma_1 = \gamma$, $\gamma_2 = c\gamma$, and $\gamma_3 = d\gamma$ the couplings to the three

leads, we obtain for the transmissions the values

$$\begin{aligned}
\mathcal{T}_{12} &= \frac{c\gamma^2}{(E-E_d)^2 + \frac{(1+c+d)^2}{4}\gamma^2} \equiv c\mathcal{T}, \\
\mathcal{T}_{13} &= \frac{d\,\gamma^2}{(E-E_d)^2 + \frac{(1+c+d)^2}{4}\gamma^2} \equiv d\,\mathcal{T}, \\
\mathcal{T}_{23} &= \frac{cd\,\gamma^2}{(E-E_d)^2 + \frac{(1+c+d)^2}{4}\gamma^2} \equiv cd\,\mathcal{T}.
\end{aligned} \tag{2.67}$$

The Onsager coefficients then read as follows:

$$\begin{aligned}
L_{11} &= L_0\,(c+d), \\
L_{12} &= L_1\,(c+d), \\
L_{13} &= -c\,L_0, \\
L_{14} &= -c\,L_1, \\
L_{22} &= L_2\,(c+d), \\
L_{23} &= -c\,L_1, \\
L_{24} &= -c\,L_2, \\
L_{33} &= c\,L_0\,(1+d), \\
L_{34} &= c\,L_1\,(1+d), \\
L_{44} &= c\,L_2\,(1+d),
\end{aligned} \tag{2.68}$$

with $L_n = \frac{T}{h}\int dE\ (-\partial_E f)\,(E-\mu)^n\mathcal{T}$.

The numerical data shown in Sec. 2.3.1 are obtained for $d = 1$, i.e. for $\gamma_1 = \gamma_3 = \gamma$. The two-terminal configuration corresponds to $c = 0$ ($\gamma_2 = 0$), while the coupling to terminal 2 is switched on progressively by increasing c.

Chapter 3

Separation of Heat and Charge Currents for Boosted Thermoelectric Conversion

Complex multi-terminal devices allow in principle to achieve a separate control of the heat and charge currents. The key issue in this context is to assess to which extent this control can be achieved and what are its possible advantages in thermoelectric thermal machines. In this chapter we push to its extreme this type of control and explore a situation where heat and charge currents flow in spatially separated parts of the system. Namely, we will enforce that one of the terminals allows only charge current and another one allows only heat current, and name this regime as *Heat-Charge Current Separation* (HCCS). It is worth stressing already at this point, that the regime of HCCS is realized notwithstanding the fact that the same carriers are responsible for heat and charge flow. As we will discuss in details in the chapter, HCCS can be naturally realized by employing superconducting reservoirs. Nonetheless, this is not a strict requirement: indeed, in principle one could spatially separate heat and charge currents in an all-normal multi-terminal device. In this case, however, a fine tuning of the parameters characterizing the thermoelectric transport needs to be performed thus making the device not easy to realize experimentally.

The three-terminal device which implements HCCS, pictorially shown in Fig. 3.1, is composed of a generic conductor connected to a superconducting reservoir (S), a normal metal reservoir (N) and a second normal reservoir whose chemical potential is set to inhibit the flow of electrical current, thus acting as a

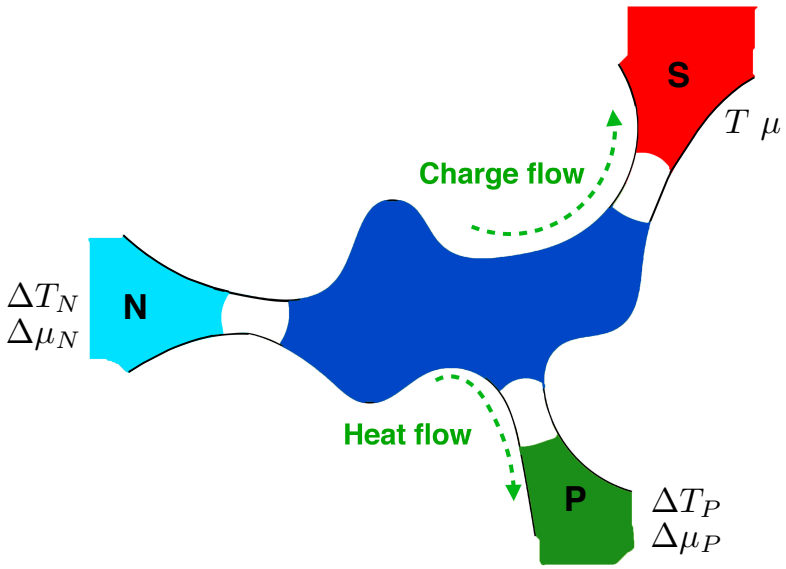

Figure 3.1 – The heat-charge current separation scheme. A generic scattering region is connected to three reservoirs labeled by the letters S (superconducting lead), P (voltage probe) and N (normal metal lead). In the main text we assume the superconducting reservoir (S) to be the reference. In any case, as pointed by the arrows, only charge flows inside lead S whereas only heat flows inside lead P.

voltage probe (P). This setup, to which we will refer to as SPN, *naturally* realizes heat-charge current separation. Indeed, a voltage probe exchanges (on average) by definition only heat (energy) with the system, whereas the superconductor, being a poor heat conductor for temperatures below the gap, can exchange only charges. This way, the heat and charge currents, flowing together out of the normal metal reservoir (N), are split and driven either towards the voltage probe (heat), or towards the superconducting reservoir (charge). In the linear response regime this setup has the advantage of admitting an effective description in terms of a 2×2 Onsager matrix, a feature which allows *inter alia* a natural way of comparing its performance to that of a standard two-terminal configuration. Using the scattering approach, we will show on general grounds that this separation allows, in the linear response regime and at small temperatures, to greatly enhance the performance of a thermal machine, namely increasing both the efficiency and the output power by roughly one order of magnitude with respect to a standard two-terminal counterpart. The root of this enhanced efficiency can be traced back to the possibility to violate in a controlled fashion the Wiedemann-Franz law in the heat-charge separation regime. On more general grounds it is worth to stress that the simultaneous presence of superconducting *and* normal terminals,

by selectively controlling the heat and charge flows through normal and Andreev scattering, introduces new degrees of freedom that are worth being explored for thermoelectric conversion.

The chapter is organized as follows: in Section 3.1 we introduce the necessary formalism and define the regime of heat-charge current separation. We then show how this regime can be attained by having one of the three terminals in the superconducting state. In order to test the performance of this thermal engine we perform an extensive analysis in Section 5.2, by varying the properties of the scattering region connecting the three reservoirs. By properly parametrizing the scattering matrix we sample randomly the scatterer and compare the efficiency of the HCCS thermal machine with that of a "conventional" two-terminal setup (Sections 3.2.1 and 3.2.2). We complete our analysis in Section 3.2.3 by discussing the case of systems consisting of quantum dots (QDs). The reason to study these examples in detail is to show that it is possible to achieve, in experimentally realizable situations, those enhanced performances that we found in the first part of Section 3.2.2. Indeed we see that our theoretical findings can be tested with current experimental capabilities. Section 3.3 is devoted to the concluding remarks. Some technical details related to the scattering formalism in the presence of Andreev scattering are summarized in the Appendices.

3.1 Heat-charge current separation

Let us consider a system composed of a conductor attached to three leads. Within the linear response regime charge and heat currents are governed by the Onsager matrix $\mathbf{L}$ via the relation

$$\begin{pmatrix} J_N^c \\ J_N^h \\ J_P^c \\ J_P^h \end{pmatrix} = \begin{pmatrix} L_{11} & L_{12} & L_{13} & L_{14} \\ L_{21} & L_{22} & L_{23} & L_{24} \\ L_{31} & L_{32} & L_{33} & L_{34} \\ L_{41} & L_{42} & L_{43} & L_{44} \end{pmatrix} \begin{pmatrix} X_N^\mu \\ X_N^T \\ X_P^\mu \\ X_P^T \end{pmatrix}, \tag{3.1}$$

where J_i^c (J_i^h) represent the charge (heat) current entering the conductor from lead i, with i = (N, P), see Fig. 3.1. We define the biases $X_i^\mu = \Delta\mu_i/T = (\mu - \mu_i)/T$ and $X_i^T = \Delta T_i/T^2 = (T - T_i)/T^2$, where μ_i and T_i are the chemical potential and temperature, respectively, relative to reservoir i =N,P and having chosen the reservoir S as reference with temperature T and chemical potential μ. Heat and charge currents flowing in lead S can be determined from the conservation of particle and energy currents. As already mentioned, HCCS consists in spatially separating heat and charge flows. In the example of Fig. 3.1 heat will only flow in lead P while charge will only flow in lead S. In this section we characterize this regime and discuss how to implement it.

On general grounds HCCS can be realized whenever two "probe" terminals are present [Gramespacher1997], one for the voltage and one for the temperature. In

fact, a voltage probe is a terminal whose voltage is adjusted in order for the charge current to vanish, while a temperature probe is a terminal whose temperature is adjusted in order for the heat current to vanish (see Appendix 3.A). Unlike a voltage probe, which is implemented simply by opening the electric circuit, making a thermal probe would require the ability to control and measure heat currents which is still very challenging in practice (although important advancements in the measurements of heat currents at the nanoscale have been recently achieved, see Refs. [Blanc2013, Meier2014]). A natural way of realizing HCCS is to replace the thermal probe with a superconducting lead which intrinsically suppresses the heat flow for low enough voltages and temperatures. On the contrary a normal metal-superconductor interface is an excellent electrical conductor due to the Andreev process that allows to carry charge current in the sub-gap regime. In the following we will detail the working principles of this implementation.

Let us consider Eq. (3.1) and take the superconducting reservoir as the reference. Assuming temperatures much smaller than the superconducting gap and using the scattering formalism one can demonstrate that the coefficients on the fourth row (column) of the Onsager matrix Eq. (3.1) are the opposite of the corresponding coefficients on the second row (column). This implies that $J_N^h = -J_P^h$ which, at first order in linear response, yields $J_S^h = 0$ by virtue of the energy conservation. In other words, it is an intrinsic property of the hybrid scattering matrix to have vanishing heat current in the superconducting lead. These observations allow us to simplify the Onsager system of equations by eliminating the redundant forth row and column, thus reducing it to a 3 by 3 problem:

$$\begin{pmatrix} J_N^c \\ J_N^h \\ J_P^c \end{pmatrix} = \begin{pmatrix} L_{11} & L_{12} & L_{13} \\ L_{21} & L_{22} & L_{23} \\ L_{31} & L_{32} & L_{33} \end{pmatrix} \begin{pmatrix} X_N^\mu \\ X^T \\ X_P^\mu \end{pmatrix}, \tag{3.2}$$

where we have introduced $X^T = X_N^T - X_P^T$ (or equivalently $\Delta T = \Delta T_N - \Delta T_P$). Now we impose the voltage probe condition $J_P^c = 0$ on reservoir P, which yields

$$X_P^\mu = -\frac{L_{31} X_N^\mu + L_{32} X^T}{L_{33}}. \tag{3.3}$$

By substituting Eq. (3.3) into Eq. (3.2) one obtains a two-terminal-like Onsager matrix:

$$\begin{pmatrix} J_N^c \\ J_N^h \end{pmatrix} = \begin{pmatrix} L'_{11} & L'_{12} \\ L'_{21} & L'_{22} \end{pmatrix} \begin{pmatrix} X_N^\mu \\ X^T \end{pmatrix}. \tag{3.4}$$

For the sake of simplicity, in the following we drop the primes for the Onsager coefficients L'_{ij} in Eq. (3.4). From the definitions of the local [Benenti2013] and non-local [Mazza2014] transport coefficients, one can introduce (local) conductances and (non-local) thermopowers described by the following two-terminal-like expressions:

$$G = \left(\frac{eJ_N^c}{\Delta\mu_N}\right)_{\Delta T=0} = \frac{L_{11}}{T}, \tag{3.5}$$

$$S = -\left(\frac{\Delta\mu_N}{e\,\Delta T}\right)_{J_N^c=0} = \frac{1}{T}\frac{L_{12}}{L_{11}}, \tag{3.6}$$

$$K = \left(\frac{J_N^h}{\Delta T}\right)_{J_N^c=0} = \frac{1}{T^2}\frac{L_{11}L_{22} - L_{21}L_{12}}{L_{11}} \tag{3.7}$$

Importantly, we can express the efficiency for heat to work conversion with the standard two-terminal formula [Benenti2013]

$$\eta = \frac{-X_N^\mu J_N^c}{J_N^h} = \frac{-L_{11}(X_N^\mu)^2 - L_{12}X_N^\mu X_P^T}{-L_{21}X_N^\mu - L_{22}X_P^T}. \tag{3.8}$$

One can also define the figure of merit $ZT = (GS^2/K)\,T$ and the power factor $Q = GS^2$. The former gives information about the maximum efficiency and the efficiency at maximum power [Curzon1975, Broeck2005] $\eta(\dot{W}_{\max}) = (\eta_C/2)\,ZT/(ZT+2)$, $\eta_C = 1-\Delta T/T$ being the Carnot efficiency, while the latter about the maximum power $\dot{W}_{\max} = Q(\Delta T)^2/4$. With these formulas the analogy between the SPN system and the two-terminal one is complete, allowing us to compare their performance.

3.2 HSSC in hybrid devices

As we shall show in this section, the heat-charge separation implemented through the SPN setup allows to control G and K separately. This will be at the origin of the enhancement of both the figure of merit ZT and the power factor Q with respect to the two-terminal setup. We will use the Landauer-Büttiker scattering formalism [Büttiker1986, Landauer1957], which is summarized in Section 1.4 for multi-terminal hybrid superconducting systems. We begin our analysis by considering low temperatures (within the Sommerfeld expansion) and studying a well-defined class of scattering matrices. Quasiparticle transmission from the normal leads into the superconductor is exponentially suppressed and thus can be ignored. Thus the scattering probabilities just involve reservoirs N and P.

In the following we will express the conductances (electrical and thermal) as well as the thermopower as functions of the parameters characterizing the scattering matrix. The aim is to sample this parameter space in order to make a statistical analysis of the thermoelectric performance. Assuming a single channel per spin per lead, in the Bogoliubov-de Gennes formalism (see Section 1.4) the total scattering matrix $\mathbf{S_{tot}}$ is 8×8. Supposing that there are no spin-mixing terms, it can be written in a diagonal block form $\mathbf{S}_{tot} = \begin{pmatrix} \mathbf{S} & 0 \\ 0 & \mathbf{S}' \end{pmatrix}$, where the basis is $(c_{\uparrow,N}, c_{\uparrow,P}, c^\dagger_{\downarrow,N}, c^\dagger_{\downarrow,P}, c^\dagger_{\uparrow,N}, c^\dagger_{\uparrow,P}, c_{\downarrow,N}, c_{\downarrow,P})$, where the operator $c_{\sigma,i}$ ($c^\dagger_{\sigma,i}$) destroys (creates) an electron with spin σ in lead $i = (N, S, P)$. The matrices $\mathbf{S}$ and $\mathbf{S}'$ are related by the particle-hole symmetry relations (see Section 1.4), so that assigning the elements of $\mathbf{S}$ is sufficient to know the whole $\mathbf{S}_{tot}$. For sake

of simplicity we will consider symmetric unitary matrices. A parametrization of such class of matrices is given by

$$\mathbf{S} = \begin{pmatrix} g_1\mathbf{S}_1 & g_2\mathbf{S}_2 \\ g_2\mathbf{S}_2^{\mathrm{T}} & g_3\mathbf{S}_3 \end{pmatrix}, \tag{3.9}$$

where $\mathbf{S}_1$ and $\mathbf{S}_3$ are 2×2 symmetric unitary matrices, $\mathbf{S}_2$ is a 2×2 unitary matrix, $\mathbf{S}_3 = \mathbf{S}_2^T\mathbf{S}_1^*\mathbf{S}_2$ and g_1, g_2, g_3 are such that the matrix $\begin{pmatrix} g_1 & g_2 \\ g_2 & g_3 \end{pmatrix}$ is unitary. For the sake of simplicity we assume the latter to be real, i.e. it can be written as $\begin{pmatrix} g(E) & \sqrt{1-g(E)^2} \\ \sqrt{1-g(E)^2} & -g(E) \end{pmatrix}$, where we made explicit the dependence on the energy E. Furthermore, we parametrize $\mathbf{S}_1$ and $\mathbf{S}_2$ as

$$\mathbf{S}_1 = \begin{pmatrix} -\rho_1(E)\,\mathrm{e}^{i(\theta_1+2\beta_1)} & \sqrt{1-\rho_1(E)^2}\,\mathrm{e}^{i\beta_1} \\ \sqrt{1-\rho_1(E)^2}\,\mathrm{e}^{i\beta_1} & \rho_1(E)\,\mathrm{e}^{-i\theta_1} \end{pmatrix} \tag{3.10}$$

and

$$\mathbf{S}_2 = \begin{pmatrix} -\rho_2(E)\,\mathrm{e}^{i(\theta_2+\beta_2+\gamma_2)} & \sqrt{1-\rho_2(E)^2}\,\mathrm{e}^{i\beta_2} \\ \sqrt{1-\rho_2(E)^2}\,\mathrm{e}^{i\gamma_2} & \rho_2(E)\,\mathrm{e}^{-i\theta_2} \end{pmatrix}, \tag{3.11}$$

assuming the phases in the matrices to be energy independent. The last simplification that we impose is the following relation between the phases: $\beta_2+\theta_2 = \beta_1+\theta_1+\frac{\pi}{2}$. Within this parametrization we assume θ_1, β_1, θ_2, β_2, and γ_2 to be real numbers and $g(E)$, $\rho_1(E)$ and $\rho_2(E)$ to be real functions of energy such that $0\le g(E)$, $\rho_1(E)$, $\rho_2(E)\le 1$ for any E. With this notation and using the expressions for the Onsager coefficients in the Landauer-Büttiker approach given in Section 1.4, the Sommerfeld expansion yields the following transport coefficients [see Eqs. (3.5)-(3.7)]:

$$\begin{aligned} G &= 8 - 8g(0)^2 \\ &+ \frac{8(-1+g(0)^2)^2}{-1-\rho_2(0)^2+g(0)^2(\rho_1(0)^2+(3-2\rho_1(0)^2)\rho_2(0)^2+2(-1+\rho_1(0)^2)\rho_2(0)^4)} \end{aligned} \tag{3.12}$$

$$\begin{aligned} S = 2\frac{\pi^2 T g(0)\rho_2(0)\big[-\rho_2(0)(-1+\rho_2(0)^2)\big[(-1+\rho_1(0)^2)g'(0)+g(0)\rho_1(0)\rho_1'(0)\big]}{-3\rho_2(0)^2+3g(0)^2(-1+\rho_1(0)^2+(3-2\rho_1(0)^2)\rho_2(0)^2+2(-1+\rho_1(0)^2)\rho_2(0)^4)} \\ - \frac{g(0)(-1+\rho_1(0)^2)(-1+2\rho_2(0)^2)\rho_2'(0)\big]}{-3\rho_2(0)^2+3g(0)^2(-1+\rho_1(0)^2+(3-2\rho_1(0)^2)\rho_2(0)^2+2(-1+\rho_1(0)^2)\rho_2(0)^4)}, \end{aligned} \tag{3.13}$$

$$K = -\frac{2\pi^2 T}{3}\Big[-1+\rho_2(0)^2+g(0)^2\big(\rho_2(0)^2-2\rho_2(0)^4+\rho_1(0)^2\big(1-2\rho_2(0)^2+2\rho_2(0)^4\big)\big)\Big], \tag{3.14}$$

where the primed quantities are derivatives with respect to energy. After the choices we made, we are left with six parameters [namely, $\rho_1(0)$, $\rho_1'(0)$, $\rho_2(0)$, $\rho_2'(0)$, $g(0)$, $g'(0)$] to control G, S and K. We stress that we do not impose time reversal symmetry on the

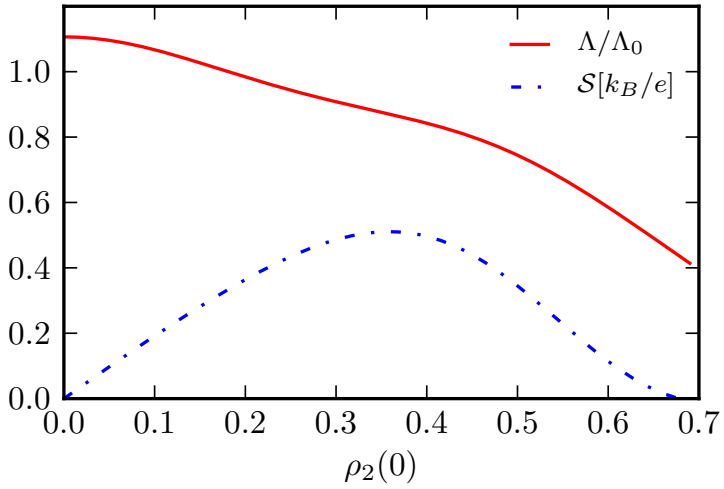

Figure 3.2 – Plot of the ratio Λ/Λ_0 and thermopower S for fixed $K = 10\,(3k_BT)/\pi^2 h$ as a function of $\rho_2(0)$. Here we show that using only one parameter $[\rho_2(0)]$ we cannot control separately the thermopower and the ratio $\Lambda = K/(GT)$. The other parameters are: $\rho_1(0) = 0.8$, $g'(0) = 0.001(k_BT)^{-1}$, $\rho_1'(0) = 0.03(k_BT)^{-1}$ and $\rho_2'(0) = 0.3(k_BT)^{-1}$.

scattering matrix $\mathbf{S}$, Eq. (3.9), although our parametrization gives rise to a symmetric Onsager matrix[1].

At this point we would like to draw the attention to the fact that the transport coefficients G, S and K are independent in a parameter region that is defined by the constraints imposed by the unitarity of the scattering matrix and from the Sommerfeld expansion. The independence of the transport coefficients can be appreciated from the way the six parameters, needed to parametrize the scattering matrix, enter Eqs. (3.12)-(3.14). Indeed, if the value of K in Eq. (3.14) is fixed, the value of G given by Eq. (3.12) is not automatically determined, but instead it can be controlled by exploiting the other parameters. The same applies to S when G and K are fixed.

We shall now discuss how the performance of the SPN system depends on these parameters. It is indeed important to verify if: i) HCCS is an advantage for thermoelectric conversion, ii) in the regime of HCCS the enhancement of the performance is generic or it requires additional fine tuning. In order to assess the above issues we will first analyze to which extent heat and charge can be controlled independently and then we will study the figure of merit as a function of the parameters characterizing the scattering matrix. Since we have to deal with six free parameters our analysis will be of statistical nature.

[1] Note that spin-dependent effects are included in this parametrization.

3.2.1 Control of heat and charge currents

Our strategy to test our ability to control the currents in the three-terminal device is to use, in the same spirit as in the Wiedemann-Franz law, the ratio between heat and electrical conductances. Using Eqs. (3.12) and (3.14) we can now calculate $\Lambda = K/(GT)$ which can be seen by inspection not to be a constant, hence violating the Wiedemann-Franz law. Note that both G and K depend only on the coefficients $\rho_1(0)$, $\rho_2(0)$, and $g(0)$. In Fig. 3.2 we plot, for a fixed value of K, the dimensionless ratio Λ/Λ_0 and the thermopower S as functions of the parameter $\rho_2(0)$. More precisely, after fixing K we extract from Eq. (3.14) the parameter $g(0)$ which is a function of $K, \rho_1(0)$, $\rho_2(0)$ and substitute it into Eq. (3.12). Moreover, we impose the condition that the next order in the Sommerfeld expansion is much smaller than the one we take into account, restricting the range of admissible values of the other parameters (e.g. $\rho_2(0)$ can at most be 0.7). For applying this condition we have to specify the values of the derivatives $g'(0)$, $\rho_1'(0)$ and $\rho_2'(0)$ even though they do not appear in Eqs. (3.12) and (3.14). We assume higher order derivatives to be zero for simplicity. The plot

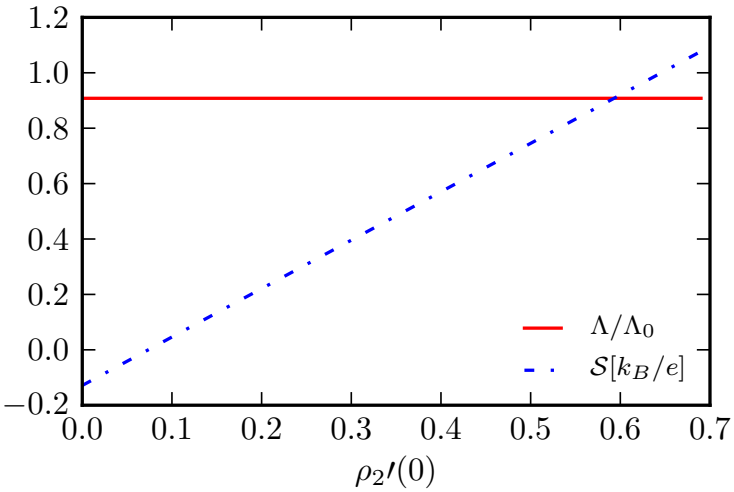

Figure 3.3 – Thermopower S from Eq. (3.13), with $K = 10\,(3k_BT)/\pi^2 h$ as a function of $\rho_2'(0)$ [in units of $(k_BT)^{-1}$]. Using the additional degrees of freedom provided by the derivatives of the parameters [here we use $\rho_2'(0)$], we gain the control of the thermopower S without affecting the ratio Λ. The other parameters are: $\rho_1(0) = 0.8$, $g'(0) = 0.001(k_BT)^{-1}$, and $\rho_1'(0) = 0.1(k_BT)^{-1}$.

shows that Λ is not a constant, but can be controlled by properly tuning the parameters of the scattering matrix. Moreover, Fig. 3.2 shows that S changes by varying $\rho_2(0)$ for fixed K. The controllability of the transport coefficients can be further increased by fixing the values of both K and Λ using the parameters $\rho_1(0)$ and $\rho_2(0)$, and tuning the derivatives to change the thermopower. This is shown in Fig. 3.3 where Λ and S are plotted as a function of $\rho_2'(0)$. Notably S spans a quite large interval of values, even changing sign. We conclude that the SPN system allows independent control of G, K

and S. This enhanced control is at the basis of the better performance that we are going to describe in the next Section.

3.2.2 Thermoelectric performance

In this section we compare on a statistical ground the thermoelectric performance of the SPN system with that of a generic two-terminal normal system by randomly generating the parameters of the scattering matrices and calculating the corresponding power factor Q and figure of merit ZT. Within the low temperature limit (Sommerfeld expansion),

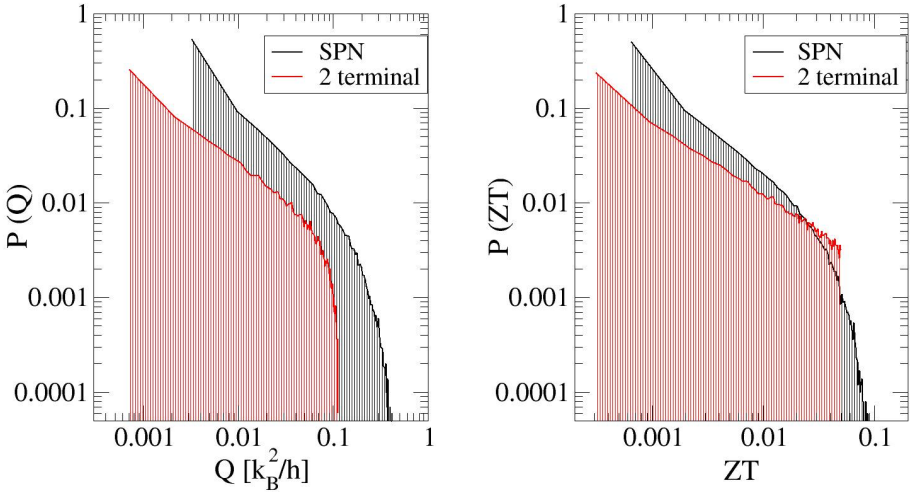

Figure 3.4 – (left) Probability histogram of the power factor $Q = GS^2$ [in units of k_B^2/h] for the SPN system (black curve) and for the corresponding normal two-terminal system (red curve). The maximum value of Q for the SPN setup is about 0.5 k_B^2/h, while it is about 0.2 k_B^2/h for the two-terminal case. (right) Probability histogram of the figure of merit ZT for the SPN system (black curve) and for the corresponding normal two-terminal case (red curve). The maximum of the SPN setup is just above 0.1, while it is about 0.05 for the two-terminal system.

we perform a numerical simulation generating the parameters of the scattering matrix, of both the two-terminal and the SPN systems. Such parameters are picked within a uniform distribution in the allowed ranges given by the conditions imposed by the unitarity of the scattering matrix[2] and the Sommerfeld expansion. In Fig. 3.4 we plot

[2]Unitarity requires that the functions $g(E)$, $\rho_1(E)$ and $\rho_2(E)$ are smaller than unity for any energy E. This implies the following condition on their derivatives with respect to energy: $\tau'(E) \leq [1 - \tau(E)]/c$, where $\tau = g, \rho_1, \rho_2$ and c is an energy scale. The same holds for the transmission amplitude of the two-terminal setup $t(E)$.

the probability of occurrence of a certain value of Q (left panel) and ZT (right panel). The plot shows that the SPN system (black histograms) has better performance than the normal two-terminal system (red histograms) for both the power factor Q and the figure of merit ZT. Indeed, the maximum value of Q for the SPN system is about 0.5 k_B^2/h, while it is about 0.2 k_B^2/h for the two-terminal one. The maximum of ZT for the SPN system is just above 0.1, while it is about 0.05 for the two-terminal system. In Fig. 3.5 we plot the correlations between Q and ZT for the same random data. Each point in the plot corresponds to a particular realization of the scattering matrix of the two-terminal or the SPN system, for which the power factor and the figure of merit are calculated.

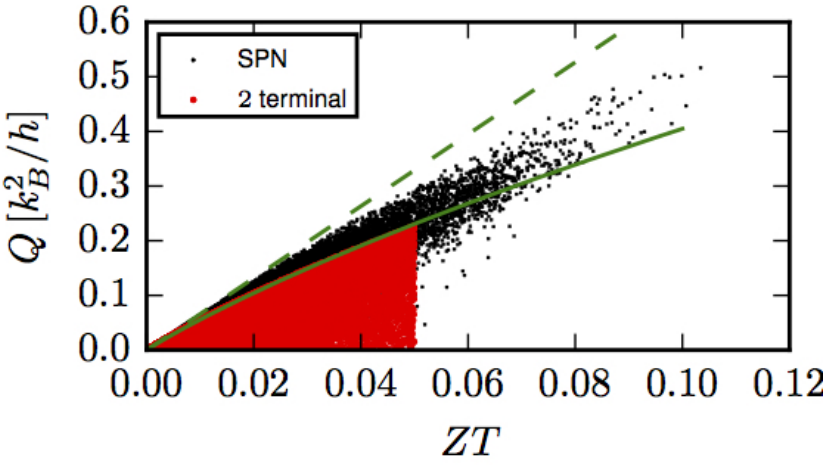

Figure 3.5 – Correlation between the values of Q and ZT for the same data as for Fig. 3.4: each point corresponds to a given random realization. Red (black) points are relative to the two-terminal (SPN) setup. The green dashed curve represents the bound of Eq. (3.15), that holds for both the SPN and the two-terminal system. The green solid curve, instead, represents the bound of Eq. (3.16), that is the stronger bound given by the unitarity on the two-terminal system.

Fig. 3.5 shows that the distribution of points presents a triangular-like shape for the two-terminal setup. An upper bound on the power factor Q is given by the unitarity of the scattering matrix. In fact, Q and ZT are related by the thermal conductance as $Q = (K/T)ZT$ and, under the Sommerfeld expansion, K is proportional to the probability of transmission of an electron from lead N to P, which cannot exceed unity. This yields an upper bound given by

$$Q \leq \frac{2\pi^2 k_B^2 ZT}{3h}. \tag{3.15}$$

This is actually true for both the two-terminal and the SPN systems. For the two-terminal system a stronger bound, which produces the curvature of the upper side of

the "triangle", is given by the constraint that must be imposed on the derivative of the transmission amplitude with respect to energy imposed by unitarity of the scattering matrix. This implies the following expression for the maximum of Q

$$Q_{\max} = \frac{2e^2}{h}\Lambda_0 ZT\left(1+\frac{c}{eT}\sqrt{\frac{ZT}{\Lambda_0^2}}\right)^{-2}, \tag{3.16}$$

where c is a given energy scale of the order of k_BT. Furthermore, for the two-terminal system the power factor Q can take all the values between 0 and $Q_{\max}$, thus filling the red "triangle" of Fig. 3.5. On the other hand, in the case of the SPN system the points are concentrated just below the line of the maximum. This is due to the fact that the value of K/T, given by Eq. (3.14), cannot take all the values between 0 and $2\pi^2 k_B^2/(3h)$ because of the constraints imposed on, and the relations between, the parameters appearing in the expression.

The bound on the maximum value of ZT, instead, is given by the conditions on the higher orders of Sommerfeld expansion, that here we impose to be at least 10 times smaller that the leading orders for both the two-terminal and the SPN system. It is interesting to notice that for the SPN system the points with the highest power factor Q are also the points with the highest figure of merit ZT: the maximum power automatically gives the maximum efficiency! In particular the points with the best thermoelectric performance for the SPN system roughly correspond to the following values of the scattering probabilities: normal reflection in lead N, $R \simeq 0$; normal transmission from lead N to lead P, $\mathcal{T} \simeq \frac{1}{4}$; Andreev reflection in lead N, $R_A \simeq \frac{3}{16}$; and Andreev transmission from lead N to lead P, $\mathcal{T}_A \simeq \frac{9}{16}$.

3.2.3 Coupled QDs in the SPN setup

We complete our analysis by assessing the thermoelectric performance of a specific SPN system composed of three coupled single-level (non-interacting) QDs ("tridot") connected to a normal lead (N), a voltage probe (P) and a superconducting lead (S), see Fig. 3.6.

The Hamiltonian describing the "tridot" reads

$$H = \begin{pmatrix} H_e & \mathbb{1}\Delta \\ \mathbb{1}\Delta^* & H_h \end{pmatrix} \tag{3.17}$$

where H_e is the Hamiltonian relative to the electrons degree of freedom, and is given by

$$H_e = \begin{pmatrix} \epsilon_1 & t_{12} & t_{13} \\ t_{12}^* & \epsilon_2 & t_{23} \\ t_{13}^* & t_{23}^* & \epsilon_3 \end{pmatrix}, \tag{3.18}$$

where ϵ_i, $i=(1,2,3)$, is the onsite energy of the $i-$th dot, while t_{ij}, $\{i,j\}=(1,2,3)$, is the coupling between dot $i-$th and dot $j-$th. Notice that $H_h = -H_e^*$ is the Hamiltonian relative to the holes, while $\Delta = 100\ k_BT$ is the superconducting gap. Note that the presence of the S lead is introduced in an effective way, whereby superconductivity is directly included in the Hamiltonian of the "tridot". The crucial point is that the superconductor chemical potential μ is fixed. Furthermore, for simplicity, we

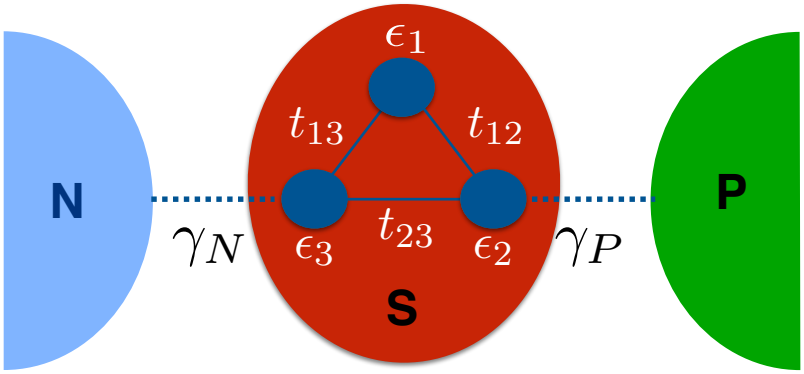

Figure 3.6 – A three coupled QDs ("tridot") system in the SPN setup. γ_N and γ_P label the coupling to the reservoirs N and P, respectively. The three QDs are coupled to a superconducting lead (S), with a fixed chemical potential.

have assumed that the superconducting pairing for all the QDs is equal as though originating from the fact that all QDs are equally coupled to the S lead. In Fig. 3.6, γ_N and γ_P are the coupling energies to the N and P lead, respectively. In order to make a statistical analysis we focus on random Hamiltonians, for the electron sector H_e, drawn from the Gaussian Orthogonal Ensemble (GOE) and from the Gaussian Unitary Ensemble (GUE). The former describe complex physical systems with time reversal symmetry (TRS), while the latter describe complex systems with broken TRS [Beenakker1997, Haake2000, Benenti2011]. The TRS breaking is encoded in the complex part of the Hamiltonian (3.18). However this does not imply the spin degeneracy breaking, since we can apply a small Aharanov-Bohm flux through the plane of the "tridot" (that breaks TRS), without a Zeeman component (that would have removed the spin degeneracy). In both cases (with and without TRS), the elements of H_e are drawn from a Gaussian probability distribution $\mathcal{N}(x, \Delta x)$, where x is the mean and Δx is the variance. We use distributions with different mean for the diagonal elements (QD energy levels) and for the off diagonal elements (couplings between QDs), in order to have a band shift. The former are drawn from a Gaussian probability distribution $\mathcal{N}(k_BT, 10^3 k_BT)$ (mean equal to k_BT, and variance equal to $10^3 k_BT$). The latter are drawn from a Gaussian probability distribution $\mathcal{N}(0, 10^3 k_BT)$. The variance is chosen in order to obtain a smooth energy profile for the transmission probabilities and to be under the Sommerfeld expansion. From the Hamiltonian (3.17) the Green function of the system is calculated for fixed values of γ_N and γ_P. The 4×4 scattering matrix (there is spin degeneracy) is finally calculated from the Green function using the Fisher-Lee relation [Datta1995]. Note that the two-terminal system, to be compared with the SPN setup, is simply described by the Hamiltonian H_e. For each random realization of the Hamiltonian of Eq. (3.17) we compute the power factor Q and the figure of merit ZT. The results are shown in Fig. 3.7, in both the panels each point in the $Q - ZT$ plane represents a single realization. We notice that both Q and ZT are one order of magnitude larger in the SPN case with respect to the two-terminal

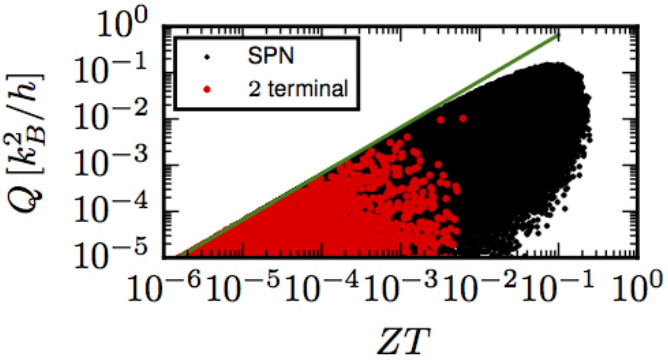

(a)

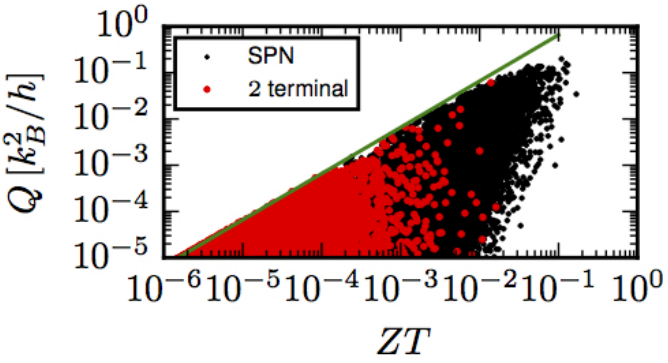

(b)

Figure 3.7 – Correlation between the power factor $Q = GS^2$ and the figure of merit ZT relative to "tridot" systems for the SPN setup (black points) and the two-terminal setup (red points). The green curve corresponds to the bound of Eq. (3.15), given by the unitarity of the scattering matrix and set a maximum value for Q as a function of ZT. In panel (a) we show the correlation for the Gaussian Orthogonal Ensemble (GOE), while in panel (b) for the Gaussian Unitary Ensemble (GUE). Both plots show that for the SPN setup both Q and ZT are one order of magnitude larger with respect to the corresponding values for the two-terminal system. Moreover it is possible to see that the increase of the performance is not due to the breaking of the TRS. The plot refers to 10^5 Hamiltonian realizations, taking $\gamma_N = \gamma_P = \gamma = 10^3\ k_B T$.

configuration for both the GOE Hamiltonian in Fig. 3.7(a), and the GUE Hamiltonian in Fig. 3.7(b). This shows a significant enhancement, on a statistical ground, in the performance of the SPN with respect to the two-terminal system. The distribution of the points is similar to that of Fig. 3.5. Since for the "tridot" model the allowed values of ZT (under Sommerfeld expansion) are much smaller than the values that we obtained from the model in the previous section (see Fig. 3.5), the bound on Q of Eq. (3.16) reduces to that of Eq. (3.15). Instead, the bound on ZT is again set by the Sommerfeld approximation. Here we notice that for the two-terminal system we cannot see the bound given in Eq. (3.16) because of the small values of ZT.

3.3 Summary

In this chapter we have analyzed the performance of a thermal machine which, by involving three reservoirs, allows for the implementation of a spatial separation between heat and charge currents in linear response. Such machine can be naturally realized by connecting a conductor to a superconducting lead, a voltage probe and a normal lead (SPN system). Interestingly, the linear-response transport equations, written in terms of the Onsager matrix, turn out to be formally equal to those of a two-terminal conventional system. Using this property we have made a comparison between the performance of these two thermal machines in terms of the power factor Q (that controls the maximum extracted power), and the figure of merit ZT (that controls the efficiency at maximum power and the maximum efficiency). Within the scattering approach we have described the SPN system with a parametrized scattering matrix. We have shown that in the low temperature limit (where the Sommerfeld expansion holds) the SPN system violates the Wiedemann-Franz law and allows, to some extent, an independent control of electrical conductance, thermal conductance and thermopower (*i.e.* of heat and charge currents). To assess the consequences of this on the thermoelectric performance of the SPN system we have made a statistical analysis by taking random values, over a uniform distribution, of the parameters contained in the scattering matrix. We have thus shown, on statistical grounds, that the SPN system exhibits much larger values of Q and ZT with respect to the two-terminal counterpart. Further improvements (more than one order of magnitude) of the thermoelectric performance of the SPN setup has been confirmed on a specific physical system composed of three coupled quantum dots. We believe that our results can be relevant in the experimental activity on thermoelectricity of nanoscale structures, which are typically conducted at low temperatures.

3.A Voltage- and temperature-probe setup

By imposing the thermal probe condition $J_N^h = 0$ on reservoir N and the voltage probe condition $J_P^c = 0$ on reservoir P, one can solve the second and third rows of Eq. (3.1) for the two biases X_N^T and X_P^μ, that will not depend directly on the currents J_N^c and J_P^h, and find:

$$\begin{pmatrix} X_N^T \\ X_P^\mu \end{pmatrix} = - \begin{pmatrix} L_{22} & L_{23} \\ L_{32} & L_{33} \end{pmatrix}^{-1} \begin{pmatrix} L_{21} & L_{24} \\ L_{31} & L_{34} \end{pmatrix} \begin{pmatrix} X_N^\mu \\ X_P^T \end{pmatrix}. \tag{3.19}$$

From the first and forth rows of Eq. (3.1) one can define an effective two-terminal-like Onsager matrix, with

$$\begin{pmatrix} J_N^c \\ J_P^h \end{pmatrix} = \begin{pmatrix} L'_{11} & L'_{12} \\ L'_{21} & L'_{22} \end{pmatrix} \begin{pmatrix} X_N^\mu \\ X_P^T \end{pmatrix}, \tag{3.20}$$

where the primed Onsager coefficients are obtained by substituting the expressions of Eq. (3.19) into Eq. (3.1). What has been given above should be considered as a definition of HCCS and not a way to implement it.

Chapter 4

Magnetic Thermal Switch for Heat Management at the Nanoscale

Heat management at the nanoscale is nowadays one of the leading research topics since to the overheating of microprocessor components is currently [Fagas2014] the most limiting factor in the development of information technology, which motivates the concern in finding alternative ways to control and evacuate heat in such devices. Controlling the heat flows in a nanostructure would be os extreme importance in many different scientific areas, including refrigeration and thermometry [Giazotto2006], coherent caloritronics [Martínez-Pérez2014], heat rectification [Martínez-Pérez2015], thermoelectric energy conversion [Snyder2008, Shakouri2011, Benenti2013, Jordan2013, Sánchez2013, Sothmann2014], and information processing by utilizing phonons [Li2012].

Theoretical works led to the possibility of controlling the heat currents and devise heat diodes [Terraneo2002] and transistors [Li2006]. First experimental implementations exploiting phononic [Chang2006, Kobayashi2009, Tian2012], electronic [Scheibner2008, Martínez-Pérez2014, Saira2007], or photonic [Chen2014] thermal currents were also reported.

It has been shown that the presence of a magnetic field breaking time reversibility could in principle enhance the thermoelectric efficiency [Benenti2011, Saito2011, Balachandran2013, Sánchez2015a, Sánchez2015b, Brandner2013a, Brandner2013b]. Interestingly a magnetic field allows for the simultaneous presence of reversible and irreversible heat currents. Indeed, in a generic multi-terminal setup, we can split the heat current J_k^h, flowing from the k-th terminal to the system, into the sum of a reversible and an irreversible part, $J_k^h = J_k^{h(r)} + J_k^{h(i)}$. Although the reversible component changes sign by reversing the magnetic field $\mathbf{B}$, the irreversible component is invariant under the inversion $\mathbf{B} \to -\mathbf{B}$. Within the linear response regime, it can be shown that only the irreversible part of the current contributes to the entropy production. On the other hand the reversible part vanishes for $\mathbf{B} = \mathbf{0}$, whereas for $\mathbf{B} \neq \mathbf{0}$ it becomes

arbitrarily large, giving rise, among other things, to the possibility of dissipationless transport, i.e., to a thermal machine operating at the Carnot efficiency with finite power output [Benenti2011].

We take advantage of the presence of reversible components of the heat currents to propose a magnetic thermal switch, a Boolean setup which allows the control of heat flow by making use of an external magnetic field as a selector of the working configuration. For a generic multi-terminal device operating in the linear response regime, we show that by properly tuning the voltage biases we can access a broad spectrum of possible operating conditions, each of these being defined in terms of the behavior of the heat currents flowing through the system. Namely, it is possible to design a *programmable* device for the management of heat flows, allowing several Boolean features, such as selected splitting, on/off switching, reversal and swap of the heat currents. For each feature, the magnetic field acts as a knob selecting one of the two possible working conditions, without the need to modify the reservoirs parameters (temperatures and electrochemical potentials): The switching from one working condition to the other is obtained by inverting the direction of the magnetic field.

A significant advantage of our approach is the absence of temperature constraints: As long as the system operates in linear response, our results hold. In particular, the method we present is valid whether the heat is transported by electrons, by phonons, or by both. Thus, remarkably, it constitutes a possible way of manipulating phononic heat currents using a magnetic field. From a practical point of view, the implementation of our theoretical results would require a full characterization of the Onsager matrix, the major difficulty being the measurement of the heat currents at the nanoscale, a challenge for which, however, important advances have been recently reported [Blanc2013, Meier2014]. Moreover, assuming the system in contact with regions having finite thermal capacitance rather than with ideally infinite reservoirs, the magnetic field switching could be used to control the temperatures of such regions, allowing for instance the initialization of qubit states or the implementation of thermal logic gate operations [Li2012]. We finally remark that there exists, in the literature, a variety of works on interferometer-based systems which, under broken time-reversal symmetry, would constitute natural physical realizations of our model (see, for instance, Refs. [Ji2003, Neder2006, Neder2007, Roulleau2007, Giovannetti2008, Deviatov2008, Altimiras2010, Hofer2015, Sothmann2014, Sánchez2015a, Sánchez2015b]).

The chapter is structured as follows: In Section 4.1 we describe the theoretical implementation of the magnetic thermal switch for a general multi-terminal setup. Then in Section 4.2 we present some results of numerical simulations using an interferometer in contact with three reservoirs as a toy model. Finally, we draw our conclusions in Section 4.3. Details of the calculations and the derivation of the scattering matrix of the interferometer are gathered in Appendix 4.3.

4.1 Magnetic thermal switch

In this section we discuss how a magnetic thermal switch can be implemented in a general multi-terminal setup. Let us consider a generic system in contact with n reservoirs at temperatures $T_k = T + \Delta T_k$ and electrochemical potentials $\mu_k = \mu + \Delta\mu_k$, T and μ being some equilibrium (reference) values. Let $\mathbf{J}_k = (J_k^c, J_k^h)$ denote the particle (J_k^c)

and heat (J_k^h) currents from the k-th terminal to the system and $\mathbf{X}_k = (X_k^\mu, X_k^T) = (\Delta\mu_k/T, \Delta T_k/T^2)$ the conjugated affinities. Within linear irreversible thermodynamics, the fluxes $\mathbf{J} = (\mathbf{J}_1, ..., \mathbf{J}_{n-1})^T$ and the conjugated affinities $\mathbf{X} = (\mathbf{X}_1, ..., \mathbf{X}_{n-1})^T$ are related as follows:

$$\mathbf{J} = \mathbf{L}\,\mathbf{X}, \tag{4.1}$$

where $\mathbf{L}$ is the Onsager matrix of kinetic coefficients [Callen1985] of dimension $2(n-1) \times 2(n-1)$. Note that, due to the constraints of particle and energy conservation, we can determine $\mathbf{J}_n$ from the fluxes $\mathbf{J}_1, ..., \mathbf{J}_{n-1}$. Moreover, we set the n-th reservoir as the reference one, with temperature T and electrochemical potential μ. In the presence of a magnetic field $\mathbf{B}$, time-reversal symmetry is broken and the Onsager matrix $\mathbf{L}$ in general is not symmetric [Callen1985, Benenti2011, Saito2011]. The currents can be separated into *reversible* components (which change sign by reversing $\mathbf{B} \to -\mathbf{B}$) and *irreversible* components (which are invariant with respect to the inversion $\mathbf{B} \to -\mathbf{B}$) [Brandner2013a, Brandner2013b]:

$$\mathbf{J}^{(r)} \equiv \frac{\mathbf{L}(\mathbf{B}) - \mathbf{L}^T(\mathbf{B})}{2}\,\mathbf{X}, \quad \mathbf{J}^{(i)} \equiv \frac{\mathbf{L}(\mathbf{B}) + \mathbf{L}^T(\mathbf{B})}{2}\,\mathbf{X}. \tag{4.2}$$

By virtue of the Onsager-Casimir relations $L_{ij}(-\mathbf{B}) = L_{ji}(\mathbf{B})$, these currents have the properties that $\mathbf{J}^{(r)}(\mathbf{B}) = -\mathbf{J}^{(r)}(-\mathbf{B})$ and $\mathbf{J}^{(i)}(\mathbf{B}) = \mathbf{J}^{(i)}(-\mathbf{B})$. In general these properties imply that $\mathbf{J}(\mathbf{B}) = \mathbf{J}^{(r)}(\mathbf{B}) + \mathbf{J}^{(i)}(\mathbf{B}) \neq \mathbf{J}^{(r)}(-\mathbf{B}) + \mathbf{J}^{(i)}(-\mathbf{B}) = \mathbf{J}(-\mathbf{B})$.

The idea of the present proposal is to set proper working conditions that enforce a given target functional dependence between the thermal currents evaluated at $\mathbf{B}$ and $-\mathbf{B}$. For instance we may ask the current $J_k^h(\mathbf{B})$ we get at the k-th contact, to be equal to twice the current $J_{k'}^h(-\mathbf{B})$ one would get at the k'-th contact when flipping the orientation of the magnetic field. More generally, given a subset K of the n terminals of the system, we will write our target functional dependence in the form of a linear constraint,

$$J_k^h(-\mathbf{B}) = \sum_{k'=1}^{n-1} x_{kk'}^{(\mathrm{target})}\, J_{k'}^h(\mathbf{B}), \qquad \forall k \in K\ , \tag{4.3}$$

where $x_{kk'}^{(\mathrm{target})}$ is an assigned $(n_0 - 1) \times (n-1)$ real matrix, with $n_0 \leq n-1$ being the number of elements of K. This allows us to define different Boolean working conditions which, while maintaining constant all the other system parameters, can be activated by simply operating on the relative orientation of the device with respect to the external magnetic field: Special instances of these devices are explicitly discussed in the following subsections.

Once the Onsager matrix $L_{ij}(\mathbf{B})$ and the coefficients $x_{kk'}^{(\mathrm{target})}$ are given, one can satisfy Eq. (4.3) by properly tuning the components of the affinity vector $\mathbf{X}$. As a matter of fact, since the conditions (4.3) are at most $n-1$ and the total number of the affinity parameters is $2(n-1)$, we can fulfill the former by only using half of the latter. In what follows we exploit this freedom to fix the values of the thermal affinity components $\{X_k^T\}$'s on each of the reservoirs, whereas using the $\{X_k^\mu\}$'s to enforce the constraint[1] (4.3). When $n_0 = n-1$, i.e., if we impose constraints on the $J_k^h(-\mathbf{B})$'s of

[1] The only limitation being not to set all of the $\{X_k^T\}$'s to be null: This configuration in fact only admits $\{X_k^\mu\} = 0\ \forall\, k$, hence no currents would flow through the device. In this scenario the $\{X_k^\mu\}$'s become explicit functions of the temperatures $\{X_k^T\}$ and of the Onsager coefficients L_{ij}.

all the terminals of the system, the procedure has the limitation of making the device operate *only* for certain precise values of the currents flowing from each k-th reservoir. Indeed, imposing $n-1$ relations of the form of Eq. (4.3) univocally determines all the $\{X_k^\mu\}$'s and hence, assuming fixed temperatures, also all the $J_k^h(\pm\mathbf{B})$'s. This limitation is naturally overcome when n_0 is strictly smaller than $n-1$. For instance, one may choose to impose only one condition (i.e., $n_0 = 1$) in order to leave all but one of the $\{X_k^\mu\}$'s unspecified. In particular, we could solve for X_1^μ to obtain:

$$X_1^\mu = a_2 X_2^\mu + \ldots + a_{n-1} X_{n-1}^\mu + f(X_1^T, \ldots, X_{n-1}^T), \tag{4.4}$$

where a_k are some functions of the Onsager matrix elements L_{ij}, whereas the function $f(X_1^T, \ldots, X_{n-1}^T)$ depends on the temperatures and on the L_{ij}. Setting $X_1^\mu =$ const, Eq. (4.4) defines a $(n\text{-}2)$-dimensional hyper-surface in the space spanned by $(X_2^\mu, \ldots, X_{n-1}^\mu)$. Assuming constant temperatures, varying the electrochemical potentials along this surface allows changing the values of the heat currents, without compromising the working operation of the device. In this way, we use the extra degrees of freedom given by the reservoirs with free electrochemical potential to widen the operational range of the device to many values of the heat currents

4.1.1 Heat current multiplier

In general, we may design a system in which the heat current in the k-th terminal becomes a fraction or a multiple of the original value when the magnetic field is reversed, which corresponds to having a diagonal matrix $x_{kk'}^{(\text{target})} = \delta_{kk'} x_k$ in Eq. (4.3): $J_k^h(-\mathbf{B}) = x_k J_k^h(\mathbf{B})$. Specifying a value for x_k makes the system operate as a Boolean *heat current multiplier* in which the two (Boolean) configurations correspond to an upward or a downward magnetic field. A illustration of such an operation for a three-terminal device is shown in Fig. 4.1(a).

On/off switch

Let us consider the specific case of a heat current multiplier in which $x_k = 0$: The device behaves as an *on/off switch for the k-th terminal*, which means $J_k^h(-\mathbf{B}) = J_k^{h(r)}(-\mathbf{B}) + J_k^{h(i)}(-\mathbf{B}) = 0$, whereas $J_k^h(\mathbf{B}) = J_k^{h(r)}(\mathbf{B}) + J_k^{h(i)}(\mathbf{B}) \neq 0$. It is then clear that $J_k^{h(i)}(\mathbf{B})$ and $J_k^{h(r)}(\mathbf{B})$ have the same magnitude and the same sign and add up giving a finite current, whereas the two terms cancel out upon magnetic field reversal, resulting in a *vanishing* heat current. This principle could be used, for instance, to implement a n-terminal *selector for the heat path* in which an upward magnetic field allows the flow of heat through l channels while blocking it into the remaining $(n-l)$ ones, and vice-versa by reversing $\mathbf{B} \to -\mathbf{B}$. A schematic of such an operation for a three-terminal device is shown in Fig. 4.1(b).

Fully reversible heat

Another interesting configuration is obtained by setting $x_k = -1$ in which case the heat current is *fully reversible*[2] ($J_k^{h(i)} = 0$). As an application, one could conceive a device in which the heat currents flowing through some (or all) the channels simultaneously flip their sign upon reversing the magnetic field. This, among other things, would offer the possibility of switching from a "refrigerator" mode for a specific reservoir to a "thermal engine" one by simply using the external magnetic field, without needing to modify the gradients in the reservoirs. A schematic of such an operation for a three-terminal device is shown in Fig. 4.1(c). Note that, by analogous considerations, $x_k = 1$ corresponds to the case of *fully irreversible* heat currents, which is however much less interesting because in this situation reversing the magnetic field has no effect.

4.1.2 Heat current swap

The matrix $x_{kk'}^{(\mathrm{target})}$ which defines our target (4.3) does not need to be diagonal. For instance let us consider the case where $x_{kk'}^{(\mathrm{target})} = x_{k'k}^{(\mathrm{target})} = 1$ and $x_{kk}^{(\mathrm{target})} = x_{k'k'}^{(\mathrm{target})} = 0$, which implements a *heat current swap* between reservoirs k and k'. This configuration couples heat currents flowing from different terminals, whereas in the previous ones the conditions were imposed on each single reservoir independently. Such a choice for $x_{kk'}^{(\mathrm{target})}$ results in having $J_k^h(\mathbf{B}) = J_{k'}^h(-\mathbf{B})$ and $J_{k'}^h(\mathbf{B}) = J_k^h(-\mathbf{B})$, i.e., the two heat currents are swapped by reversing the magnetic field, as pictorially shown in Fig. 4.1(d) for a three-terminal case. Besides, we notice that in this situation the reversible and irreversible components of the heat currents satisfy the conditions: $J_k^{h(i)} = J_{k'}^{h(i)}$ and $J_k^{h(r)} = -J_{k'}^{h(r)}$.

It is worth stressing that in a generic multi-terminal setup different working conditions can co-exist: For instance, some channels can be configured as heat current selectors, whereas others may operate as multipliers, make heat reversal or swap.

4.2 Three-terminal model

In order to illustrate the effects discussed in the previous section, we study a simple noninteracting model consisting of a three-terminal interferometer sketched in Fig. 4.2. We assume for simplicity low temperatures, so that electrons are the only heat carriers. Under these conditions, the electronic transport through the device is coherent, which allows us to follow a scattering approach [Datta1995]. The system consists of an interference loop, for example, made by two clean wires and connected to three electronic reservoirs with temperatures T_k and electrochemical potentials μ_k ($k = 1, 2, 3$). A magnetic field $\mathbf{B}$ orthogonal to the interferometer plane generates a magnetic flux Φ piercing the loop, which will be the relevant parameter in the following discussion (from here on, we will assume Φ to be expressed in units of $h/2e$). A scattering region S_s is inserted into channel 1, having the effect of breaking the particle-hole symmetry $E \to -E$ (having set $\mu = 0$ as the reference zero energy) in order to have

[2] Note, however, that in general the entropy production rate is nonzero, due to the irreversible component of the particle current.

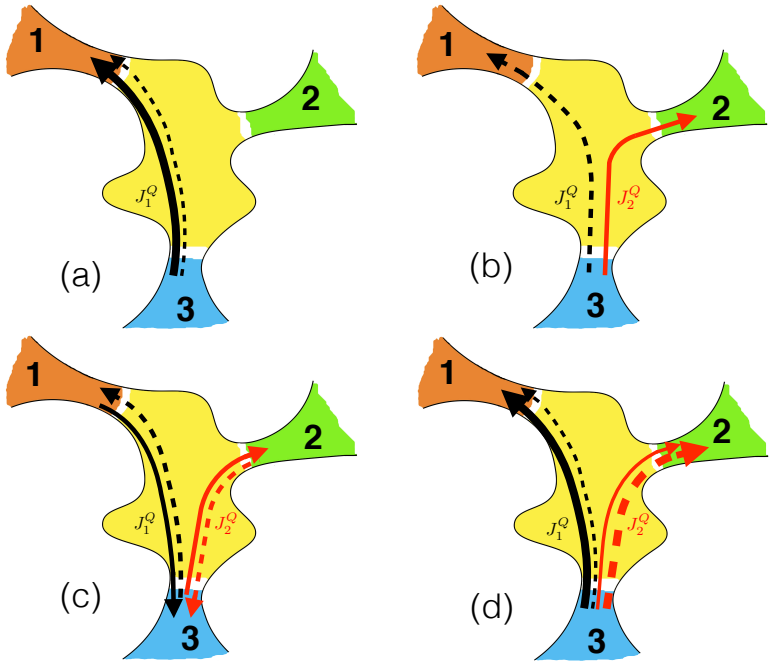

Figure 4.1 – Examples of operational principles for a three-terminal magnetic thermal switch. The different panels illustrate the heat-current (a) multiplier, (b) selector, (c) reversal and (d) swap configurations, respectively. The working operation is selected by choosing either $+\mathbf{B}$ or $-\mathbf{B}$. Solid[dashed] lines correspond to $J^h(+\mathbf{B})[J^h(-\mathbf{B})]$, whereas black(red) lines refer to currents flowing from terminal 1(2). Notice that in panel (a) lines of different thicknesses have been used to emphasize the increase/decrease of the heat currents magnitude before and after the magnetic field reversal.

finite non-diagonal Onsager coefficients. The specific choice of such scatterer is not important for the present discussion, as it does not alter the results at a qualitative level. Further details on the computation of the scattering matrix of this system are given in Appendix 4.A. Following the notation of the previous section, we set the reservoir 3 as the reference one ($\{\mu_3, T_3\} \equiv \{\mu, T\}$), and we express the particle and heat currents flowing from the other two reservoirs via the following 4×4 linear system [Mazza2014]:

$$\begin{pmatrix} J_1^c \\ J_1^h \\ J_2^c \\ J_2^h \end{pmatrix} = \begin{pmatrix} L_{11} & L_{12} & L_{13} & L_{14} \\ L_{21} & L_{22} & L_{23} & L_{24} \\ L_{31} & L_{32} & L_{33} & L_{34} \\ L_{41} & L_{42} & L_{43} & L_{44} \end{pmatrix} \begin{pmatrix} X_1^\mu \\ X_1^T \\ X_2^\mu \\ X_2^T \end{pmatrix}. \tag{4.5}$$

The coefficients L_{ij} are functions of the magnetic flux Φ and therefore of the applied magnetic field $\mathbf{B}$. Their explicit expressions are given by Eqs. (4.16), derived in

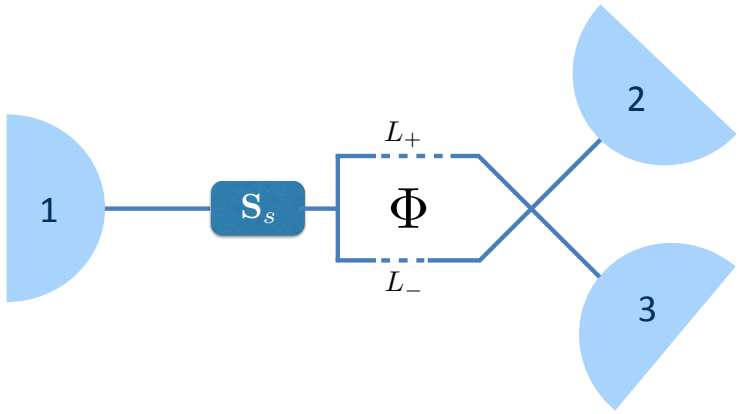

Figure 4.2 – Sketch of the three-terminal magnetic thermal switch studied numerically: an electronic interferometer, pierced by a magnetic flux Φ and in contact with three reservoirs at different temperatures T_k and electrochemical potentials μ_k $(k = 1, 2, 3)$. The scattering region S_s inside channel 1 breaks the particle-hole symmetry. L_+ and L_- are the interference paths and must be different in order to observe interference at the end of the device.

Appendix 4.B. The reversible (r) and irreversible (i) components of the heat currents J_1^h and J_2^h are as follows[3]:

$$\begin{aligned}
J_1^{h(r)} &= \frac{L_{23} - L_{32}}{2} X_2^\mu + \frac{L_{24} - L_{42}}{2} X_2^T, \\
J_1^{h(i)} &= L_{21} X_1^\mu + L_{22} X_1^T + \frac{L_{23} + L_{32}}{2} X_2^\mu + \frac{L_{24} + L_{42}}{2} X_2^T, \\
J_2^{h(r)} &= \frac{L_{41} - L_{14}}{2} X_1^\mu + \frac{L_{42} - L_{24}}{2} X_1^T, \\
J_2^{h(i)} &= \frac{L_{41} + L_{14}}{2} X_1^\mu + \frac{L_{42} + L_{24}}{2} X_1^T + L_{43} X_2^\mu + L_{44} X_2^T.
\end{aligned} \tag{4.6}$$

Once the L_{ij} coefficients *for a given magnetic flux* Φ_0 are calculated, for fixed $X_{1,2}^T$ different Boolean working conditions can be achieved by tuning the electrochemical potentials (and hence $X_{1,2}^\mu$) in order to impose Eq. (4.3) in both channels 1 and 2. Then, the switch is realized by reversing the magnetic field $\mathbf{B} \to -\mathbf{B}$, and hence the flux $\Phi_0 \to -\Phi_0$. In order to illustrate the effects outlined in the previous section, we focus here below on the same four working conditions, by properly choosing the values of $x_{kk'}^{(\text{target})}$ appearing in Eq. (4.3). The numerical results are summarized in Fig. 4.3: Notice that both the heat (symbols) and the particle (dashed lines) currents are shown, to stress that they are not constrained to follow the same behaviors.

[3] We have used the fact that, due to the symmetries of the scattering matrix, the Onsager matrix is block diagonal, and therefore $L_{21} = L_{12}$ and $L_{43} = L_{34}$.

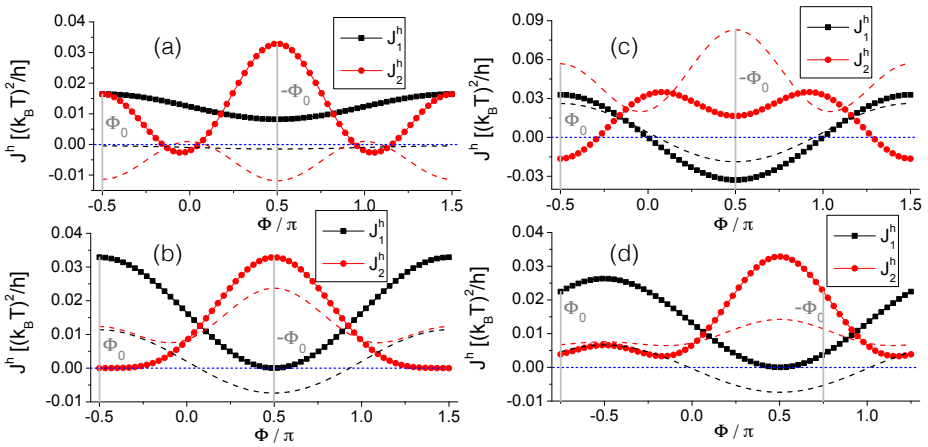

Figure 4.3 – Working operations of the three-terminal magnetic thermal switch discussed in the text. The heat currents through channels 1 (black squares) and 2 (red circles) are shown as a function of the magnetic flux Φ enclosed in the interferometer. For completeness, the particle currents (black and red dashed lines) are also shown, to emphasize that they do not follow the same behaviors as the heat currents. (a) *Heat current multiplier*: By reversing Φ from $\Phi_0 = -\pi/2$ to $-\Phi_0 = +\pi/2$, J^h_1 is halved whereas J^h_2 is doubled. (b) *Heat path selector*: For $\Phi_0 = -\pi/2$, J^h_1 is finite whereas J^h_2 is blocked. The situation is opposite by reversing Φ to $-\Phi_0$. (c) *Heat current reversal*: By reversing Φ from $-\pi/2$ to $+\pi/2$, the signs of both J^h_1 and J^h_2 flip. (d) *Heat current swap*: By reversing Φ from $-3\pi/4$ to $+3\pi/4$, the values of J^h_1 and J^h_2 are interchanged. The parameters are $k_BT = 1$, $\mu = 0$, $X^T_1 = 0.025$, $X^T_2 = 0.01$ [except in (c), where $X^T_1 = -0.005$ and $X^T_2 = 0.005$] and the difference between the interference paths in the upper/lower interferometer arms is $\Delta(kL) \equiv k(L_+ - L_-) = \pi/2$. Dotted blue lines are guides to the eye at $J^h = 0$, whereas gray lines highlight the magnetic flux values $\Phi = \pm\Phi_0$ selecting the two Boolean configurations.

- *Heat current multiplier*, $(x_1, x_2) = (1/2, 2)$. In this case the heat currents satisfy:

$$J^h_1(-\mathbf{B}) = \frac{1}{2}\, J^h_1(+\mathbf{B}),$$
$$J^h_2(-\mathbf{B}) = 2\, J^h_2(+\mathbf{B}), \tag{4.7}$$

  that is, by reversing the magnetic field J^h_1 is halved whereas J^h_2 is doubled. Under these conditions, by using Eqs. (4.3) and (4.6), it is straightforward to see that the reversible and irreversible components of the heat currents are related via: $J^{h(i)}_1(\mathbf{B}) = 3J^{h(r)}_1(\mathbf{B})$ and $J^{h(i)}_2(\mathbf{B}) = -3J^{h(r)}_2(\mathbf{B})$. The behavior of the heat currents flowing through the interferometer as a function of the magnetic flux in this configuration is shown in Fig. 4.3(a) for the interferometer described above.

- *Heat path selector*, $(x_1, 1/x_2) = (0, 0)$. In this case the heat currents satisfy

$J_1^h(\mathbf{B}) \neq 0$, $J_2^h(\mathbf{B}) = 0$ and $J_1^h(-\mathbf{B}) = 0$, $J_2^h(-\mathbf{B}) \neq 0$, i.e., for an upward magnetic field, heat transfer is allowed between the system and reservoir 1, while being blocked between the system and reservoir 2. This situation is reversed by changing $\mathbf{B} \to -\mathbf{B}$ ($\Phi_0 \to -\Phi_0$). Furthermore, according to Eqs. (4.3) and (4.6), the reversible and irreversible components of the heat currents are related via: $J_1^{h(i)}(\mathbf{B}) = J_1^{h(r)}(\mathbf{B})$ and $J_2^{h(i)}(\mathbf{B}) = -J_2^{h(r)}(\mathbf{B})$. The behavior of J_1^h and J_2^h is shown in Fig. 4.3(b).

- *Heat current reversal*, $(x_1, x_2) = (-1, -1)$. In this case the heat currents are purely reversible, that is, $J_1^{h(i)} = J_2^{h(i)} = 0$. Reversing the magnetic flux through the interferometer makes them simultaneously change their sign. The behavior of J_1^h and J_2^h is shown in Fig. 4.3(c). Note that at $\Phi_0 = -\pi/2$ both J_1^h (black squares) and J_1^c (black dashed line) are positive. This, together with the fact that $X_1^\mu > 0$ in this case, means that the system is acting as a *local refrigerator* [Entin-Wohlman2015] for the reservoir 1, exploiting a positive $\Delta\mu_1$ to extract heat from a cold bath ($X_1^T < 0$). Conversely, at $\Phi = -\Phi_0 = \pi/2$, both J_1^h and J_1^c have changed their sign: the system is now performing work driving particles against $\Delta\mu_1$, thus operating as a thermal engine. Notice that the same reasoning does not hold for reservoir 2 in which, upon reversing the magnetic flux, the sign of J_2^h flips whereas that of J_2^c does not.
- *Heat current swap*, $(x_{12}, x_{21}) = (1, 1)$. The heat currents satisfy $J_1^h(\mathbf{B}) = J_2^h(-\mathbf{B})$ and $J_2^h(\mathbf{B}) = J_1^h(-\mathbf{B})$, that is, the two heat currents are swapped by reversing the magnetic field. Furthermore, according to Eqs. (4.3) and (4.6), the reversible and irreversible components of the heat currents are related via: $J_1^{h(i)}(\mathbf{B}) = J_2^{h(i)}(\mathbf{B})$ and $J_1^{h(r)}(\mathbf{B}) = -J_2^{h(r)}(\mathbf{B})$. The behavior of J_1^h and J_2^h is shown in Fig. 4.3(d).

4.3 Summary

We have shown that a magnetic thermal switch can be implemented within the framework of linear response, taking advantage of the generic existence of reversible and irreversible heat currents when time reversal symmetry is broken. Such a device could allow the implementation of several Boolean features, such as on/off switching, reversal, selected splitting, and swap of the heat currents. For each feature, the switching from one working condition to the other is obtained by inverting the direction of an applied magnetic field. Quite interestingly, it is possible to change the operating mode of the device (from a power generator to a refrigerator) with respect to one of the reservoirs by inverting the external driving parameter, i.e., the magnetic field, at fixed electrochemical potentials and temperatures of the reservoirs.

A further advantage of our magnetic switch would arise in the perspective of conceiving a more complex programmable system, made of (for instance) an array of N simpler subsystems. These may be set up to operate in a variety of independent configurations, but always defined in terms of conditions of the form Eq. (4.3). We could imagine designing an array of N elements that are all initialized in the same state (say, for upward magnetic field $\mathbf{B}$), but that upon reversing $\mathbf{B} \to -\mathbf{B}$ go to (possibly all different) final states. We stress once more that acting on a *single* parameter - the

magnetic field - would be enough to achieve this operation and to reinitialize them in a subsequent moment, if needed.

Note that, although we have illustrated the magnetic thermal switch for a low-temperature interferometer model, with the heat carried by the electrons, the mechanism discussed in this chapter is generic for any system with the time-reversal symmetry broken by a magnetic field. A magnetic thermal switch could be in principle implemented also when both fermionic and bosonic reservoirs are present. Indeed, as shown in Ref. [Entin-Wohlman2012] due to the electron-phonon coupling the Onsager kinetic coefficients connecting the phononic heat currents from the bosonic reservoirs to the affinities for the fermionic terminals, in general are not even functions of the magnetic field. As a consequence, the phononic heat current generally exhibits a reversible component, and our theory can be applied.

4.A Modeling the interferometer

In this section we outline the procedure followed to compute the scattering matrix of our interferometric system. We start by considering an interferometer realized by connecting two four-arms beam-splitters via two clean wires (see Fig. 4.4). For simplicity, we assume the beam splitters to be identical and symmetric, that means, each one is described by a scattering matrix of the form:

$$S_{bs} = \begin{pmatrix} r_{11} & t_{12} & t_{13} & t_{14} \\ t_{21} & r_{22} & t_{23} & t_{24} \\ t_{31} & t_{32} & r_{33} & t_{34} \\ t_{41} & t_{42} & t_{43} & r_{44} \end{pmatrix} = \\ = \begin{pmatrix} 0 & 1/\sqrt{2} & 1/\sqrt{2} & 0 \\ 1/\sqrt{2} & 0 & 0 & 1/\sqrt{2} \\ 1/\sqrt{2} & 0 & 0 & -1/\sqrt{2} \\ 0 & 1/\sqrt{2} & -1/\sqrt{2} & 0 \end{pmatrix}. \tag{4.8}$$

The matrix S_{bs} describes a 50:50 beam splitter of electron waves, for which all the reflection terms are zero, and such that particles entering through one arm can be transmitted into two of the other three, with equal probability one half. According to the notation of Fig. 4.4, we have to compose the scattering matrices of the two individual beam splitters with the free propagation phase terms associated with the two interference paths. These terms are products of both the geometric (Aharonov-Bohm) phase and the dynamical phase exponentials:

$$f_{25} = f_g^+ \times f_d^+, \quad f_{38} = (f_g^-)^* \times f_d^-, \\ f_{52} = (f_g^+)^* \times f_d^+, \quad f_{83} = f_g^- \times f_d^-, \tag{4.9}$$

where $f_g^+ \, f_g^- = \exp\{i\Phi\}$, $f_d^\pm = \exp\{ikL_\pm\}$, the $\pm$ signs denote the upper (+) and lower (-) interference arms of lengths $L_\pm$, the complex conjugation accounts for the electron traveling direction, Φ denotes the magnetic flux enclosed in the interferometer and k is the Fermi wavevector. For simplicity we neglect the energy dependence of the free-propagations. The resulting scattering matrix describes the propagation among channels 1,4,6 and 7, and reads

$$S_i^{(1)} = \begin{pmatrix} 0 & 0 & t_{16} & t_{17} \\ 0 & 0 & t_{46} & t_{47} \\ t_{61} & t_{64} & 0 & 0 \\ t_{71} & t_{74} & 0 & 0 \end{pmatrix}, \tag{4.10}$$

where the various coefficients t_{pq} account for the different possible paths along which particles can travel from p to q,

$$t_{16} = t_{12} f_{25} t_{56} + t_{13} f_{38} t_{86}, \quad t_{17} = t_{12} f_{25} t_{57} + t_{13} f_{38} t_{87}, \\ t_{46} = t_{42} f_{25} t_{56} + t_{43} f_{38} t_{86}, \quad t_{47} = t_{42} f_{25} t_{57} + t_{43} f_{38} t_{87}, \\ t_{61} = t_{65} f_{52} t_{21} + t_{68} f_{83} t_{31}, \quad t_{71} = t_{75} f_{52} t_{21} + t_{78} f_{83} t_{31}, \\ t_{64} = t_{65} f_{52} t_{24} + t_{68} f_{83} t_{34}, \quad t_{74} = t_{75} f_{52} t_{24} + t_{78} f_{83} t_{34}. \tag{4.11}$$

Now, since we are interested in a three-terminal configuration, we impose that one of the channels (say, channel 4) behaves as a purely reflective mirror characterized by a reflection amplitude $r = -1$. The interferometer scattering matrix thus reduces to a 3×3 matrix,

$$S_i^{(2)} = \begin{pmatrix} r'_{11} & t'_{16} & t'_{17} \\ t'_{61} & r'_{66} & t'_{67} \\ t'_{71} & t'_{76} & r'_{77} \end{pmatrix} = \begin{pmatrix} 0 & t_{16} & t_{17} \\ t_{61} & t_{64}\, r\, t_{46} & t_{64}\, r\, t_{47} \\ t_{71} & t_{74}\, r\, t_{46} & t_{74}\, r\, t_{47} \end{pmatrix}. \tag{4.12}$$

Finally, in order to break the particle-hole symmetry, we insert in channel 1 an energy-dependent scattering region, described by a scattering matrix

$$S_s = \begin{pmatrix} \rho & i\tau \\ i\tau & \rho \end{pmatrix}, \tag{4.13}$$

where $\rho, \tau \geq 0$ and such that

$$\tau = \begin{cases} 1, & \text{if} \quad E > 0 \\ 0, & \text{elsewhere,} \end{cases} \tag{4.14}$$

with $\rho^2 = 1 - \tau^2$. This energy step would naturally be implemented using a well tuned electronic constriction, such as a quantum point contact [Houten1992]. The final expression for the scattering matrix of the whole system is as follows:

$$\begin{aligned} S &= \begin{pmatrix} r''_{11} & t''_{16} & t''_{17} \\ t''_{61} & r''_{66} & t''_{67} \\ t''_{71} & t''_{76} & r''_{77} \end{pmatrix} = \\ &= \begin{pmatrix} \rho & i\tau\, t'_{16} & i\tau\, t'_{17} \\ i\tau\, t'_{61} & r'_{66} + t'_{61}\, \rho\, t'_{16} & t'_{67} + t_{61}\, \rho\, t'_{17} \\ i\tau t'_{71} & t'_{76} + t'_{71}\, \rho\, t'_{16} & r'_{77} + t_{71}\, \rho\, t'_{17} \end{pmatrix}. \end{aligned} \tag{4.15}$$

It is worth observing that, having initialized all the r_{pq} and t_{pq} in Eq. (4.8), the remaining (relevant) free parameters in the scattering matrix above are the difference between the paths in the upper/lower interference arms, $\Delta L = L_+ - L_-$, and the magnetic flux enclosed in the interferometer loop, Φ [see Eq. (4.9)].

4.B Calculation of the Onsager coefficients

We set, for simplicity, channel 7 (see Fig. 4.4) as the lead connected to the reference reservoir. Moreover, we set the relative dynamical phase $k\Delta L = \pi/2$ in order to maximize the effect of the sign flip of $\mathbf{B}$. Using the Landauer-Büttiker formalism[Landauer1957, Büttiker1986] and the scattering coefficients from Appendix 4.A, we compute the Onsager coefficients,

$$\begin{aligned} L_{11} &= \frac{T}{h} \int \mathrm{d}E\, (-\partial_E f)\, \tau^2, \\ L_{12} &= \frac{T}{h} \int \mathrm{d}E\, E\, (-\partial_E f)\, \tau^2 = L_{21}, \end{aligned}$$

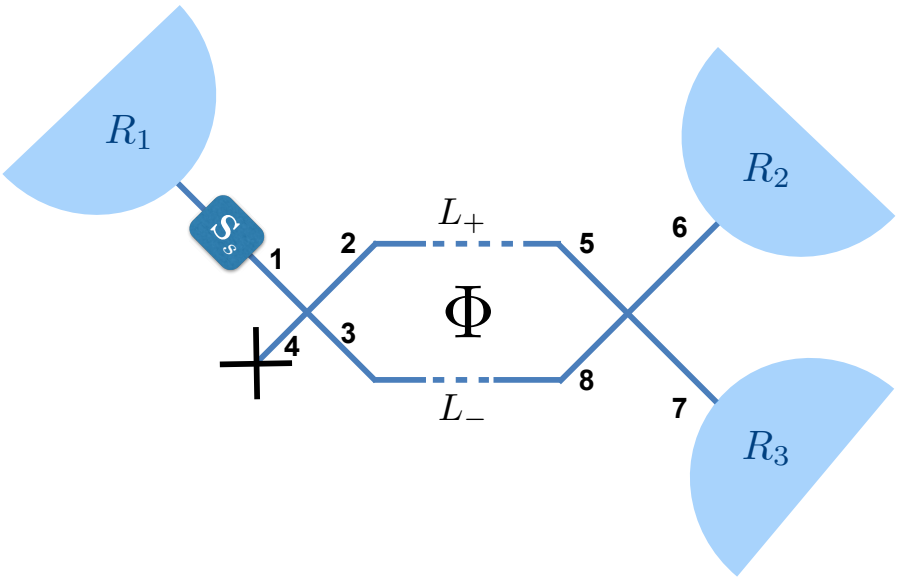

Figure 4.4 – Sketch of the system used to model the interferometer discussed in Sec. 4.2. Two identical four-arm beam splitters are connected via two clean electronic waveguides of lengths L_+ and L_-, forming an interference loop which is pierced by a magnetic flux Φ. A scatterer S_s is inserted into arm 1 in order to break the particle-hole symmetry. The numbers from 1 to 8 refer to the arms of the beam splitters and label the transmission and reflection amplitudes t_{ij} and r_{ij} (in particular, channel 4 is assumed to be totally reflective). The system is connected to three electronic reservoirs R_1, R_2, and R_3.

$$
\begin{aligned}
L_{22} &= \frac{T}{h} \int \mathrm{d}E\, E^2\, (-\partial_E f)\, \tau^2, \\
L_{33} &= \frac{T}{h} \int \mathrm{d}E\, (-\partial_E f) \left[1 - \frac{1}{4} \cos^2\Phi\, (1+\rho)^2\right], \\
L_{34} &= \frac{T}{h} \int \mathrm{d}E\, E\, (-\partial_E f) \left[1 - \frac{1}{4} \cos^2\Phi\, (1+\rho)^2\right] = L_{43}, \\
L_{44} &= \frac{T}{h} \int \mathrm{d}E\, E^2\, (-\partial_E f) \left[1 - \frac{1}{4} \cos^2\Phi\, (1+\rho)^2\right], \\
L_{13} &= \frac{T}{h} \int \mathrm{d}E\, (-\partial_E f) \left[-\frac{1}{2} \tau^2\, (1+\sin\Phi)\right], \\
L_{14} &= \frac{T}{h} \int \mathrm{d}E\, E\, (-\partial_E f) \left[-\frac{1}{2} \tau^2\, (1+\sin\Phi)\right] = L_{23}, \\
L_{24} &= \frac{T}{h} \int \mathrm{d}E\, E^2\, (-\partial_E f) \left[-\frac{1}{2} \tau^2\, (1+\sin\Phi)\right],
\end{aligned}
$$

$$
\begin{aligned}
L_{31} &= \frac{T}{h} \int \mathrm{d}E \; (-\partial_E f) \left[-\frac{1}{2} \tau^2 \left(1 - \sin\Phi\right) \right], \\
L_{41} &= \frac{T}{h} \int \mathrm{d}E \, E \; (-\partial_E f) \left[-\frac{1}{2} \tau^2 \left(1 - \sin\Phi\right) \right] = L_{32}, \\
L_{42} &= \frac{T}{h} \int \mathrm{d}E \, E^2 \; (-\partial_E f) \left[-\frac{1}{2} \tau^2 \left(1 - \sin\Phi\right) \right],
\end{aligned} \tag{4.16}
$$

where $f = [\exp\{E/k_B T\} + 1]^{-1}$ is the equilibrium Fermi distribution at temperature T and $\mu = 0$.

Chapter 5

Thermoelectric efficiency for multi-level interacting quantum dots

The recent growing number of experiments on thermoelectric systems at the nanoscale pushed the theoretical research towards the study of more and more complex designs. When the nanostructure is very small the effect of the electron-electron Coulomb interaction on thermal machines becomes important. This issue has received a growing attention recently [Liu2010, T Kuo2012, Muralidharan2012, Karwacki2013, Torfason2013, Koch2014, Lim2014, Chen2015].

A very large literature exists on thermoelectricity with non-interacting quantum dots, that has already been review in this Thesis in Section 1.5. However, very few papers deal with the thermoelectricity of interacting quantum dots [Boese2001, Trocha2012, Torfason2013, Koch2014, Monteros2014, Buddhiraju2015], and the majority of them study the problem of a single level (or two levels) interacting quantum dot [Liu2010, Muralidharan2012]. In this Chapter we extend the existing knowledge of the two-terminal one (or two) levels quantum dot to multi-level and multi-terminal formalism.

The aim of this work is to study the role that the electron-electron interaction plays in quantum dot based thermal machines. In particular we want to study the behavior of a three-terminal system when such an interaction enters the game. The system that we analyze is a multi-level quantum dot in the limit of sequential tunneling (very narrow level broadening), attached to two or three terminals. We first derive the expression for the heat and particle currents for a two-terminal system, by following the work done in Refs. [Beenakker1991, Beenakker1992]. Then we generalize those equations to three-terminal systems using the expressions derived for the three-terminal Onsager problem in Chapter 2 for the maximum power and the efficiency at maximum power. We will established how the Coulomb interaction affects the thermodynamics relevant quantity (power and efficiency).

This chapter is organized as follows. In Section 5.1 we will derive the analytical formulas for the heat and charge currents within linear response for the multi-level quantum dot. In Section 5.2 we will recover the well known results of Ref. [Beenakker1992] for the thermopower and the electrical conductance of a two-terminal systems and we will complete it with the study with the efficiency and the efficiency at maximum power. Then three-terminal systems follow: we will show how a third terminal could be useful to enhance both the efficiency and the power of a quantum thermal machine also when the Coulomb interaction plays a significant role. Finally Section 5.3 is devoted to the conclusions.

5.1 Three-terminal model

5.1.1 General framework

In this section, generalizing the paper of Beenakker [Beenakker1992], we will derive the linear response expressions for the heat and charge currents of a three-terminal system attached to an interacting quantum dot. The quantum dot is a confined region, with discrete levels that can host zero or one electron, which is weakly coupled (via tunnel barriers) to three electron metallic reservoirs, described by the Fermi distribution

$$f_i(E-\mu_i) = \left[1+\exp\left(\frac{E-\mu_i}{k_B T_i}\right)\right]^{-1} \tag{5.1}$$

where μ_i is the chemical potential and $k_B T_i$ is the temperature in the i-th lead, $i = \{1,2,3\}$. We assume that between the reservoirs there is a small temperature difference with respect to a reference value (although the reservoir itself is in thermal equilibrium) $\Delta T_i = T_i - T$ as well as a small voltage difference $\Delta\mu_i = -(\mu_i - \mu)$. The values of temperature and chemical potential of the third reservoir have been taken as the reference values: $\mu = \mu_3$ and $T = T_3$. The quantum dot has single-electron energy level at energies E_p ($p = 1, 2, \dots$). The levels are labeled in ascending order and measured relative to the bottom of the potential well that defines the quantum dot (E_{BW}). Because the number of electrons in the QD, that we label with N, can only take integer values, an electrostatic potential difference $\phi(Q)$ is developed between the QD and the reservoirs even if $\mu_i = 0$ ($Q = -eN$ is the charge on the QD). We assume that the QD has a capacitance C independent on the number of electrons N in the QD. Then ϕ is expressed in terms of this capacitance: $\phi(Q) = Q/C + \phi_{\text{ext}}$, including also a contribution ϕ_{ext} from external charges. The electrostatic energy then takes the form

$$U(N) = \frac{(Ne)^2}{2C} - Ne\phi_{\text{ext}}. \tag{5.2}$$

We denote with γ_i the tunnel rates from reservoir i, and assume that each level E_p is coupled to the reservoirs in the same way (no dependence on p in the γ's). This will have important consequences on the local and non local thermopowers, that we will discuss later. At this point we have to make an assumption to simplify the calculations: we consider the thermal energy $k_B T$ and the level spacing $\Delta E_p = E_{p+1} - E_p$ much grater than the level width $h(\gamma_1 + \gamma_2 + \gamma_3)$, so that virtual tunnel processes can be

disregarded. With these assumptions we can describe the transport through the QD by rate equations [Ziman1972].

Energy conservation upon tunneling from an initial state p in the QD (containing N electrons) to a final state in the $j-$th reservoir at energy $E^{f,j}$ (in excess of the local conduction band bottom), requires that:

$$E^{f,j}(N) = E_p + U(N) - U(N-1) - \Delta\mu_j. \tag{5.3}$$

The energy conservation condition for tunneling from an initial state $E^{i,j}$ in the $j-$th reservoir to a final state p in the QD (containing N electrons) is given by

$$E^{i,j}(N) = E_p + U(N+1) - U(N) - \Delta\mu_j, \tag{5.4}$$

The stationary current through the $j-$ lead is given by

$$J_j^c = -e\sum_{p=1}^{\infty}\sum_{\{n_i\}}\gamma_j P(\{n_i\})\Big[\delta_{n_p,0}f_j(E^{i,j}-\mu_j) - \delta_{n_p,1}[1-f_j(E^{f,j}(N)-\mu_j)]\Big]. \tag{5.5}$$

The first summation is over all the energy levels in the QD, while the second is over all the possible configuration that the N electrons (in the QD) can realize, each with stationary probability $P(\{n_i\})$. In equilibrium this probability is given by the Gibbs distribution in the grand canonical ensemble

$$P_{\rm eq}(\{n_i\}) = Z^{-1}\exp\left[-\frac{1}{k_BT}\left(\sum_{i=1}^{\infty}E_i n_i + U(N) - N\mu\right)\right], \tag{5.6}$$

where $\sum_i n_i = N$ and Z is the partition function that normalize the probability. The non-equilibrium probability distribution $P(\{n_i\})$ is a stationary solution of the kinetic equation [Beenakker1992]

$$\frac{\partial}{\partial t}P(\{n_i\}) = 0 \tag{5.7}$$

This kinetic equation is equivalent to the set of detailed balance equations (one for each level $p = 1, 2, \dots$)

$$\begin{aligned}
&P(\{n_i\})\delta_{n_p,1}\Big[\gamma_1(1-f_1(E^{f,1}(N+1)-\mu)) + \gamma_2(1-f_2(E^{f,2}(N+1)-\mu)) + \\
&+\gamma_3(1-f_3(E^{f,3}(N+1)-\mu))\Big] = \\
&= P(\{n_i\})\delta_{n_p,0}\Big[\gamma_1 f_1(E^{i,1}(N+1)-\mu) + \gamma_2 f_2(E^{i,2}(N+1)-\mu) + \\
&+\gamma_3 f_3(E^{i,3}(N+1)-\mu)\Big]
\end{aligned} \tag{5.8}$$

5.1.2 Linear response

In order to make the linear response approximation we need to make an expansion in both the Fermi function and the stationary probability. Since the latter is more usual (and simple) we start from the probability expansion. We substitute $P(\{n_i\}) =$

$P_{\rm eq}(\{n_i\})\Big[1+\Psi(\{n_i\})\Big]$ into the detailed balance equations (5.8). Then we can expand to the first order in ΔT_j and $\Delta\mu_j$. We define

$$T_3 \equiv T, \quad T_1 \equiv T+\Delta T_1, \quad T_2 \equiv T+\Delta T_2, \quad f(\epsilon) = [1+\exp{(\epsilon/k_BT)}]^{-1},$$

so that now we can write:

$$f_1(\epsilon-\Delta\mu_1) = f(\epsilon) - \epsilon\Delta T_1/Tf'(\epsilon) + \Delta\mu_1 f'(\epsilon), \tag{5.9}$$
$$f_2(\epsilon-\Delta\mu_2) = f(\epsilon) - \epsilon\Delta T_2/Tf'(\epsilon) + \Delta\mu_1 f'(\epsilon), \tag{5.10}$$
$$f_3(\epsilon) = f(\epsilon), \tag{5.11}$$

where we have abbreviated $\epsilon_p = E_p+U(N+1)-U(N)-\mu$. By substituting in Eq. (5.8) we obtain:

$$\begin{aligned} &P_{\rm eq}(\{n_i\})\,[1+\Psi(\{n_i\})]\,\delta_{n_p,1}\Big\{\gamma_1\,(1-f_1(\epsilon_p+\Delta\mu_1)) + \gamma_2\,(1-f_2(\epsilon_p+\Delta\mu_2)) + \\ &+\gamma_3\,(1-f(\epsilon_p))\Big\} = \\ &= P_{\rm eq}(\{n_i\})\,[1+\Psi(\{n_i\})]\,\delta_{n_p,0}\Big\{\gamma_1 f_1(\epsilon_p+\Delta\mu_1) + \gamma_2 f_2(\epsilon_p+\Delta\mu_2) + \gamma_3 f(\epsilon_p)\Big\}. \end{aligned} \tag{5.12}$$

Now we analyze each of the two sides of this Equation, starting from the right hand side,

$$\begin{aligned} \text{RHS} &= P_{\rm eq}(\{n_i\})\,[1+\Psi(\{n_i\})]\,\delta_{n_p,1}\Big\{\gamma_1\left(1-f(\epsilon_p)+\frac{\epsilon_p\Delta T_1}{T}f'(\epsilon_p)-\Delta\mu_1 f'(\epsilon_p)\right)+ \\ &+\gamma_2\left(1-f(\epsilon_p)+\frac{\epsilon_p\Delta T_2}{T}f'(\epsilon_p)-\Delta\mu_2 f'(\epsilon_p)\right)+\gamma_3(1-f(\epsilon_p))\Big\} = \\ &= P_{\rm eq}(\{n_i\})\delta_{n_p,1}\Big[\gamma_{\rm tot}\,(1-f(\epsilon_p)) + \Psi(\{n_i\})\delta_{n_p,1}\gamma_{\rm tot}\,(1-f(\epsilon_p)) + \\ &+\gamma_1 f'(\epsilon_p)\left(\frac{\epsilon_p\Delta T_1}{T}-\Delta\mu_1\right)+\gamma_2 f'(\epsilon_p)\left(\frac{\epsilon_p\Delta T_2}{T}-\Delta\mu_2\right)\Big]. \end{aligned} \tag{5.13}$$

Analogously the left hand side reads

$$\begin{aligned} \text{LHS} &= P_{\rm eq}(\{n_i\})\,[1+\Psi(\{n_i\})]\,\delta_{n_p,0}\Big\{\gamma_1\left(f(\epsilon_p)-\frac{\epsilon_p\Delta T_1}{T}f'(\epsilon_p)+\Delta\mu_1 f'(\epsilon_p)\right)+ \\ &+\gamma_2\left(f(\epsilon_p)-\frac{\epsilon_p\Delta T_2}{T}f'(\epsilon_p)+\Delta\mu_2 f'(\epsilon_p)\right)+\gamma_3 f(\epsilon_p)\Big\} = \\ &= P_{\rm eq}(\{n_i\})\delta_{n_p,0}\Big[\gamma_{\rm tot} f(\epsilon_p) + \Psi(\{n_i\})\delta_{n_p,0}\gamma_{\rm tot} f(\epsilon_p) + \\ &+\gamma_1 f'(\epsilon_p)\left(-\frac{\epsilon_p\Delta T_1}{T}+\Delta\mu_1\right)+\gamma_2 f'(\epsilon_p)\left(-\frac{\epsilon_p\Delta T_2}{T}+\Delta\mu_2\right)\Big]. \end{aligned} \tag{5.14}$$

Now using the properties of the Fermi functions and of the Gibbs distribution

$$1-f(\epsilon_p) = f(\epsilon_p)\,\mathrm{e}^{\epsilon_p/k_BT} \tag{5.15}$$

$$k_B T f'(\epsilon_p) = -f(\epsilon_p)\left[1+\mathrm{e}^{-\epsilon_p/k_B T}\right]^{-1} \tag{5.16}$$

$$P_{\mathrm{eq}}(\{n_i\})\delta_{n_p,1} = P_{\mathrm{eq}}(\{n_i\})\delta_{n_p,0}\,\mathrm{e}^{-\epsilon_p/k_B T}, \tag{5.17}$$

a lot of terms cancel with each other and it is possible to obtain an equation for the Ψ's

$$\Psi(\{n_i\})\delta_{n_p,1} = \Psi(\{n_i\})\delta_{n_p,0} + \frac{1}{k_B T \gamma_{\mathrm{tot}}}\left[\gamma_1\left(\epsilon_p\frac{\Delta T_1}{T} - \Delta\mu_1\right) + \gamma_2\left(\epsilon_p\frac{\Delta T_2}{T} - \Delta\mu_2\right)\right]. \tag{5.18}$$

This equation has to be used in the linearization of the current in Eq. (5.5), the result is the expression of the particle and heat currents

$$\begin{aligned} J_1^c &= \frac{e}{k_B T}\sum_{p=1}^{\infty}\sum_{\{n_i\}}\frac{\gamma_1}{\gamma_{\mathrm{tot}}}P_{\mathrm{eq}}(\{n_i\})\delta_{n_p,0}f(\epsilon_p)\Big[\Delta\mu_1\left(\gamma_2+\gamma_3\right) + \\ &+ \frac{\epsilon_p\Delta T_1}{T}\left(-\gamma_2-\gamma_3\right) + \Delta\mu_2(-\gamma_2) + \frac{\epsilon_p\Delta T_2}{T}\gamma_2\Big] \end{aligned} \tag{5.19}$$

$$\begin{aligned} J_1^h &= -\frac{1}{k_B T}\sum_{p=1}^{\infty}\sum_{\{n_i\}}\frac{\gamma_1}{\gamma_{\mathrm{tot}}}P_{\mathrm{eq}}(\{n_i\})\delta_{n_p,0}f(\epsilon_p)\epsilon_p\Big[\Delta\mu_1\left(\gamma_2+\gamma_3\right) + \\ &+ \frac{\epsilon_p\Delta T_1}{T}\left(-\gamma_2-\gamma_3\right) + \Delta\mu_2(-\gamma_2) + \frac{\epsilon_p\Delta T_2}{T}\gamma_2\Big] \end{aligned} \tag{5.20}$$

$$\begin{aligned} J_2^c &= \frac{e}{k_B T}\sum_{p=1}^{\infty}\sum_{\{n_i\}}\frac{\gamma_2}{\gamma_{\mathrm{tot}}}P_{\mathrm{eq}}(\{n_i\})\delta_{n_p,0}f(\epsilon_p)\Big[\Delta\mu_1(-\gamma_1) + \frac{\epsilon_p\Delta T_1}{T}\gamma_1 + \\ &+ \Delta\mu_2\left(\gamma_1+\gamma_3\right) + \frac{\epsilon_p\Delta T_2}{T}\left(-\gamma_1-\gamma_3\right)\Big] \end{aligned} \tag{5.21}$$

$$\begin{aligned} J_2^h &= -\frac{1}{k_B T}\sum_{p=1}^{\infty}\sum_{\{n_i\}}\frac{\gamma_2}{\gamma_{\mathrm{tot}}}P_{\mathrm{eq}}(\{n_i\})\delta_{n_p,0}f(\epsilon_p)\epsilon_p\Big[\Delta\mu_1(-\gamma_1) + \frac{\epsilon_p\Delta T_1}{T} + \\ &+ \Delta\mu_2\left(\gamma_1+\gamma_3\right) + \frac{\epsilon_p\Delta T_2}{T}\left(-\gamma_1-\gamma_3\right)\Big]. \end{aligned} \tag{5.22}$$

We can write these expressions in a more compact form using the Onsager matrix

$$\begin{pmatrix} J_1^c \\ J_1^h \\ J_2^c \\ J_2^h \end{pmatrix} = \begin{pmatrix} L_{11} & L_{12} & L_{13} & L_{14} \\ L_{21} & L_{22} & L_{23} & L_{24} \\ L_{31} & L_{32} & L_{33} & L_{34} \\ L_{41} & L_{42} & L_{43} & L_{44} \end{pmatrix} \begin{pmatrix} X_1^\mu \\ X_1^T \\ X_2^\mu \\ X_2^T \end{pmatrix} \tag{5.23}$$

From these equations we can easily identify the Onsager coefficients, see Appendix 5.A, (in the presence of time reversal symmetry the matrix is symmetric), and define the transport coefficients to obtain the expression for the electrical conductance G_{ij}, the thermopower S_{ij} and the thermal conductivity K_{ij} for the three-terminal case (see also Chapter 2)

$$G_{ij} = \left(\frac{eJ_i^c}{\Delta\mu_j}\right)_{\substack{\Delta T_k=0\ \forall k,\\ \Delta\mu_k=0\ \forall k\neq j}}, \tag{5.24}$$

$$S_{ij} = -\left(\frac{\Delta\mu_i}{e\Delta T_j}\right)_{\substack{J_k^c=0\ \forall k,\\ \Delta T_k=0\ \forall k\neq j}}, \tag{5.25}$$

$$K_{ij} = \left(\frac{J_i^h}{\Delta T_j}\right)_{\substack{J_k^c = 0\ \forall k, \\ \Delta T_k = 0\ \forall k \neq j}} . \tag{5.26}$$

If we set $\gamma_1 = 0$, i.e. we disconnect one of the terminals, we recover the two-terminal expressions for the currents and the transport coefficients that were derived in Ref. [Beenakker1992]. Notice that we could have set $\gamma_2 = 0$ as well, but not γ_3, since terminal 3 is our reference for the temperatures and the chemical potentials.

5.2 Results

In this Section we will discuss the results that we obtained for the effect of the Coulomb interaction in a quantum dot on the thermoelectric efficiency. We will analyze in detail the three-terminal system. We will show the results for the local and non-local transport coefficients as well as the efficiency at maximum power and the power. We will complete this Section with the study of the effect of the third terminal on the performance of the quantum dot. In Appendix 5.B we discuss the results for the two-terminal systems. In the whole discussion we will set $k_B T = 1$ as the unit of the energy scale.

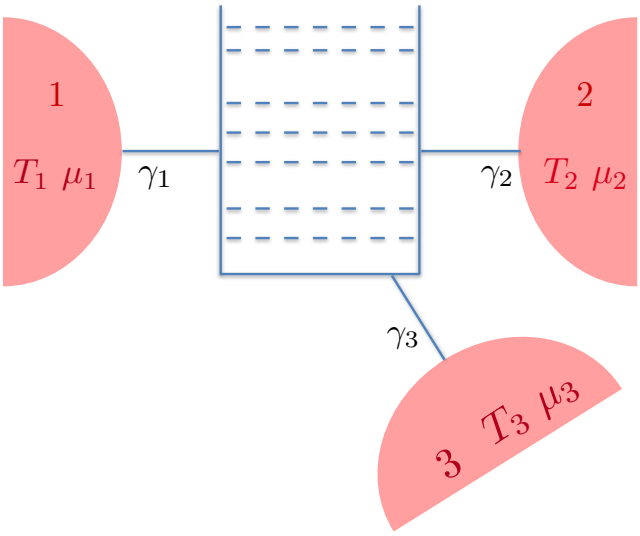

Figure 5.1 – Schematic representation of the three-terminal system. The three leads are kept at different temperatures and chemical potentials and are connected through a multi level quantum dot. γ_i is the coupling to the i-th lead, $i = (1, 2, 3)$. In the non-interacting case the separation between the levels is given by δE.

5.2.1 Three-terminal systems

Now we will describe the thermoelectric transport in a system composed by a multi-level quantum dot attached to three fermionic reservoirs each described by a chemical potential and a termperature, as in Fig. 5.1.

Dependence on the chemical potential

For a pure three-terminal fermionic system we have to deal with four independent currents (two charge currents and two heat currents), but the model of the interacting quantum dot remains the same. In a three-terminal setup (with time reversal symmetry)

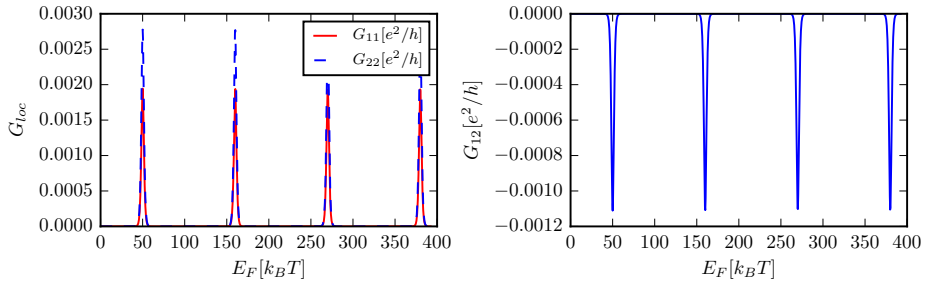

Figure 5.2 – In this figure we plot the electrical conductance G_{ij}. In the left panel we have the two local conductance G_{11} and G_{22}, while in the right panel we have the non-local conductance G_{12}. Although the position of the resonances is the same for all the quantities, in the left panel it is possible to see how G_{11} and G_{22} have peaks of very different height. This difference is mainly due to the different couplings γ_i. The parameters used are: $e^2/2C = 50\,k_BT$, $\delta E = 10\,k_BT$, $\gamma_1 = 0.01\,k_BT$, $\gamma_2 = 0.02\,k_BT$, $\gamma_3 = 0.015\,k_BT$

we have nine independent coefficients: three electrical conductance G_{11}, G_{22} and G_{12}, three thermopower S_{11}, S_{22} and S_{12} and three thermal conductance K_{11}, K_{22} and K_{12}. We start by analyzing the electrical conductance and the thermopower, as in the two-terminal case. In Fig. 5.2 we can see that the two local electrical conductance are quite different. This is due to the different couplings to the reservoirs 1 and 2 (γ_1 and γ_2). The non local conductance is negative, but we stress that here are no sign requirements on the non local coefficients. The peaks remain in the same positions as in the two-terminal case (see Fig. 5.9), because the third terminal cannot change the intrinsic properties of the QD. In Fig. 5.3 we can appreciate how the two local thermopower are equal, while the non local thermopowers $S_{12} = S_{21}$ are zero. This is always true if the couplings to the leads do not depend on energy. An analytical proof of that could be found in Chapter 2. The local thermopowers exhibit the same oscillations described in Fig. 5.9.

In order to study the efficiency we choose the thermal gradients in order to have heat adsorbed only from terminal 2 and in order to have the same Carnot efficiency as in the two-terminal case, therefore $\Delta T_1 = 0$ and $\Delta T_2 = 0.005\,k_BT$. From Fig. 5.4 we

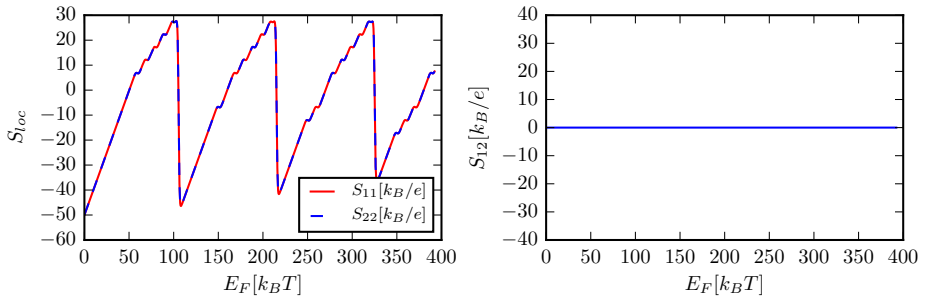

Figure 5.3 – In this figure we plot the electrical conductance S_{ij}. In the left panel we have the two local conductance S_{11} and S_{22}, while in the right panel we have the non-local conductance S_{12}. The two local thermopowers S_{11} and S_{22} are equal, while the non-local thermopower S_{12} is zero. This is a consequence of the energy independent couplings that we used. The parameters used are: $e^2/2C = 50\,k_BT$, $\delta E = 10\,k_BT$, $\gamma_1 = 0.01\,k_BT$, $\gamma_2 = 0.02\,k_BT$, $\gamma_3 = 0.015\,k_BT$.

can see that there are always regions where the extracted power W is negative, and therefore it is impossible to define the heat to work conversion efficiency. However we can also see that we can reach pretty high efficiency and efficiency at maximum power. In particular the latter is fixed to the Curzon-Ahlborn efficiency ($\eta_{CA} = \eta_C/2$) for low values of the chemical potential. This is due to the fact that in that region there is a

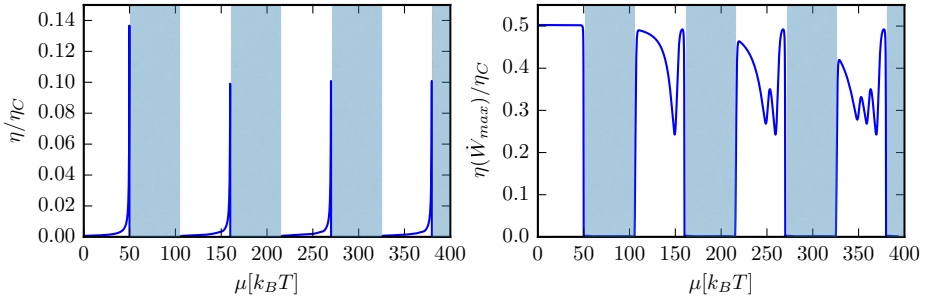

Figure 5.4 – In this figure we plot the efficiency η (left panel) and the efficiency at maximum power $\eta(\dot{W}_{\max})$ (right panel) normalized to the Carnot efficiency. There are some regions, shadowed in the two panels, where the extracted power $\dot{W}$ is negative, therefore the efficiency of heat to work conversion cannot be defined. We chose the parameters in order to adsorb heat only from reservoir 2. Moreover since $\Delta T_1 = 0$ the Carnot efficiency has the two-terminal expression $\eta_C = 1 - T_3/T_1$. The parameters used are: $e^2/2C = 50\,k_BT$, $\delta E = 10\,k_BT$, $\gamma_1 = 0.01\,k_BT$, $\gamma_2 = 0.02\,k_BT$, $\gamma_3 = 0.015\,k_BT$, $\Delta T_1 = 0$, $\Delta T_2 = 0.005\,k_BT$, $\Delta\mu_1 = 0.001\,k_BT$ and $\Delta\mu_2 = 0.002\,k_BT$.

single energy level with very very small width (the systems is essentially a single level non-interacting quantum dot, off resonance). It is also interesting to notice that in the three-terminal case the oscillation of the efficiency at maximum power now reflect the behavior of the negative branch of the thermopower, thus they increase at each charging energy step.

Dependence on the third terminal

In this last paragraph we want to explore the effect of the presence of the third terminal on the efficiency and the power of the quantum dot.
In order to study the effect of the third terminal on the system we will set the couplings to leads 2 a 3 equal between each other $\gamma_2 = \gamma_3 = \gamma = 0.02\,k_BT$ and show the plots of the efficiency and the power as a function of the coupling of lead 1 γ_1, that spans from 0 to γ, thus going from a pure two-terminal system ($\gamma_1 = 0$ to a pure three-terminal one $\gamma_1 = \gamma$), for different values of the charging energy E_C. We want to stress that we set $\Delta T_1 = 0$, in this way the Carnot efficiency is equal to the two-terminal Carnot efficiency $\eta_C = \Delta T_2/T$ and does not change as the coupling to lead 1 is turned on, thus allowing for a comparison of the efficiency in these two cases.

The results are shown in Fig. 5.5. A systematic increase of the efficiency as the coupling γ_1 is turned on has been found for many different values of the thermal and chemical potential gradients. This means that a third terminal could be useful

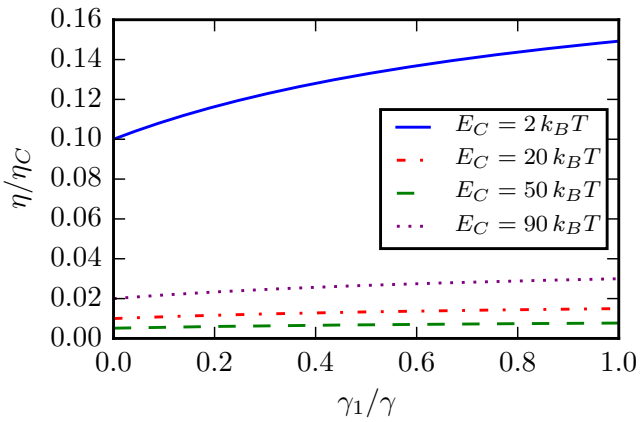

Figure 5.5 – Efficiency η/η_C as a function of the coupling γ_1 for different values of the charging energy $E_C = (2, 20, 50, 90)k_BT$, with a fixed level spacing $\delta E = 20\,k_BT$. We are spanning from the non-interacting to the interacting regime, and we find a systematic increase of the efficiency as the coupling to lead 1 is turned on. This increase is not monotonic in E_C, but there is no reason why it should be. The other parameters used are $\mu = 100\,k_BT$, $\gamma_2 = \gamma_3 = \gamma = 0.02\,k_BT = \gamma_3$, $\Delta T_1 = 0$, $\Delta T_2 = 0.005\,k_BT$, $\Delta\mu_1 = 0.0001\,k_BT$ and $\Delta\mu_2 = -0.0001\,k_BT$.

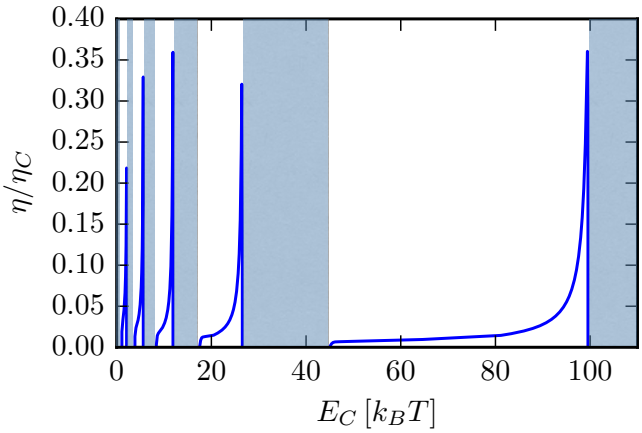

Figure 5.6 – Efficiency (left) for the interacting quantum dot as a function of the charging energy $E_C = e^2/2C$. In this plot a behavior similar to the one observed in Fig. 5.4 arise. The peaks of the efficiency are observed at the resonances' energies $\epsilon_p = E_p + U(N+1) - U(N) - \mu$. In the shadowed zones in the left panel, the QD is not acting as a thermal machine, and it is not possible to define an heat to work conversion efficiency. The parameters used are $\mu = 100\,k_BT$, $\gamma_1 = 0.01\,k_BT$, $\gamma_2 = 0.02\,k_BT$, $\gamma_3 = 0.015\,k_BT$, $\Delta T_1 = 0$, $\Delta T_2 = 0.005\,k_BT$, $\Delta\mu_1 = 0.0001\,k_BT$ and $\Delta\mu_2 = -0.0001\,k_BT$.

to enhance the efficiency also for an interacting system. The strongly interacting or non-interacting regimes $E_C = 2\,k_BT$ or $E_C = 90\,k_BT$ are the ones that manifest the most evident increase. In the intermediate regimes $E_C = (20, 50)k_BT$ this is less visible but still present, although we want to stress that in all the cases the increase is about the 50%. The non-monotonic behavior as a function of the charging energy can be understood from Fig. 5.6, where we plot the efficiency as a function of the charging energy E_C. It is possible to see a peak structure similar to the one in Fig. 5.4, and indeed increasing the charging energy has the same effect as moving the chemical potential in the leads. However, it is interesting to notice that a machine that is not performing work in the non-interacting case, can start to behave as a thermal machine by increasing the charging energy. We want to make the same analysis also for the power extracted from the machine, because the strong feature in the non-interacting case as shown in Chapter 2 was that the third terminal could enhance both the power and the efficiency at the same time. As it is possible to see in Fig. 5.7 also an increase in the power $\dot{W}$ has been found. We decided to plot the four different curves in four panels, because the values are very different one from another. This is due to the fact that as the charging energy is changed the chemical potential of the leads could be in resonance with a level or not, thus allowing for a very wide range of values of $\dot{W}$. However the important thing is the positive slope that the power always shows. This means that also in the interacting case turning on the coupling to a third terminal could be very useful for enhancing the performance of the quantum dot. In our model

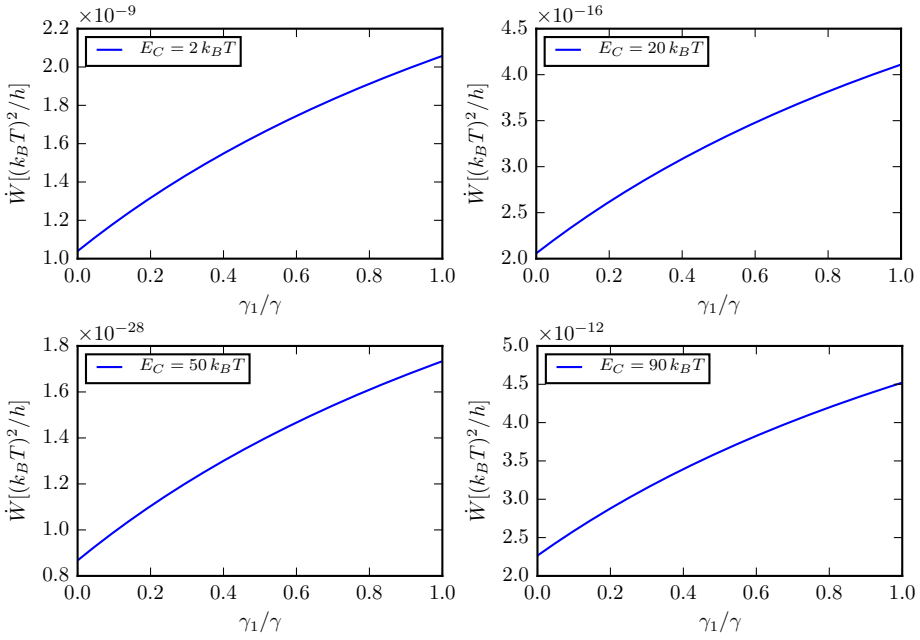

Figure 5.7 – Power $\dot{W}$ as a function of the coupling γ_1 for different values of the charging energy $E_C = (2, 20, 50, 90)k_BT$, with a fixed level spacing $\delta E = 20\,k_BT$. We are spanning from the non-interacting to the interacting regime, and we find a systematic increase of the power as the coupling to lead 1 is turned on. The values of the power $\dot{W}$ could vary significantly as the charging energy varies, going from high values (when resonant with a level) to very low values (from a level). The other parameters used are the same as in Fig. 5.5.

the efficiency at maximum power $\eta(\dot{W}_{\max})$ doesn't depend on the couplings γ_j. It is possible to see in the structure of the transport coefficients G, S and K that in the ratio of the Onsager coefficients the coupling terms simplify with each other. This is a limitation of our model and not a physical feature, this is why we do not show them.

5.3 Summary

In this chapter we have extended the general formalism for linear-response of interacting two-terminal systems to multi-terminal ones. In particular, we have worked out analytical expressions for the currents and the Onsager coefficients in the three-terminal case. We have recovered the known results in the literature for the conductance and the thermopower of an interacting quantum dot, completing the knowledge of the two-terminal systems studying the efficiency, the power and the efficiency at maximum power. For a

three-terminal case we have shown that a third terminal can be useful to improve the thermoelectric performance of a system with respect to the two-terminal case. This remains true also for the strongly interacting case, where moreover oscillations of the efficiency at maximum power, due to the oscillations of the thermopower, have been observed. Our analysis could be extended also to cases in which time-reversal symmetry is broken by a magnetic field or including bosonic or superconducting terminals. It is an interesting open problem to understand in such instances both thermoelectric performance in realistic systems and fundamental bounds on efficiency for power generation and cooling.

5.A Onsager coefficients for the interacting QD

The Onsager coefficients for a three-terminal interacting quantum dot with many levels take the following form

$$
\begin{aligned}
L_{11} &= \frac{e}{k_BT}\frac{\gamma_1}{\gamma_{\rm tot}}\sum_{p=1}^{\infty}\sum_{\{n_i\}} P_{\rm eq}(\{n_i\})\delta_{n_p,0} f(\epsilon_p)(\gamma_2+\gamma_3),\\
L_{12} &= -\frac{e}{k_BT}\frac{\gamma_1}{\gamma_{\rm tot}}\sum_{p=1}^{\infty}\sum_{\{n_i\}} P_{\rm eq}(\{n_i\})\delta_{n_p,0} f(\epsilon_p)\epsilon_p(\gamma_2+\gamma_3),\\
L_{13} &= -\frac{e}{k_BT}\frac{\gamma_1}{\gamma_{\rm tot}}\sum_{p=1}^{\infty}\sum_{\{n_i\}} P_{\rm eq}(\{n_i\})\delta_{n_p,0} f(\epsilon_p)\gamma_2,\\
L_{14} &= \frac{e}{k_BT}\frac{\gamma_1}{\gamma_{\rm tot}}\sum_{p=1}^{\infty}\sum_{\{n_i\}} P_{\rm eq}(\{n_i\})\delta_{n_p,0} f(\epsilon_p)\epsilon_p\gamma_2,\\
L_{22} &= \frac{1}{k_BT}\frac{\gamma_1}{\gamma_{\rm tot}}\sum_{p=1}^{\infty}\sum_{\{n_i\}} P_{\rm eq}(\{n_i\})\delta_{n_p,0} f(\epsilon_p)\epsilon_p^2(\gamma_2+\gamma_3),\\
L_{23} &= \frac{1}{k_BT}\frac{\gamma_1}{\gamma_{\rm tot}}\sum_{p=1}^{\infty}\sum_{\{n_i\}} P_{\rm eq}(\{n_i\})\delta_{n_p,0} f(\epsilon_p)\epsilon_p\gamma_2,\\
L_{24} &= -\frac{1}{k_BT}\frac{\gamma_1}{\gamma_{\rm tot}}\sum_{p=1}^{\infty}\sum_{\{n_i\}} P_{\rm eq}(\{n_i\})\delta_{n_p,0} f(\epsilon_p)\epsilon_p^2\gamma_2,\\
L_{33} &= \frac{e}{k_BT}\frac{\gamma_2}{\gamma_{\rm tot}}\sum_{p=1}^{\infty}\sum_{\{n_i\}} P_{\rm eq}(\{n_i\})\delta_{n_p,0} f(\epsilon_p)(\gamma_1+\gamma_3),\\
L_{34} &= -\frac{e}{k_BT}\frac{\gamma_2}{\gamma_{\rm tot}}\sum_{p=1}^{\infty}\sum_{\{n_i\}} P_{\rm eq}(\{n_i\})\delta_{n_p,0} f(\epsilon_p)\epsilon_p(\gamma_1+\gamma_3),\\
L_{44} &= \frac{1}{k_BT}\frac{\gamma_2}{\gamma_{\rm tot}}\sum_{p=1}^{\infty}\sum_{\{n_i\}} P_{\rm eq}(\{n_i\})\delta_{n_p,0} f(\epsilon_p)\epsilon_p^2(\gamma_1+\gamma_3).
\end{aligned}
\tag{5.27}
$$

Here k_BT is the temperature, γ_i, with $i=\{1,2,3\}$ is the total coupling to the ith lead and $\gamma_{\rm tot}=\sum_i\gamma_i$. It is interesting to notice that the off-diagonal blocks $\begin{pmatrix} L_{13} & L_{14}\\ L_{23} & L_{24}\end{pmatrix}$ and its symmetric counterpart, do not depend on γ_3 since they connect lead 1 and 2. The diagonal blocks instead, do depend on all the couplings.

5.B Two-terminal system

In this Appendix, we recover the two-terminal results for the electrical conductance G and the thermopower S of Ref. [Beenakker1992]. Then we will discuss also the efficiency,

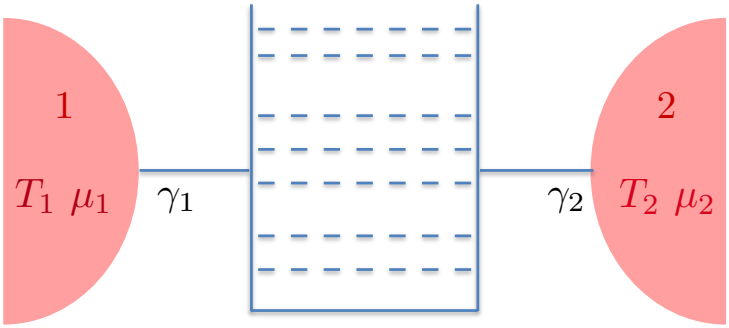

Figure 5.8 – Schematic representation of the two-terminal multi level quantum dot. The two leads are kept at different temperatures and chemical potentials and are connected through a multi level quantum dot. γ_1 and γ_2 are the coupling to the leads. In the non-interacting case the separation between the levels is given by δE.

the efficiency at maximum power and the power.

5.B.1 Behavior as a function of the chemical potential

We started by recovering of the results obtained in Ref. [Beenakker1992], for a two terminal system. i.e. the behavior of the electrical conductance G and of the thermopower S as we vary the chemical potential in the leads. The regime that we analyze is the quantum regime: $k_BT \ll \delta E$, we also assume $\delta E \ll e^2/2C$. The temperature is small enough to resolve all the energy levels of the QD, that are moreover split by the charging energy, that is the dominant energy scale. In Fig. 5.9 we can notice that our results coincide with the approximated ones. In the electrical conductance G that the position of the resonances is given by $\epsilon_p = E_p + U(N+1) - U(N) - \mu$, where $E_p = p\,\delta E$, $p = 0, 1, 2, \ldots$ are the QD's level without interaction. The thermopowers' structure however, deserves a little more explanation. We can observe two different kind of oscillations. The long period oscillation, due to changes of the number of electrons in the quantum dot, and whose period is given by $\Delta\mu = \delta E + e^2/C$ (the same periodicity shown by the conductance resonances); and the short period oscillations, due to energy differences between the ground state and the excited states in the QD at constant number of electrons, and whose period is given by $\Delta\mu = \delta E$. The approximated formulas of Ref. [Beenakker1992] are the following

$$G_B = \frac{e^2}{4k_BT}\frac{\gamma_1\gamma_2}{\gamma_{\rm tot}}\cosh^{-1}\left(\frac{\Delta_{\rm min}}{2k_BT}\right)\left[\mathrm{Int}\left(\frac{|\Delta_{\rm min}|}{\delta E}\right)+1\right], \tag{5.28}$$

$$S_B = -\frac{1}{eT}\left[-\frac{\delta E}{2}\mathrm{Int}\left(\frac{\Delta_{\rm min}}{\delta E}\right)+\Delta_{\rm min}\right]. \tag{5.29}$$

Where $\mathrm{Int}(x)$ is the integer part of x for $x > 0$ and minus the integer part of $|x|$ for $x < 0$, $\Delta_{\rm min} = E_{N_{\rm min}} + (N_{\rm min} - 1/2)\frac{e^2}{C} - e\phi_{\rm ext} - \mu$ and $N_{\rm min}$ is the term that gives the

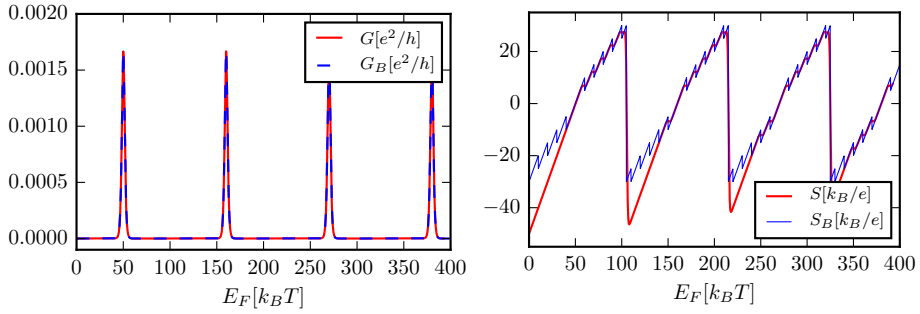

Figure 5.9 – In this figure we compare the electrical conductance G (left) and the thermopower S (right) obtained from a full calculation of the QD's energy level (full red line), and obtained in Ref. [Beenakker1992] with approximated formulas (blue dashed line). In these graphics the parameters used are $e^2/2C = 50\,k_BT$, $\delta E = 10\,k_BT$, $\gamma_1 = 0.01\,k_BT$ and $\gamma_2 = 0.02\,k_BT$.

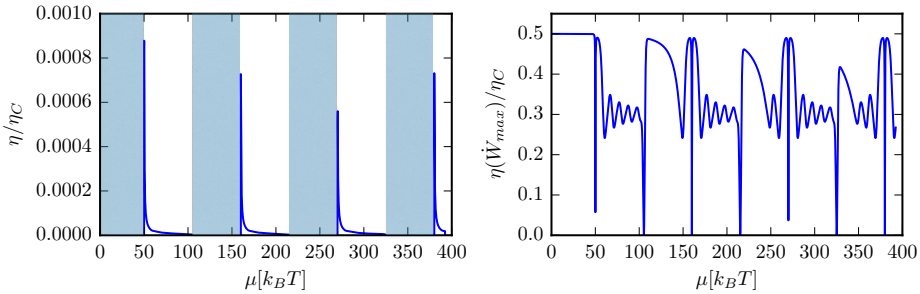

Figure 5.10 – Efficiency (left) and efficiency at max power (right) for the interacting quantum dot as a function of the chemical potential in the leads. In the shadowed zones in the left panel, the QD is not acting as a thermal machine, and it is not possible to define an heat to work conversion efficiency. This is no longer true for the efficiency at maximum power (right panel) that only depends on the figure of merit ZT. In the right panel we can observe an interesting fine structure in the efficiency at maximum power, with a series of oscillations that reflect the thermopower's oscillations. In these graphics the parameters used are $e^2/2C = 50\,k_BT$, $\delta E = 10\,k_BT$, $\gamma_1 = 0.01\,k_BT$, $\gamma_2 = 0.02\,k_BT$, $X^\mu = -1 \times 10^{-5}\,k_BT$ and $X^T = 0.05\,k_BT$.

dominant contribution to the sums over N in Eqs. (5.19)-(5.22). We can see that in Eqs. (5.28) and (5.29) there are no longer sums over the levels or over the electrons of the QD, thus they work for a dot with an infinite number of levels (there are no upper nor lower bounds in the spectrum).

We start our analysis by calculating the relevant thermodynamic quantities such

as the efficiency, the power and the efficiency at maximum power of the interacting quantum dot. We start by analyzing the case of a QD with fixed charging energy. The variation of the efficiency η and of the efficiency at max power $\eta(\dot{W}_{\max})$ as a function of the chemical potential in the leads is shown in Fig. 5.10 There are some regions, shadowed in the left panel of Fig. 5.10, in which the extracted power $\dot{W}$ is negative, therefore we cannot define an heat to work conversion efficiency and it is not a thermal machine. It is interesting to notice that the efficiency at maximum power (Fig. 5.10, right panel) is very sensitive to the thermopower's fine structure, that manifest in a series of oscillations with period δE, that precisely correspond to the thermopower's oscillation.

Conclusions

In this thesis we have presented our work about the properties of multi-terminal thermoelectric machines. In the first place we have developed the general framework for a three-terminal system, the Onsager matrix and his (local and non-local) properties. We then have used this framework to develop and design new applications for the improvement of the thermoelectric performance and the heat management at the nanoscale.

In the first Chapter we developed the general theory to tackle the problem, providing the definitions for local and non-local transport coefficients, as well as the expressions for the generalized figures of merit that characterize the efficiency at maximum power in three-terminal systems. Studying the problem we derived the new expression for the Carnot efficiency that must be used. By means of two solid state models (based on quantum dots), we showed how a third terminal could enhance both the efficiency and the power extracted by a three-terminal system used as a quantum thermal machine. This work provided a solid basis for all the researchers who want to study the thermoelectric transport in three-terminal devices.

Once the general theory was developed we explored different possible applications that could be implemented in a multi-terminal system. In the first place we focalized on the thermoelectric efficiency at the nanoscale. In such systems, with a proper energy filtering mechanism, the ZT figure of merit could be enhanced arbitrarily, but the price of very low power has to be paid. We managed to develop a scheme to achieve an enhancement of both the figure of merit ZT and the power factor Q. This could be obtained by spatially separating the heat and charge currents into different parts of the systems (we want to stress that this is impossible in a two-terminal system). The analytical results showed how, at low temperatures, it was possible to have a great improvement of thermoelectric performance with respect to the two-terminal system. The main reason of that was the possibility of violating the Wiedemann-Franz low in a controlled fashion, thus having a complete control on the ratio G/K. Driven by those results we tested our heat-charge separation scheme on a wide class of devices, in a system whose three terminals were a normal lead, a superconductor and a voltage probe, founding a systematic increasing in both the ZT and the Q.

By adding a magnetic field to the multi-terminal system, in order to break the time-reversal symmetry, we realized that it could be possible to design a device for controlling

the heat flows. In fact, thanks to the Onsager reciprocity relations, the currents could be separated in their reversible and irreversible parts, according to their behavior when the sign of the magnetic field is inverted. This difference allowed for the implementation of several Boolean working conditions, such as (but not limited to) on/off switch, reversal, selected splitting and swap of the heat currents in the device. For each feature the Boolean behavior was obtained by reversing the direction of the applied magnetic field. A further significant advantage manifests in the possibility of designing an array of those devices, in order to have many different working conditions implemented at once. The great potentiality of this mechanism is based on the fact that the whole systems is controlled simply by reversing a magnetic field. We also showed the possibility to implement such a device in a low temperature three-terminal interferometer model, where the heat is carried by the electrons. However, our theoretical model is valid for any system with broken time-reversal symmetry. This means that also a phononic heat current could be controlled by a magnetic field in this device.

Finally we have investigated the consequences, on thermoelectric performance, of Coulomb interaction in multi-levels quantum dots. In particular we have considered the sequential tunneling regime (where the levels' broadening is negligible) for Coulomb blockaded quantum dots. We have worked out analytical expressions for the currents and the Onsager coefficients in the three-terminal case. First we have recovered the known results, for the two-terminal case, for the conductance and the thermopowers and then we have studied the efficiency, the power and the efficiency at maximum power. For a three-terminal case we have shown that a third terminal can be useful to improve the thermoelectric performance of a system with respect to the two-terminal systems even for the strongly interacting case. Interestingly, oscillations of the efficiency at maximum power, that reflect the oscillations of the thermopower, arise from the interplay between the charging energy and the quantization of the levels. A promising further development could be the extension to the case in which time-reversal symmetry is broken by a magnetic field or including bosonic or superconducting terminals. It is an interesting open problem to understand in such instances both thermoelectric performance and fundamental bounds on efficiency for power generation and cooling.

Acknowledgements

First, I greatly thank my supervisor Prof. Rosario Fazio and Prof. Vittorio Giovannetti for their constant help and support during the three years of my PhD. The results contained in this thesis have deeply benefited from frequent discussions with both of them and from the guidance of their physical insight. A special thanks is for Doc. Fabio Taddei, whose great enthusiasm always gave me strong motivations to love this job. I thank all the people with whom I had the pleasure to collaborate during the realization of this work: Doc. Riccardo Bosisio, Stefano Valentini and Prof. Giuliano Benenti. Working with them has given me the opportunity to interact with a stimulating scientific environment. Finally, I thank all my past and present colleagues in the Condensed Matter and Quantum Information group at Scuola Normale Superiore for all the moments shared together and for making the last three years such an unforgettable experience.

Pisa – November 6, 2015

List of personal publications

The following works have been published during my PhD scholarship at Scuola Normale Superiore.

[Mazza2014] F. Mazza, R. Bosisio, G. Benenti, V. Giovannetti, R. Fazio and F. Taddei, *Thermoelectric efficiency of three-terminal quantum thermal machines*, New J. Phys. **16**, 085001 (2014).

–

[Mazza2015] F. Mazza, S. Valentini, R. Bosisio, G. Benenti, V. Giovannetti, R. Fazio and F. Taddei, *Separation of heat and charge currents for boosted thermoelectric conversion*, Phys. Rev. B **91**, 245435 (2015).

–

[Bosisio2015b] R. Bosisio, S. Valentini, F. Mazza, G. Benenti, R. Fazio, V. Giovannetti and F. Taddei, *A magnetic thermal switch for heat management at the nanoscale*, Phys. Rev. B **91**, 205420 (2015).

–

[preprint] F. Mazza, R. Bosisio, G. Benenti, R. Fazio, and F. Taddei, *Thermoelectric efficiency for multi-level interacting quantum dots.*

–

Bibliography

[Altimiras2010] C. Altimiras, H. le Sueur, U. Gennser, A. Cavanna, D. Mailly and F. Pierre, *Non-equilibrium edge-channel spectroscopy in the integer quantum Hall regime*, Nat. Phys. **6**, 34 (2010).

[Andresen2011] B. Andresen, *Current Trends in Finite-Time Thermodynamics*, Angewandte Chemie International Edition **50**, 2690 (2011).

[Apertet2012] Y. Apertet, H. Ouerdane, C. Goupil and P. Lecoeur, *Thermoelectric internal current loops inside inhomogeneous systems*, Phys. Rev. B **85**, 033201 (2012).

[Ashcroft1976] N. W. Ashcroft and N. D. Mermim, *Solid State Physics* (Saunders College Publishing, 1976).

[Balachandran2013] V. Balachandran, G. Benenti and G. Casati, *Efficiency of three-terminal thermoelectric transport under broken time-reversal symmetry*, Phys. Rev. B **87**, 165419 (2013).

[Bedkihal2013] S. Bedkihal, M. Bandyopadhyay and D. Segal, *The probe technique far from equilibrium: Magnetic field symmetries of nonlinear transport*, Euro. Phys. J. B **86**, 506 (2013).

[Beenakker1991] C. W. J. Beenakker, *Theory of Coulomb-blockade oscillations in the conductance of a quantum dot*, Phys. Rev. B **44**, 1646 (1991).

[Beenakker1992] C. W. J. Beenakker and a. a. M. Staring, *Theory of the thermopower of a quantum dot*, Phys. Rev. B **46**, 9667 (1992).

[Beenakker1997] C. W. J. Beenakker, *Random-matrix theory of quantum transport*, Rev. Mod. Phys. **69**, 731 (1997).

[Benenti2011] G. Benenti, K. Saito and G. Casati, *Thermodynamic Bounds on Efficiency for Systems with Broken Time-Reversal Symmetry*, Phys. Rev. Lett. **106**, 230602 (2011).

[Benenti2013] G. Benenti, G. Casati, T. Prosen and K. Saito, *Fundamental aspects of steady state heat to work conversion*, arXiv preprint arXiv:1311.4430 (page 28) (2013).

[Blanc2013] C. Blanc, A. Rajabpour, S. Volz, T. Fournier and O. Bourgeois, *Phonon heat conduction in corrugated silicon nanowires below the Casimir limit*, Appl. Phys. Lett. **103**, 043109 (2013).

[Boese2001] D. Boese and R. Fazio, *Thermoelectric effects in Kondo-correlated quantum dots*, EPL (Europhysics Letters) **56**, 576 (2001).

[Bosisio2014] R. Bosisio, C. Gorini, G. Fleury and J.-L. Pichard, *Gate-modulated thermopower of disordered nanowires: II. Variable-range hopping regime*, New J. Phys. **16**, 095005 (2014).

[Bosisio2015a] R. Bosisio, C. Gorini, G. Fleury and J.-L. Pichard, *Using Activated Transport in Parallel Nanowires for Energy Harvesting and Hot-Spot Cooling*, Phys. Rev. Applied **3**, 054002 (2015).

[Bosisio2015b] R. Bosisio, S. Valentini, F. Mazza, G. Benenti, R. Fazio, V. Giovannetti and F. Taddei, *Magnetic thermal switch for heat management at the nanoscale*, Phys. Rev. B **91**, 205420 (2015).

[Brandner2013a] K. Brandner, K. Saito and U. Seifert, *Strong Bounds on Onsager Coefficients and Efficiency for Three-Terminal Thermoelectric Transport in a Magnetic Field*, Phys. Rev. Lett. **110**, 070603 (2013).

[Brandner2013b] K. Brandner and U. Seifert, *Multi-terminal thermoelectric transport in a magnetic field: Bounds on Onsager coefficients and efficiency*, New J. Phys. **15**, 1 (2013).

[Broeck2005] C. Van den Broeck, *Thermodynamic Efficiency at Maximum Power*, Phys. Rev. Lett. **95**, 190602 (2005).

[Buddhiraju2015] S. Buddhiraju and B. Muralidharan, *Optimal single quantum dot heat-to-pure-spin-current converters*, Physica B: Condensed Matter **478**, 153 (2015).

[Büttiker1986] M. Büttiker, *Four-Terminal Phase-Coherent Conductance*, Phys. Rev. Lett. **57**, 1761 (1986).

[Büttiker1988] M. Büttiker, *Coherent and sequential tunneling in series barriers*, IBM J. Res. Dev. **32**, 63 (1988).

[Callen1985] H. B. Callen, *Thermodynamics and an Introduction to Thermostatistics* (John Wiley And Sons Inc, 1985), second edition.

[Carnot1824] N. L. S. Carnot, *Réflexions sur la puissance motrice du feu et sur les machines propres à développer cette puissance* (Libraire Chez Bachelier, Paris, 1824).

[Chang2006] C. W. Chang, D. Okawa, A. Majumdar and A. Zettl, *Solid-State Thermal Rectifier*, Science **314**, 1121 (2006).

[Chen2014] Z. Chen, C. Wong, S. Lubner, S. Yee, J. Miller, W. Jang, C. Hardin, A. Fong, J. E. Garay and C. Dames, *A photon thermal diode*, Nat. Commun. **5** (2014).

[Chen2015] S. Chen, J. Wang, G. Casati and G. Benenti, *Thermoelectricity of interacting particles: A numerical approach*, Phys. Rev. E **92**, 032139 (2015).

[Claughton1996] N. R. Claughton and C. J. Lambert, *Thermoelectric properties of mesoscopic superconductors*, Phys. Rev. B **53**, 6605 (1996).

[Curzon1975] F. L. Curzon and B. Ahlborn, *Efficiency of a Carnot engine at maximum power output*, Am. J. Phys. **43**, 22 (1975).

[Datta1995] S. Datta, *Electronic Transport in Mesoscopic Systems* (Cambridge University Press, 1995).

[De Groot1962] S. R. De Groot and P. Mazur, *Nonequilibrium Thermodynamics: Transport and Rate Processes in Physical and Biological Systems* (North-Holland Publ. Co., 1962).

[Deviatov2008] E. V. Deviatov and A. Lorke, *Experimental realization of a Fabry-Perot-type interferometer by copropagating edge states in the quantum Hall regime*, Phys. Rev. B **77**, 161302 (2008).

[Dresselhaus2007] M. S. Dresselhaus, G. Chen, M. Y. Tang, R. G. Yang, H. Lee, D. Z. Wang, Z. F. Ren, J.-P. Fleurial and P. Gogna, *New Directions for Low-Dimensional Thermoelectric Materials*, Adv. Mater. **19**, 1043 (2007).

[Dubi2011] Y. Dubi and M. Di Ventra, *Colloquium: Heat flow and thermoelectricity in atomic and molecular junctions*, Rev. Mod. Phys. **83**, 131 (2011).

[Engl2011] T. Engl, J. Kuipers and K. Richter, *Conductance and thermopower of ballistic Andreev cavities*, Phys. Rev. B **83**, 205414 (2011).

[Entin-Wohlman2010] O. Entin-Wohlman, Y. Imry and A. Aharony, *Three-terminal thermoelectric transport through a molecular junction*, Phys. Rev. B **82**, 115314 (2010).

[Entin-Wohlman2012] O. Entin-Wohlman and A. Aharony, *Three-terminal thermoelectric transport under broken time-reversal symmetry*, Phys. Rev. B **85**, 085401 (2012).

[Entin-Wohlman2015] O. Entin-Wohlman, Y. Imry and A. Aharony, *Enhanced performance of joint cooling and energy production*, Phys. Rev. B **91**, 054302 (2015).

[Eom1998] J. Eom, C.-J. Chien and V. Chandrasekhar, *Phase Dependent Thermopower in Andreev Interferometers*, Phys. Rev. Lett. **81**, 437 (1998).

[Esposito2009] M. Esposito, K. Lindenberg and C. V. den Broeck, *Thermoelectric efficiency at maximum power in a quantum dot*, EPL (Europhysics Letters) **85**, 60010 (2009).

[Esposito2010] M. Esposito, R. Kawai, K. Lindenberg and C. Van den Broeck, *Efficiency at Maximum Power of Low-Dissipation Carnot Engines*, Phys. Rev. Lett. **105**, 150603 (2010).

[Fagas2014] G. Fagas, L. Gammaitoni, D. Paul and G. A. Berini, *ICT-Energy-Concepts Towards Zero-Power Information and Communication Technology* (InTech, 2014).

[Fisher1981] D. S. Fisher and P. A. Lee, *Relation between conductivity and transmission matrix*, Phys. Rev. B **23**, 6851 (1981).

[Fleurial1996] J.-P. Fleurial, A. Borshchevsky, A. Caillat, D. Morelli and G. Meisner, *Proceedings of the 15th International Conference on Thermoelectrics*, Eds. T. Caillat, J.-P- Fleurial, A. Borshchevsky, Piscataway (1996).

[Gentle1998] J. E. Gentle, *Numerical Linear Algebra for Applications in Statistics* (Springer New York, 1998).

[Giazotto2006] F. Giazotto, T. T. Heikkilä, A. Luukanen, A. M. Savin and J. P. Pekola, *Opportunities for mesoscopics in thermometry and refrigeration: Physics and applications*, Rev. Mod. Phys. **78**, 217 (2006).

[Giovannetti2008] V. Giovannetti, F. Taddei, D. Frustaglia and R. Fazio, *Multichannel architecture for electronic quantum Hall interferometry*, Phys. Rev. B **77**, 155320 (2008).

[Gramespacher1997] T. Gramespacher and M. Büttiker, *Nanoscopic tunneling contacts on mesoscopic multiprobe conductors*, Phys. Rev. B **56**, 13026 (1997).

[Haake2000] F. Haake, *Quantum Signatures of Chaos* (Springer Berlin, 2000).

[Harman2002] T. C. Harman, P. J. Taylor, M. P. Walsh and B. E. LaForge, *Quantum Dot Superlattice Thermoelectric Materials and Devices*, Science **297**, 2229 (2002).

[Hicks1993] L. D. Hicks and M. S. Dresselhaus, *Thermoelectric figure of merit of a one-dimensional conductor*, Phys. Rev. B **47**, 16631 (1993).

[Hofer2015] P. P. Hofer and B. Sothmann, *Quantum heat engines based on electronic Mach-Zehnder interferometers*, Phys. Rev. B **91**, 195406 (2015).

[Horvat2012] M. Horvat, T. Prosen, G. Benenti and G. Casati, *Railway switch transport model*, Phys. Rev. E **86**, 052102 (2012).

[Hou2013] C. Y. Hou, K. Shtengel and G. Refael, *Thermopower and Mott formula for a Majorana edge state*, Phys. Rev. B **88** (2013).

[Houten1992] H. van Houten, C. W. J. Beenakker and B. J. van Wees, *Nanostructured Systems*, volume 35 of *Semiconductors and Semimetals* (Academic Press Boston, 1992).

[Humphrey2002] T. E. Humphrey, R. Newbury, R. P. Taylor and H. Linke, *Reversible Quantum Brownian Heat Engines for Electrons*, Phys. Rev. Lett. **89**, 116801 (2002).

[Humphrey2005] T. E. Humphrey and H. Linke, *Reversible Thermoelectric Nanomaterials*, Phys. Rev. Lett. **94**, 096601 (2005).

[Imry2008] Y. Imry, *Introduction to Mesoscopic Physics* (Oxford University Press, 2008), second edition.

[Ioffe1958] A. F. Ioffe, *Semiconductor Thermoelements and Thermoelectric Cooling* (Pion Ltd, 1958).

[Jacquet2009] P. Jacquet, *ThermoElectric Transport Properties of a Chain of Quantum Dots with Self-Consistent Reservoirs*, J. Stat. Phys. **134**, 709 (2009).

[Jacquod2010] P. Jacquod and R. S. Whitney, *Coherent Thermoelectric Effects in Mesoscopic Andreev Interferometers*, EPL (Europhysics Letters) **91**, 67009 (2010).

[Ji2003] Y. Ji, Y. Chung, D. Sprinzak, M. Heiblum, D. Mahalu and H. Shtrikman, *An electronic Mach-Zehnder interferometer*, Nature **422**, 415 (2003).

[Jiang2005] Z. Jiang and V. Chandrasekhar, *Thermal Conductance of Andreev Interferometers*, Phys. Rev. Lett. **94**, 147002 (2005).

[Jiang2012] J. H. Jiang, O. Entin-Wohlman and Y. Imry, *Thermoelectric three-terminal hopping transport through one-dimensional nanosystems*, Phys. Rev. B **85**, 1 (2012).

[Jiang2013] J. H. Jiang, O. Entin-Wohlman and Y. Imry, *Hopping thermoelectric transport in finite systems: Boundary effects*, Phys. Rev. B **87**, 1 (2013).

[Jiang2014a] J. H. Jiang, *Enhancing efficiency and power of quantum-dots resonant tunneling thermoelectrics in three-terminal geometry by cooperative effects*, J. Appl. Phys. **116**, 194303 (2014).

[Jiang2014b] J. H. Jiang, *Thermodynamic bounds and general properties of optimal efficiency and power in linear responses*, Phys. Rev. E **90**, 042126 (2014).

[Jordan2013] A. N. Jordan, B. Sothmann, R. Sánchez and M. Büttiker, *Powerful and efficient energy harvester with resonant-tunneling quantum dots*, Phys. Rev. B **87**, 1 (2013).

[Karwacki2013] Ł. Karwacki, P. Trocha and J. Barnaś, *Spin-dependent thermoelectric properties of a Kondo-correlated quantum dot with Rashba spin–orbit coupling*, Journal of Physics: Condensed Matter **25**, 505305 (2013).

[Kobayashi2009] W. Kobayashi, Y. Teraoka and I. Terasaki, *An oxide thermal rectifier*, Appl. Phys. Lett. **95**, 171905 (2009).

[Koch2014] T. Koch, J. Loos and H. Fehske, *Thermoelectric effects in molecular quantum dots with contacts*, Phys. Rev. B **89**, 155133 (2014).

[Kosloff2014] R. Kosloff and A. Levy, *Quantum Heat Engines and Refrigerators: Continuous Devices*, Annu. Rev. Phys. Chem. **65**, 365 (2014).

[Landauer1957] R. Landauer, *Spatial Variation of Currents and Fields Due to Localized Scatterers in Metallic Conduction*, IBM J. Res. Dev. **1**, 223 (1957).

[Leijnse2014] M. Leijnse, *Thermoelectric signatures of a Majorana bound state coupled to a quantum dot*, New J. Phys. **16**, 015029 (2014).

[Li2006] B. Li, L. Wang and G. Casati, *Negative differential thermal resistance and thermal transistor*, Appl. Phys. Lett. **88**, 143501 (2006).

[Li2012] N. Li, J. Ren, L. Wang, G. Zhang, P. Hänggi and B. Li, *Colloquium: Phononics: Manipulating heat flow with electronic analogs and beyond*, Rev. Mod. Phys. **84**, 1045 (2012).

[Lim2014] J. S. Lim, R. López and D. Sánchez, *Orbital caloritronic transport in strongly interacting quantum dots*, New Journal of Physics **16**, 015003 (2014).

[Liu2010] J. Liu, Q.-f. Sun and X. C. Xie, *Enhancement of the thermoelectric figure of merit in a quantum dot due to the Coulomb blockade effect*, Phys. Rev. B **81**, 245323 (2010).

[Lopez2014] R. Lopez, M. Lee, L. Serra and J. S. Lim, *Thermoelectrical detection of Majorana states*, Phys. Rev. B **89**, 205418 (2014).

[Machon2013] P. Machon, M. Eschrig and W. Belzig, *Nonlocal Thermoelectric Effects and Nonlocal Onsager relations in a Three-Terminal Proximity-Coupled Superconductor-Ferromagnet Device*, Phys. Rev. Lett. **110**, 047002 (2013).

[Mahan1996] G. D. Mahan and J. O. Sofo, *The best thermoelectric*, Proceedings of the National Academy of Sciences of the United States of America **93**, 7436 (1996).

[Mahan1997] G. Mahan, B. Sales and J. Sharp, *Thermoelectric Materials: New Approaches to an Old Problem*, Phys. Today **50**, 42 (1997).

[Majumdar2004] A. Majumdar, *Thermoelectricity in Semiconductor Nanostructures*, Science **303**, 777 (2004).

[Marciani2014] M. Marciani, P. W. Brouwer and C. W. J. Beenakker, *Time-delay matrix, midgap spectral peak, and thermopower of an Andreev billiard*, Phys. Rev. B **90**, 045403 (2014).

[Martínez-Pérez2014] M. Martínez-Pérez, P. Solinas and F. Giazotto, *Coherent Caloritronics in Josephson-Based Nanocircuits*, J. Low Temp. Phys. **175**, 813 (2014).

[Martínez-Pérez2015] M. J. Martínez-Pérez, A. Fornieri and F. Giazotto, *Rectification of electronic heat current by a hybrid thermal diode*, Nat. Nanotechnol. **10**, 303 (2015).

[Mazza2014] F. Mazza, R. Bosisio, G. Benenti, V. Giovannetti, R. Fazio and F. Taddei, *Thermoelectric efficiency of three-terminal quantum thermal machines*, New J. Phys. **16**, 085001 (2014).

[Mazza2015] F. Mazza, S. Valentini, R. Bosisio, G. Benenti, V. Giovannetti, R. Fazio and F. Taddei, *Separation of heat and charge currents for boosted thermoelectric conversion*, Phys. Rev. B **91**, 245435 (2015).

[Meier2014] T. Meier, F. Menges, P. Nirmalraj, H. Hölscher, H. Riel and B. Gotsmann, *Length-Dependent Thermal Transport along Molecular Chains*, Phys. Rev. Lett. **113**, 060801 (2014).

[Monteros2014] A. Monteros, G. Uppal, S. McMillan, M. Crisan and I. Ţifrea, *Thermoelectric transport properties of a T-shaped double quantum dot system in the Coulomb blockade regime*, The Euro. Phys. J. B **87** (2014).

[Morelli1995] D. T. Morelli, T. Caillat, J.-P. Fleurial, A. Borshchevsky, J. Vandersande, B. Chen and C. Uher, *Low-temperature transport properties of p -type* $CoSb_3$, Phys. Rev. B **51**, 9622 (1995).

[Muralidharan2012] B. Muralidharan and M. Grifoni, *Performance analysis of an interacting quantum dot thermoelectric setup*, Phys. Rev. B **85**, 1 (2012).

[Nakpathomkun2010] N. Nakpathomkun, H. Q. Xu and H. Linke, *Thermoelectric efficiency at maximum power in low-dimensional systems*, Phys. Rev. B **82** (2010).

[Neder2006] I. Neder, M. Heiblum, Y. Levinson, D. Mahalu and V. Umansky, *Unexpected Behavior in a Two-Path Electron Interferometer*, Phys. Rev. Lett. **96**, 016804 (2006).

[Neder2007] I. Neder, N. Ofek, Y. Chung, M. Heiblum, D. Mahalu and V. Umansky, *Interference between two indistinguishable electrons from independent sources*, Nature **448**, 333 (2007).

[Onsager1931] L. Onsager, *Reciprocal Relations in Irreversible Processes.*, Phys. Rev. **37**, 405 (1931).

[Ozaeta2014] A. Ozaeta, P. Virtanen, F. S. Bergeret and T. T. Heikkilä, *Predicted Very Large Thermoelectric Effect in Ferromagnet-Superconductor Junctions in the Presence of a Spin-Splitting Magnetic Field*, Phys. Rev. Lett. **112**, 057001 (2014).

[Parsons2003] A. Parsons, I. Sosnin and V. Petrashov, *Phase periodic thermopower in normal metal/superconductor nanostructures*, Physica E **18**, 316 (2003), 23rd International Conference on Low Temperature Physics (LT23).

[Peltier1834] J. C. A. Peltier, *Nouvelles expériences sur la caloricité des courants électrique*, Annales de Chimie et de Physique **56**, 371 (1834).

[Roulleau2007] P. Roulleau, F. Portier, D. C. Glattli, P. Roche, A. Cavanna, G. Faini, U. Gennser and D. Mailly, *Finite bias visibility of the electronic Mach-Zehnder interferometer*, Phys. Rev. B **76**, 161309 (2007).

[Saira2007] O.-P. Saira, M. Meschke, F. Giazotto, A. M. Savin, M. Möttönen and J. P. Pekola, *Heat Transistor: Demonstration of Gate-Controlled Electronic Refrigeration*, Phys. Rev. Lett. **99**, 027203 (2007).

[Saito2011] K. Saito, G. Benenti, G. Casati and T. Prosen, *Thermopower with broken time-reversal symmetry*, Phys. Rev. B **84**, 3 (2011).

[Sánchez2011a] D. Sánchez and L. Serra, *Thermoelectric transport of mesoscopic conductors coupled to voltage and thermal probes*, Phys. Rev. B **84**, 201307 (2011).

[Sánchez2011b] R. Sánchez and M. Büttiker, *Optimal energy quanta to current conversion*, Phys. Rev. B **83**, 1 (2011).

[Sánchez2013] R. Sánchez, B. Sothmann, A. N. Jordan and M. Büttiker, *Correlations of heat and charge currents in quantum-dot thermoelectric engines*, New J. Phys. **15**, 125001 (2013).

[Sánchez2015a] R. Sánchez, B. Sothmann and A. N. Jordan, *Chiral Thermoelectrics with Quantum Hall Edge States*, Phys. Rev. Lett. **114**, 146801 (2015).

[Sánchez2015b] R. Sánchez, B. Sothmann and A. N. Jordan, *Heat diode and engine based on quantum Hall edge states*, New J. Phys. **17**, 075006 (2015).

[Scheibner2008] R. Scheibner, M. König, D. Reuter, A. D. Wieck, C. Gould, H. Buhmann and L. W. Molenkamp, *Quantum dot as thermal rectifier*, New J. Phys. **10**, 083016 (2008).

[Schmiedl2008] T. Schmiedl and U. Seifert, *Efficiency at maximum power: An analytically solvable model for stochastic heat engines*, EPL (Europhysics Letters) **81**, 20003 (2008).

[Seebeck1822] T. J. Seebeck, *Ueber den Magnetismus der galvanische Kette*, Abhandlungen der Deutschen Akademie der Wissenschaften zur Berlin (1822).

[Shakouri2011] A. Shakouri, *Recent Developments in Semiconductor Thermoelectric Physics and Materials*, Annu. Rev. Mater. Res. **41**, 399 (2011).

[Snyder2008] G. J. Snyder and E. S. Toberer, *Complex thermoelectric materials*, Nature Mater. **7**, 105 (2008).

[Sothmann2012a] B. Sothmann and M. Büttiker, *Magnon-driven quantum-dot heat engine*, EPL (Europhysics Letters) **99**, 27001 (2012).

[Sothmann2012b] B. Sothmann, R. Sánchez, A. N. Jordan and M. Büttiker, *Rectification of thermal fluctuations in a chaotic cavity heat engine*, Phys. Rev. B **85**, 205301 (2012).

[Sothmann2013] B. Sothmann, R. Sánchez, A. N. Jordan and M. Büttiker, *Powerful energy harvester based on resonant-tunneling quantum wells*, New J. Phys. **15**, 095021 (2013).

[Sothmann2014] B. Sothmann, R. Sánchez and A. N. Jordan, *Quantum Nernst engines*, EPL (Europhysics Letters) **107**, 47003 (2014).

[T Kuo2012] D. T Kuo and Y.-C. Chang, *Effects of interdot hopping and Coulomb blockade on the thermoelectric properties of serially coupled quantum dots*, Nanoscale Research Letters **7**, 257 (2012).

[Terraneo2002] M. Terraneo, M. Peyrard and G. Casati, *Controlling the Energy Flow in Nonlinear Lattices: A Model for a Thermal Rectifier*, Phys. Rev. Lett. **88**, 094302 (2002).

[Tian2012] H. Tian, D. Xie, Y. Yang, T.-L. Ren, G. Zhang, Y.-F. Wang, C.-J. Zhou, P.-G. Peng, L.-G. Wang and L.-T. Liu, *A Novel Solid-State Thermal Rectifier Based On Reduced Graphene Oxide*, Sci. Rep. **2** (2012).

[Titov2008] M. Titov, *Thermopower oscillations in mesoscopic Andreev interferometers*, Phys. Rev. B **78**, 224521 (2008).

[Torfason2013] K. Torfason, A. Manolescu, S. I. Erlingsson and V. Gudmundsson, *Thermoelectric current and Coulomb-blockade plateaus in a quantum dot*, Physica E: Low-dimensional Systems and Nanostructures **53**, 178 (2013).

[Trocha2012] P. Trocha and J. Barna, *Large enhancement of thermoelectric effects in a double quantum dot system due to interference and Coulomb correlation phenomena*, Phys. Rev. B **85**, 1 (2012).

[Venkatasubramanian2001] R. Venkatasubramanian, E. Siivola, T. Colpitts and B. O'Quinn, *Thin-film thermoelectric devices with high room-temperature figures of merit*, Nature **413**, 597 (2001).

[Vineis2010] C. J. Vineis, A. Shakouri, A. Majumdar and M. G. Kanatzidis, *Nanostructured Thermoelectrics: Big Efficiency Gains from Small Features*, Advanced Materials **22**, 3970 (2010).

[Virtanen2004a] P. Virtanen and T. Heikkilä, *Thermopower in Andrew Interferometers*, J. Low Temp. Phys. **136**, 401 (2004).

[Virtanen2004b] P. Virtanen and T. T. Heikkilä, *Thermopower Induced by a Supercurrent in Superconductor-Normal-Metal Structures*, Phys. Rev. Lett. **92**, 177004 (2004).

[Volta1794] A. Volta, *Nuova memoria sull'elettricità animale*, Lettere al signor Abate Anton Maria Vassalli (1794).

[Zheng2008] J.-C. Zheng, *Recent advances on thermoelectric materials*, Frontiers of Physics in China **3**, 269 (2008).

[Ziman1972] J. M. Ziman, *Principles of the Theory of Solids* (Cambridge University Press, 1972), Cambridge Books Online.